Fuzzy Logic Based Proportional Integral with Anti-windup Dynamic Control of Grid-Tied Microgrid

(Case Study: ASTU Student Cafeteria)

Raji Ababe Sori

A Thesis Submitted to

Department of Electrical Power and Control Engineering

School Electrical Engineering and Computing

Presented in Partial Fulfillment of the Requirement of the degree of Master of Science in Electrical Power and Control Engineering (Specialization in Control Engineering)

Office of Graduate Studies

Adama Science and Technology University

September, 2021

Adama, Ethiopia

Fuzzy Logic Based Proportional Integral with Anti-windup Dynamic Control of Grid-Tied Microgrid

(Case Study: ASTU Student Cafeteria)

Raji Ababe Sori

Advisor: Tafese Asrat(PhD)

A Thesis Submitted to

Department of Electrical Power and Control Engineering

School Electrical Engineering and Computing

Presented in Partial Fulfillment of the Requirement of the degree of Master of Science in Electrical Power and Control Engineering (Specialization in Control Engineering)

Office of Graduate Studies

Adama Science and Technology University

September, 2021

Adama, Ethiopia

DECLARATION OF STUDENT

I hereby declare that this Master Thesis entitled “Fuzzy Logic Based Proportional Integral with Anti-windup Dynamic Control Of Grid-Tied Microgrid (Case Study: ASTU Student Cafeteria)” is my original work. That is, it has not been submitted for the award of any academic degree, diploma or certificate in any other university. All sources of materials that are used for this thesis have been duly acknowledged through citation.

Raji Ababe Sori	_________________________	_________________
Name of the student	Signature	Date

RECOMMENDATION OF ADVISOR

I, the advisor of this thesis, hereby certify that I have read the revised version of the thesis entitled "Fuzzy Logic based Proportional integral with anti-windup dynamic control of Grid-Tied Microgrid (Case Study: ASTU Student Cafeteria) " prepared under my guidance by Raji Ababe Sori submitted in partial fulfillment of the requirements for the degree of Masters of Science in Electrical Power and Control Engineering (Specialization in Control Engineering) Therefore, I recommend the submission of revised version of the thesis to the department following the applicable procedures.

Tafese Asrat(PhD)	______________	28/09/2021
Major Advisor	Signature	Date

APPROVAL SHEET

I, the advisors of the thesis entitled **"Fuzzy Logic Based Proportional Integral with Anti-windup Dynamic Control of Grid-Tied Microgrid (Case Study: ASTU student Cafeteria)"** and developed by **Raji Ababe Sori**, hereby certify that the recommendation and suggestions made by the board of examiners are appropriately incorporated into the final version of the thesis.

Tafese Asrat(PhD)		28/09/2021
Major Advisor	Signature	Date

We, the undersigned, members of the Board of Examiners of the thesis by Raji Ababe Sori have read and evaluated the thesis entitled "Fuzzy Logic Based Proportional Integral with Anti-windup Dynamic Control of Grid-Tied Microgrid (Case Study: ASTU student Cafeteria)" and examined the candidate during open defense. This is, therefore, to certify that the thesis is accepted for partial fulfillment of the requirement of the degree of Master of Science in Electrical Power and Control Engineering (Specialization in Control Engineering)

Milkias Berhanu(PhD)		23.09.2021
Chairperson	Signature	Date
Molla Biweta (PhD)		29/09/2021
Internal Examiner	Signature	Date
Kemal R. (PhD)		Sep. 28/2021
External Examiner	Signature	Date

Final approval and acceptance of the thesis is contingent upon submission of its final copy to the Office of Postgraduate Studies (OPGS) through the Department Graduate Council (DGC) and School Graduate Committee (SGC).

Department Head	Signature	Date
School Dean	Signature	Date
Office of Postgraduate Studies, Dean	Signature	Date

ACKNOWLEDGEMENTS

First, of all my gratitude, goes to omniscience of Almighty God. It gives me great pride to appreciate all the wonderful, brilliant people who contributed directly and indirectly to make this thesis work completed. Next my heartiest gratitude, profound and deep respect go to my research advisor, Tefese Asrat(PhD) for his friendly attitude, guidance, and inspiration through the research process and course-work, for all the emails, meetings, advice, suggestions and sharing of many good ideas.

I am especially grateful to the Department of Electrical and computer engineering of Adama Science and Technology University (ASTU) for providing their all support. I also would like to thank my colleagues for all their supports. Finally, I must express my gratitude to my parents, for their encouragement and support.

TABLE OF CONTENTS

LIST OF TABLES

LIST OF FIGURES

LIST OF SYMBOLS

Symbols	Description
a	Diode ideality factor
G	Actual irradiance in W/m^2
I_d	Diode saturation current,
I_{pv}	Light generated current of the photovoltaic cell
I_{scn}	Short-circuit current at the nominal condition
K	Boltzmann constant (1.38×10^{-23}) JK^{-1}
N_p	Number of cells connected in parallel
N_s	Number of cells connected in series
q	Electronic charge (1.602×10^{-19})
R_p	Shunt resistance (Ω)
R_s	Series resistance (Ω)
T	Module operating temperature in Kelvin
ΔT	Deviation from the nominal temp in Kelvin
V_d	Voltage across the diode:
V_{ocn}	Open circuit current at the nominal condition

LIST OF ABBREVIATIONS

AC ·	Alternating current
BESS ·	Battery energy storage systems
BJT ·	Bipolar Junction Transistor
CHP ·	Combined heat and power, combined heat and power
DC ·	Direct current
DG ·	Distributed generation
DOD ·	Depth of Discharge
EMS ·	Energy management system
IEEE ·	Institute of Electrical and Electronics Engineer
IGBT ·	Insulated Gate Bipolar Transistor, Insulated Gate Bipolar transistor
KVL ·	Kirchhoff's Voltage Law
LFP ·	Lithium Iron Phosphate
MATLAB ·	Matrix Laboratory
MG ·	Microgrid
MOSFET ·	Metal–oxide–semiconductor field-effect transistor
MPC ·	Model predictive control
MPP	Maximum power point
MPPT ·	Maximum Power Point Track
NASA ·	National Aeronautics and Space
NPC ·	Neutral Point Clamped
P&O ·	Perturb and observe
PCC ·	Point of common coupling
PEVSI ·	Power electronic based static voltage source inverter

PI ·	Proportional-integral
PLL ·	Phase-Locked-Loop
PR ·	Proportional Resonant
PV ·	Photovoltaic system
PWM ·	Pulse Width Modulation
RES ·	Renewable Energy Source
SCR ·	Short circuit ratio
SG ·	Synchronous generator
SIT ·	Static induction transistor
SOC ·	State of charge
STC ·	Standard Test Conditions
SVPWM	Space vector pulse width modulation
UK ·	United Kingdom
UPS	Uninterruptable Power Supply
USA ·	United State of America
VCO ·	Voltage Controlled Oscillator
VIR ·	Virtual inertia response Inverter

ABSTRACT

Economic aspects, environmental issue, social and technical aspects are key factors for revolution of electric grid to develop microgrid. The grid tied microgrid consisting of solar photovoltaic system and battery energy storage system is modelled to support load without interruption. The frequency and voltage fluctuation are major problems in a grid tied microgrid due to intermittent nature of solar photovoltaic system while battery energy storage system acts as a master unit which is responsible for setting up the voltage and frequency at the point of common coupling by balancing active power. This research work focuses on active power regulation, frequency and voltage control at the point of common coupling between microgrid and utility grid. Microgrid needs good frequency dynamic performance, good voltage amplitude dynamic performance and well regulated active power at the point of common coupling. Microgrid components are analyzed by using MATLAB/Simulink. Mathematical modelling of the proposed system is performed. Fuzzy logic based proportional integral with anti-windup and proportional integral anti-windup voltage and current controllers are designed to control the current and voltage output of three phase three level neutral point clamped voltage source inverter connected to battery energy storage system, utility grid and loads at the point of common coupling. Fuzzy logic based Proportional integral (PI) with anti-windup and PI anti windup controller are compared based on their dynamic frequency performance and dynamic voltage amplitude performance during different operation mode of microgrid. Fuzzy-PI anti-windup gives settling time of 12:00 hour of frequency with overshoot of 0.1976% per 50Hz in a grid connected operation of microgrid with varying solar irradiance at point of common coupling. But, PI anti wind up results settling time of 12:30 hour with overshoot of 0.1997% for the same conditions. Also, Fuzzy-PI anti windup gives settling time of 3.97 minute of voltage amplitude with overshoot of 4.4634% in the same condition. But, PI anti windup results settling time of 4 minute of voltage amplitude with overshoot of 4.4766% in the same condition. The detailed analysis of microgrid dynamic operation control is performed by conducting three scenario. In all cases system parameters maintained within the acceptable range for stable operation of grid tied microgrid. In general fuzzy PI anti-windup is recommended for microgrid dynamic control.

Key words: *Active power, Frequency, Fuzzy logic PI anti windup, Grid-tied Microgrid, PI anti-windup and Voltage*

CHAPTER ONE

INTRODUCTION

1.1 Background of the study

Economic inflation, population increase, technological progress, and environmental changes are now demanding decentralized generation in place of conventional centralized generation. The centralized power generation systems have several disadvantages: first, most power generation plants rely on fossil fuels, which increases carbon dioxide emissions and wastes heat; second, the supply of a large amount of energy through transformers and long transmission and distribution lines; third, power losses and voltage drops due to long transmission lines and transformers are major problems; fourth, it does not provide an economically viable solution to power poor and isolated communities[1].

In order to reduce the dependency on electricity generation from fossil fuels, decentralized renewable energy technologies are becoming increasingly important as alternative energy sources in the energy supply systems of many countries[2][3].With regard to the coordinated integration of the decentralized generation (DG) with the energy of the public grid, the concept of the microgrid was developed. A typical microgrid are low-medium-voltage distribution systems that represent a network of renewable or alternative energy sources (e.g. photovoltaics, wind energy), fuel cells, diesel generators, biomass, geothermal and marine energy systems (waves and tides, etc.), energy storage (batteries, supercapacitors, electric vehicles, etc.), suitable energy conversion devices, flexible loads and control units[4]. Microgrid operates in island (standalone) and grid-tied mode in accordance with the availability of utility supply in terms of power quality and reliability. When the microgrid (MG) is connected to the utility, it has the advantage of power supply and power quality support[5]. When utility power is interrupted due to faults, the loads on an MG are shared between micro-sources and voltage and frequency control is switched to an individual control system known as a micro-source controller (MSC).When microgrid is grid-tied power flow is controlled (regulated) so that a certain amount of active and reactive power is supplied from the network to MG or vice versa. In addition, microgrids can provide improvements in local power quality and voltage regulation. Keeping the voltage and frequency within the allowable standard values is an important requirement in microgrid design[6]. Such introduction of microgrids permits larger distributed generation by interconnecting several micro supplys, that usually uses a single interface(usually power electronic based static voltage source electrical converter (PEVSI) to the utility grid[7].

Thus, main concern in grid interconnected microgrid is electric power transaction and revenue maximization as well as management of microgrid from the economical point of view. In contrast, maintenance of voltage and frequency fluctuation are the major problems in an isolated microgrid as it is not connected to the large-scale electric grid. In the present scenario, the power demand of remote villages is mostly fulfilled by the diesel generator. However, the diesel generator is not the best solution for such places due to high operating cost, environmental pollution, and transportation cost of fuel[8]. The combination of the solar PV generation and battery energy storage systems becomes an attractive solution in such a remote area. The variable nature of the solar PV resources can be partially overcome by a combination of both PV and BESS into an optimal combination and so the system becomes more reliable compared with the system having no storage systems. Furthermore, the integration of these two becomes an attractive solution to run and provide better reliability because the weakness of one system can be compensated by the strength of the other one at any time [9]. However, in the isolated microgrid, power generation does not match with power consumption, mainly due to the load profile and intermittent nature of renewable energy resources such as the wind and solar PV. As the wind and solar PV generation depend highly on weather conditions like wind speed and intensity of light, the output power from those resources are fluctuating in nature[10]. To connect to utility grid intermittent nature produces variable frequency AC and DC voltage. This different kinds of voltage amplitude and frequency converted to the same voltage amplitude and frequency with voltage source inverte control of microgrid which allows the microgrid to connect to utility. Several techniques and algorithms have been proposed by researchers for grid tied microgrid voltage source inverter control to the point where the microgrid is connected with the main grid through a breaker mechanism known by point of common coupling. Among the proposed techniques are conventional PI, MPC, H-infinity have been widely used for grid tied microgrid inverter control. One of the control strategy which has been applied to the grid-connected system is the model predictive control (MPC). The advantages of model predictive control are fast dynamic response and accurate reference tracking. However, this controller has a model based regulator and therefore it is quite sensitive to parameter variations, uncertainties, inaccuracies and delays[1]. Proportional-integral (PI) controllers are used in several research studies to control currents on the AC side. In these control schemes, the DC link voltage is controlled by a voltage control loop in which a PI controller acts on the DC voltage error in order to provide references for the alternating current in the stationary frame (abc or dq) or synchronous (dq) frame. PI Current regulators ensure that a clean and in-phase alternating current feeds the grid[11] . Since the reference signals for the current controllers in this scheme are sinusoidal, a PI controller implemented in standard way under a stationary frame is not able to adequately track these references, and this results in steady-state error due to the limited controller gain at the frequency of interest. Also, this controller does not support large set point deviation which causes saturation of the system.

In this research work, the comparison of fuzzy PI with anti-windup and PI anti windup inverter control was applied which well suits with parameter variation, reduces steady state error while large set point changes while the integral anti windup reduces saturation of the system. The solar array is controlled with MPPT to generate maximum power using perturb and observe algorithm techniques. The inverter uses PWM switching techniques. The result shows the proposed technique gives better dynamic performance with less steady state error and better set point tracking.

1.2 Statement of the Problem

Coordinated integration of distributed generation (DG) with utility power to support local load without interruption, the microgrid concept has been developed. The performance of distributed generation such as photovoltaic and wind generators is heavily influenced by weather conditions; indeed, this intermittent energy from renewable sources consequently has some serious effects on the operation of the electrical system. Frequent integration of distributed generation in distribution lines may cause voltage fluctuation which accordingly damages the voltage-regulating devices. They also may cause frequency deviation of power systems which depreciate stability of system at point of common coupling.However,the the voltage and frequency deviation under different kinds of microgrid operation needs research to control the overall microgrid operation to perform with less disturbance under parameter variations. In fact, the more distributed generation grows the more storage capacity is required. If renewable energies are to provide a huge amount of microgrid power, they will need to maintain some power in reserve. On the other hand, the sunlight or wind is not always present or predictable. So, it requires battery energy storage systems (BESS). Battery energy storage system (BESS) store power during normal operation and inject power during a fault, to maintain the proper microgrid frequency and voltage. Therefore, the photovoltaic systems in micro grids requires advanced and reliable control units that can be used not only for voltage regulation, but also for frequency regulation. The grid needs this type of renewable generator to help to regulate voltage and frequency. Intelligent mechanisms are required to make microgrid and utility grid interact properly. On the other hand, control techniques used in conventional distributed generation systems are mainly linear. However, to have RES and storage elements working together, sophisticated switching power electronics devices are required. In the case when the application calls for less power losses or large power transfer, it is necessary to use different types of converters with more power electronics switches. Since the aforementioned system distributed generation with battery energy storage system had severe nonlinear behavior, the use of a simple linear controller is not adequate for such applications and doesn't provide good performances. Therefore, it needs best and robust controller. In this research work, the fuzzy-PI with anti-windup and PWM inverter switching technique are proposed and developed. The proposed control and system modelling is implemented and simulated by using MATLAB software.

1.3 Research Questions

This work intends to answer the following basic research questions.

- How renewable energy resources can improve the operation and stability of the regional Electric grid?
- How can voltage and frequency deviation adjusted in different operation modes of microgrid?
- How can controller decrease non linearity and steady state error of microgrid system?
- How battery energy storage system benefit microgrid during transient operation?

1.4 Objectives of the study

1.4.1 General objective

The main objective of this research is to design and model a grid connected microgrid composed of a solar PV system, system controller and battery energy storage system using MATLAB/Simulink for ASTU student cafeteria.

1.4.2 Specific objectives

The specific objectives of this research thesis are:

- To assess the energy demand of ASTU student cafeteria load.
- To model suitable microgrid for ASTU student cafeteria load.
- To manage the active power flow at the point of common coupling
- To adjust frequency and voltage magnitude deviation in the modelled microgrid due to parameter variation.
- To design appropriate controller which compensate imbalance in a microgrid.

1.5 Scope of the Study

The thesis focuses on the mathematical modeling and simulation design of both the islanded and grid tied microgrid. Simulation of microgrid dynamics using MATLAB Simulink/script for the campus level microgrid application are implemented. The microgrid consisting of solar PV and battery using inverter driving techniques are developed and discussed.

1.6 Limitations of the Study

This study comes across limitations on different phases of the research process. Power delivered or absorbed by the battery is only based on the frequency change without battery state of charge. Load sharing between inverters considering the factors like battery state of charge, renewable generation and load profile. Therefore, the load sharing between inverters considering the factors like battery state of charge is not included in this research. Further, coordination and control of multiple Microgrid is not considered in this study.

1.7 Motivation of the Study

Generating electricity from conventional power sources has always been a major cause of air pollution, and great efforts have been made to develop cleaner power generation technologies. However, relatively new concerns about global warming and sustainability have begun to transform the way energy systems work and expand. Renewable energies have drawn the most attention in comparison with conventional energy generations in recent years. Accordingly, Ethiopia has abundant Renewable energies. Besides having abundant Renewable energy resources Ethiopia have been using hydro power generation system while the other optional power generation resources which requires less cost and easy operation like Solar and wind power generation is not used to their extent of existence. Therefore, a micro-grid (MG) concept is needed to integrate the renewable energy sources (RES) in the electric grid for greater support and operation of existing system.

1.8 Significance of the Study

The microgrid not only provides emergency network backup for the ASTU student cafeteria, but can also be used to reduce costs or connect to a local resource that is too small or unreliable for grid network use. The cafeteria is more energy-independent and partly more environmentally friendly.

1.9 Thesis Organization

This thesis organizes into five chapters.

Chapter One: This chapter contains an introduction, study background, problem and study objectives as well as the scope and limitations of this study.

Chapter Two: This chapter contains the literature review, in this chapter articles, journals and related papers are discussed and a large part of the theoretical knowledge on the topics of this work is discussed.

Chapter Three: This chapter applies different methodology, also describes the data required for this study, and describes all equations, procedures and mathematical calculations. Also describes the modeling of the components of the microgrid and the control of the battery energy storage system and solar photovoltaic systems in MATLAB Simulink / Scripts. Chapter Four: In this chapter the result and discussions were presented.

Finally, in Chapter five, an overall system conclusion, recommendations and future works related to this study were stated.

CHAPTER TWO
LITERATURE REVIEW

2.1 Chapter Overview

This chapter explains the definition of a micro grid and the structure of a typical micro grid. The properties and problems of the micro grid are introduced and checked. Closely related work, especially in various control methods, along with their merits and demerits are examined and discussed.

2.1.1 Definition of Microgrid

In Author [12],dictates microgrid as: “the micro grid concept assumes a number of loads and micro-sources that work as a single controllable system that supplies energy and heat to its local area". Alternatively, a "micro grid is a small network in which distributed generators and electrical consumers are combined and efficiently controlled in an integrated manner"[13].Alternatively, "a micro grid can be defined as a low-voltage network (for example a small urban area, a shopping center or an industrial park) with its consumers and several small modular generation systems connected to them that provide energy and heat for the local supply"[14].

Microgrid can be designed for grid-connected or isolated operation. In addition to electrical consumers, heat consumers are often also connected to this small power system[15]. A microgrid is a decentralized group of generation sources and loads that is normally connected and works synchronously with the conventional wide area synchronous network (macro grid), but can also be separated in "island mode" and works autonomously depending on physical or economic conditions [16]. In this way, microgrids improve the security of supply within the microgrid and can provide emergency power and switch between island and network mode. As a controllable unit, a microgrid can effectively integrate several sources of decentralized generation, especially renewable energy[17]. Typical microgrid structure is as shown in figure 2.1.

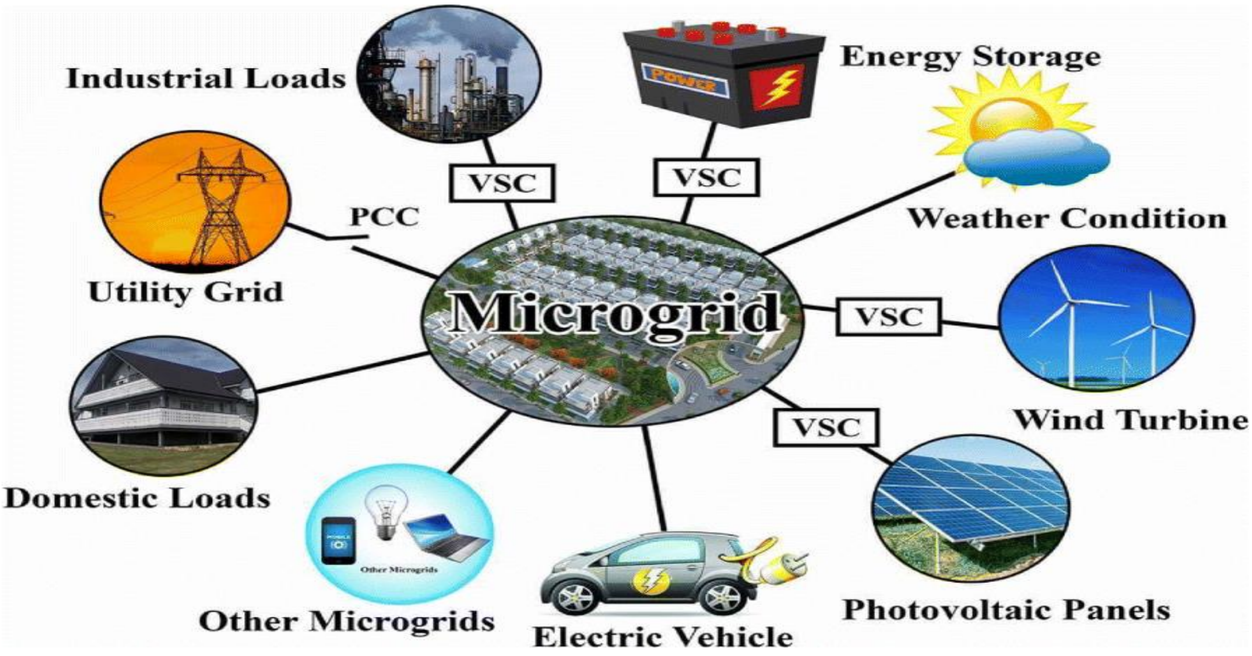

Figure 2.1 Microgrid architecture structure[18]

2.1.2 Types of Microgrids

There are many kinds of microgrid depending on their size and geographical area of requirement. Some of the most known was:

I. Campus environment/institutional microgrids

The main purpose of campus microgrids are to combine the generations in place to support multiple loads located in a very narrow geographic area where they can be easily managed by a single owner[19][20].

ii. Community microgrids

Community microgrids can serve hundreds of customers and support nearby energy penetration (power, heating and cooling). In a community microgrid, some households may have renewable resources that can meet needs for themselves and those of their neighbors in the same community. The common microgrid can also have a central or decentralized energy store to support community loads[21].

iii. Remote off-grid microgrids

These microgrids are never connected to the macro grid (public grid), but constantly work offline for economic or geographic reasons. Generally, "off-grid" microgrids are built in areas far away from any transmission and distribution infrastructure, so they are not connected to the public grid[22].

iv. Military-based microgrids

These microgrids are actively used with attention on the physical and cyber security of military systems so as to ensure a reliable power supply without having to rely on the macro grid [23].

2.1.3 Operation modes of a microgrid

This section introduces the main operating modes: grid connection mode, once interacting with utility grid; island mode refers to autonomous operation; and transient operation mode, as the name implies, is that the temporary condition when the main grid is disconnected or restored [24].

I. Grid Connected Mode

In the grid-connected mode, the working principle of the microgrid is to export energy into and out of the grid, balance power flow and energy management, and provide support to the grid through a series of auxiliary services such as voltage and frequency control regulation, dispatch service and operating power reserve depend on load and power generation conditions [25][18].

II. Islanded Mode

The island mode of the microgrid can be intentional or unintentional. On the one hand, there can be deliberate island formation during scheduled maintenance work or if the network quality can endanger the operation of the microgrid[26]. On the other hand, the unintended island occurs due to faults, contingencies or other unplanned events. [27][4].

III. Transient operating mode

Transient operation mode refers to a temporary state between a device connected to the grid and islanded mode, and vice versa. In a microgrid, disconnection and reconnection to the PCC should be as smooth and fast as possible, because the recovery process must be absolutely reliable and run under minimal or trouble-free conditions. A method of synchronizing voltage amplitude, frequency and phase and coordinated sequence connection of decentralized generator sets are needed to ensure a smooth transition [28].

2.2 Control Methods of Microgrids

This section describes microgrid control layers based on the hierarchical control method: primary, secondary and tertiary[10]. The primary layer guarantees a precise power sharing between the inverters, by adding virtual inertia that emulates the physical characteristics of conventional power systems through voltage amplitude and frequency regulation. The secondary control restores the voltage amplitude and frequency deviations caused by the droop control[29]. The tertiary layer manages the power flow among the microgrid and the utility grid at the point of common coupling with utility.

2.3 Basic Components in Microgrid

A typical microgrid are low-to-medium voltage distribution plants, which constitutes an interconnection of renewable or alternative energy sources (e. g solar photovoltaics, wind power, etc.), energy storage units (batteries, super capacitors, electric vehicles, etc.), suitable power conversion devices, flexible loads, and control units[4].

Local alternative generation units: A microgrid represents several types of generation sources that are a combination of renewable or alternative energy sources (e.g.solar and wind energy)[23]. For the purpose of this thesis solar photovoltaic is reviewed.

2.3.1 Solar Photovoltaic system (PV)

Due to its quiet operation and its relatively small size, the photovoltaic system is an attractive renewable energy source for decentralized power generation[30]. The photovoltaic system generates energy when it is exposed to sunlight, but several interface components are required to convert, control, conduct, distribute and store the electrical energy generated by the photovoltaic system [31].

a. PV Array: A photovoltaic array is an interconnected set of modules a photovoltaic array is an interconnected collection of photovoltaic modules, one of which is shown in the illustration to the right.

b. Photovoltaic cell: Photovoltaic cells (solar cells) are covered with a protective laminate and become a photovoltaic module, and it is the basic combination component of photovoltaic systems. [32].

c. PV module: The combining of cells is called a Photovoltaic module or sometimes called a photovoltaic panel. Most of the time cells are connected in series to increase the voltage rating of the photovoltaic module or panel. Figure 2.2 shows the photovoltaic structure of PV cell, module, and array.

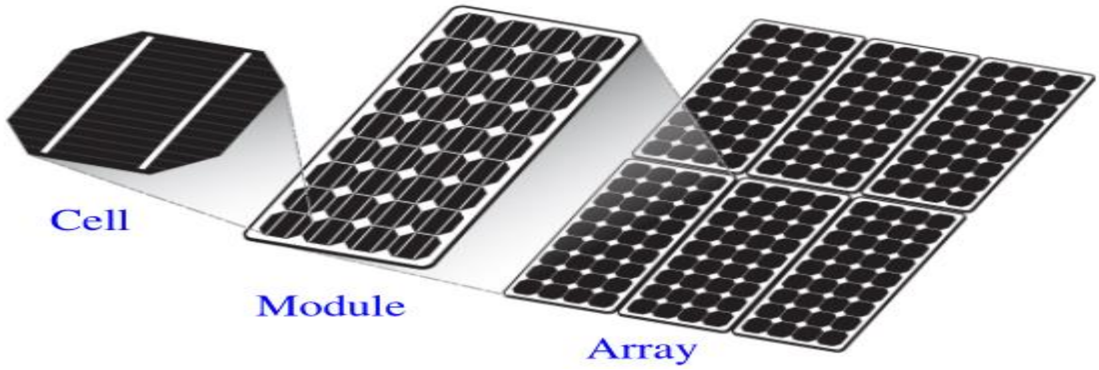

Figure 2.2 Structure of PV cell, module and array[33]

Types of Solar photovoltaic Cells

Photovoltaic cells are manufactured in a different way with different materials. The material used for solar panel constructions is silicon which contains semiconductor properties[32]. Types of photovoltaic cell that dominate the world market are categorized into three: Monocrystalline, polycrystalline and thin film.

a. Monocrystalline silicon photovoltaic cell

The first commercially introduced or the first-generation solar cells are made from monocrystalline silicon cell, which has an extremely pure form of silicon. A Monocrystalline silicon cell is very efficient and has high heat resistant ability.

b. Polycrystalline silicon photovoltaic cell

Polycrystalline or multi-crystalline photovoltaic cells contain many small grains of the crystal rather than a single similar crystal structure. Also, they are made by casting a cube-shaped ingot by using molten silicon, then packed and sawn the same with monocrystalline photovoltaic cells. It is cheaper but less efficient than a monocrystalline cell.

c. Thin film

Even so, the crystalline Photovoltaic cells are dominating the market, cells they also made from a thin film. This makes them durable and more flexible. This type of thin-film photovoltaic cell is amorphous silicon which is resulted from depositing thin layers of silicon onto a glass[34].

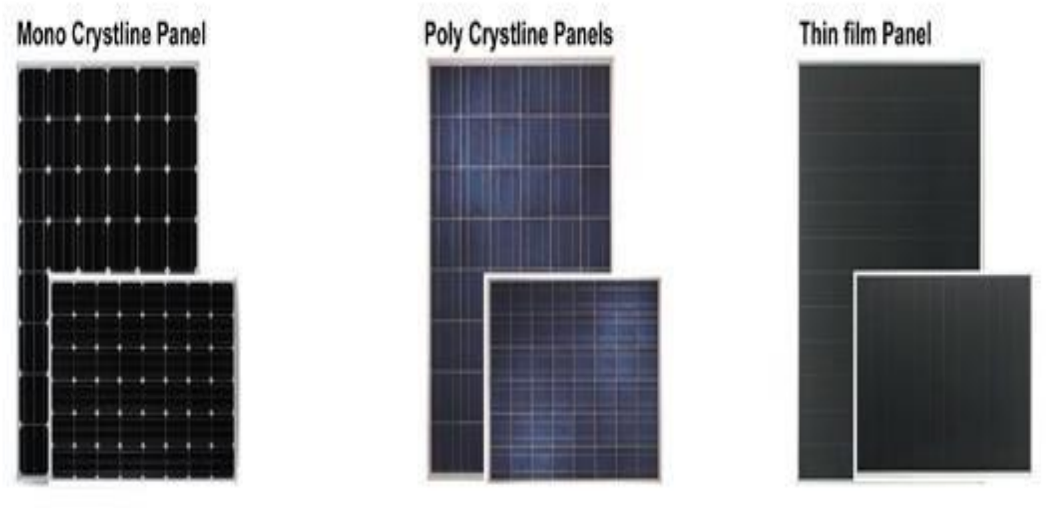

Figure 2.3 Types of solar photovoltaic cells[35]

Types of the photovoltaics are described as in table 2.1.

Table 2.1 Summary of types of Photovoltaics

Types of cell	**Efficiency rate**	**Advantage**	**Disadvantage**
Monocrystalline cell	20%	Highly efficient, Durable	Most expensive
Polycrystalline cell	15%	Less expensive, improving efficiency	Slightly lower efficiency not as durable
Thin film (amorphous cell)	7- 10%	Low cost, easily Produced	Shorter warranties, shorter lifespan

2.3.2 Factors that Affect Reliability and Performance of PV Cell

I. Solar Cell Conversion Efficiency (η)

The efficiency of a PV solar cell is the ratio of the generated maximum output power to the incident or input power. Some of the output parameters affect how efficient a solar PV cell is and they defined as follows[36].

$$\eta = \frac{V_{oc} \times I_{sc} \times FF}{P_{in}} \tag{2.1}$$

Where: V_{oc} = Open circuit voltage, density, I_{sc} = the short circuit current, P_{in} = the incident light power on the device, and FF = the fill factor.

ii. Short Circuit Current

The short-circuit current is the current found when the negative and positive terminals of the cell are short-circuited; also, the voltage between the negative and positive terminals is zero, which corresponds with zero load resistance. It depends on the spectrum of the incident light and incident photon flux density[36].

iii. Open Circuit Voltage

The open-circuit voltage is the maximum voltage in absence of current flows through the external circuit. In open Circuit Voltage, the solar PV cell terminals are opened or disconnected from a load. It is the maximum voltage that a photovoltaic solar cell can deliver under any illumination.

iv. Fill factor

Fill factor (FF) is one of the important parameters to identify the efficiency of the solar photovoltaic module. The fill factor value gives an idea of the quality of the PV array, and the closer to unity the more power the array can provide. Because of the existence of parasitic elements in the photovoltaic cell, the value of FF decreases. Due to this, the values of the fill factor are between 0.7 and 0.8. It is the ratio of theoretical power to the maximum power and mathematically expressed as following[37].

I-V Curve with varying Fill Factor of solar cell is shown in figure 2.4.

$$FF = \frac{V_{mp} \times I_{mp}}{V_{oc} \times I_{sc}} \tag{2.2}$$

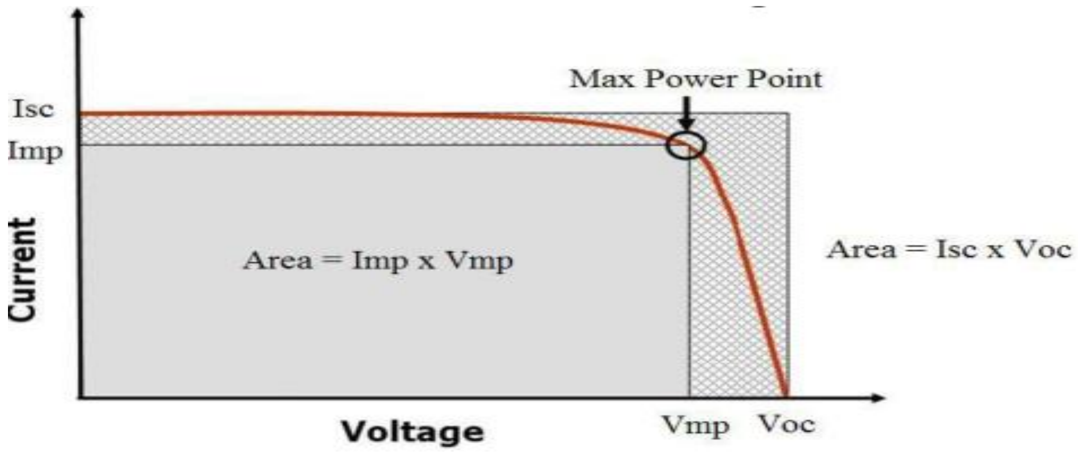

Figure 2.4 I-V Curve with varying fill factor of solar cell[38]

2.3.3 Energy Storage System

The energy storage system is a critical component used in a microgrid that is based on renewable energy sources. It will help to provide voltage stability and smooth out the fluctuations that occurred in renewable energy generation[39].

There are different types of energy storage systems such as the battery, fuel cell compressed air, Flywheel, compressed air, and super-capacitor. Among them, the battery is selected for review.

Battery

Generally, there are two classification of energy storage batteries: primary and secondary batteries.

a. Primary Batteries These batteries are not rechargeable and, if discharged, cannot be recharged and must be disposed of. They are cheap, lightweight, energy-tight, and are mainly used for portable electronic devices. However, primary batteries are not used in photovoltaic systems because they cannot be recharged[40].

b. Secondary Batteries: This battery can store and deliver electrical energy, which means it can be charged and recharged several times. They are more expensive than the primary batteries and are used in applications that involve some discharge and charge cycles, like in solar photovoltaic systems[40].

For grid connection and standalone (islanded) microgrid design there are different battery technologies are there in the market. From those battery technologies the most adapted categories are Lead acid and Lithium ion battery. Table 2.2 describe clearly their performance.

Table 2.2 Summary of battery comparison of lead acid and lithium-ion battery

Points of difference	Lithium-ion batteries	Lead-acid batteries
Weight	Light	Heavy
Discharge rate	Less Discharge rate	High discharge rate
Initial cost	High, expected to decrease	Cheaper
Life cycle	4000 cycles at 10% discharge	1750 cycles at 10% discharge
	500 cycles at 95% discharge	250 cycles at
	Longer expected life time	Shorter expected lifetime
Efficiency	High	Low
Replacement Cycle	7-8 years	2-3 years
Application area	Gaining popularity in domestic grid-tied	Typically used for off-grid properties wherever a lot of energy storage is needed

In most cases, lithium-ion battery technology is superior to lead-acid battery because of its reliability and efficiency, among other things.

2.3.4 Power Conversion Device

DC to DC converters

DC to DC converters is the power electronic circuit that converts a DC voltage from one level to another voltage level. There are types of conversion methods such as linear, electronic, magnetic, switched-mode, capacitive. Among them, the circuits described in this thesis work are switched-mode DC-DC converters. This is the electronic device that is used whenever a change of direct current electrical power from one voltage level to another voltage level is needed[41].

DC to DC converters is especially important because, unlike AC, DC cannot simply be stepped down or stepped up using a transformer. So, the DC-DC converter is used as a transformer. They essentially just change the input power into various impedance levels. Therefore, whatever the output voltage levels, the output of power comes from the input. There are different kinds of dc-to-dc converter that can be used to change voltage level to another level. Some of them were discussed below[42] .

i. The buck converter

The buck converter is used in circuits that step down the voltage level from the input voltage according to its requirement. Buck converter is simple and low cost. A buck converter operation starts with a switch that is open which means no current flow in any part of a circuit and when the switch is closed, the current passes through the inductor, slowly at first, however building up over time. When the switch is closed the inductor pulls current through the diode, and this means the voltage at the output of the inductor is lower than the first[43].

ii. The boost Converter:

A boost converter which is called a step-up converter is a power converter that has an output DC voltage that is greater than its input DC voltage. Where the power (P = VI) must be conserved, the source current is higher than the output current. This converter has the same components as the buck converter, but it produces an output voltage greater than the source.

iii. Buck-boost converter:

The other basic switched-mode converter is the buck-boost converter. The output of this buck-boost converter will be either lower or higher than the input voltage[39].

DC to AC converters (Inverter)

It is an electrical device that has the opposite function with the rectifier. As known, the Photovoltaic panel produces DC power, and therefore this grid connected Photovoltaic system has an inverter, which is used for DC to AC conversion. [44].

2.4 Components of Control Techniques

2.4.1 Maximum power point tracker (MPPT)

A maximum power point tracker is used to extract the maximum power from the photovoltaic module or panel under varying irradiance and temperature. The point at which the photovoltaic module produces the maximum power is called the maximum PowerPoint.

The output characteristic of the Photovoltaic array is influenced by the variation of temperature and irradiance. When temperature and irradiance change, the photovoltaic module may not work at the maximum PowerPoint. Therefore, to overcome this problem perturb and observe (P&O) method is selected for maximum power generation. It is the type of maximum PowerPoint tracking technique and it can extract maximum power from PV module at any time and provide solar energy efficiency. Also, to get maximum power the fill factor plays a great role[45].

The output power induced within the PV module depends on the temperature and irradiance of solar cells. So, to increase the efficiency of the system, it's necessary to trace the maximum PowerPoint of the photovoltaic array. The photovoltaic module features a distinctive operating point that can provide maximum energy to the load. This point is known as the maximum PowerPoint which is a nonlinear variation with cell temperature and solar irradiance and shown in figure 2.5.

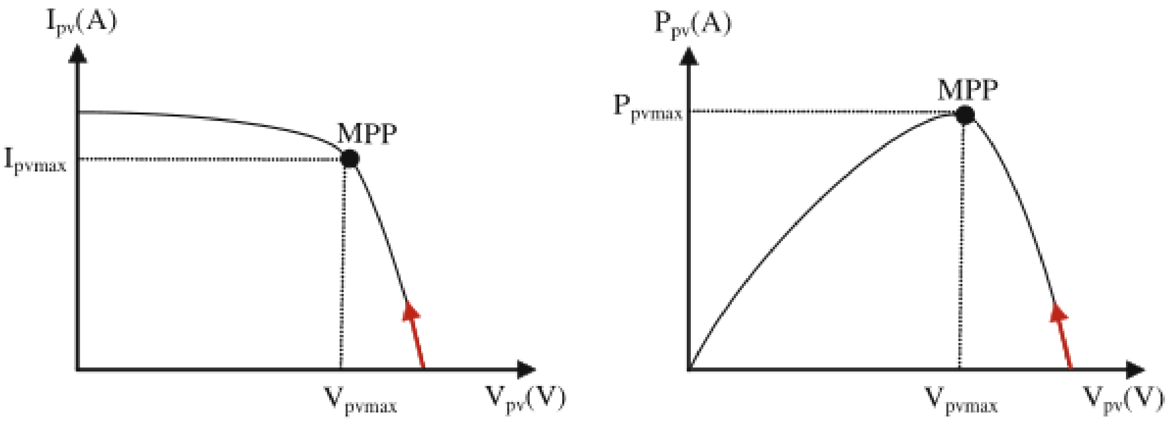

Figure 2.5 Maximum power points of I-V and P-V curves[46]

2.4.2 Perturb & Observe Technique.

This is the easiest method. The perturb & observe algorithm principle states that as the operating voltage of the photovoltaic panel is perturbed by a small increment if the produced power (ΔP) change in power is positive then we must go in the direction of MPP and then keep on perturbing in the similar direction. If a change in power is negative, it is going away from the direction of MPP, and the sign of perturbing supplied must be changed [47].

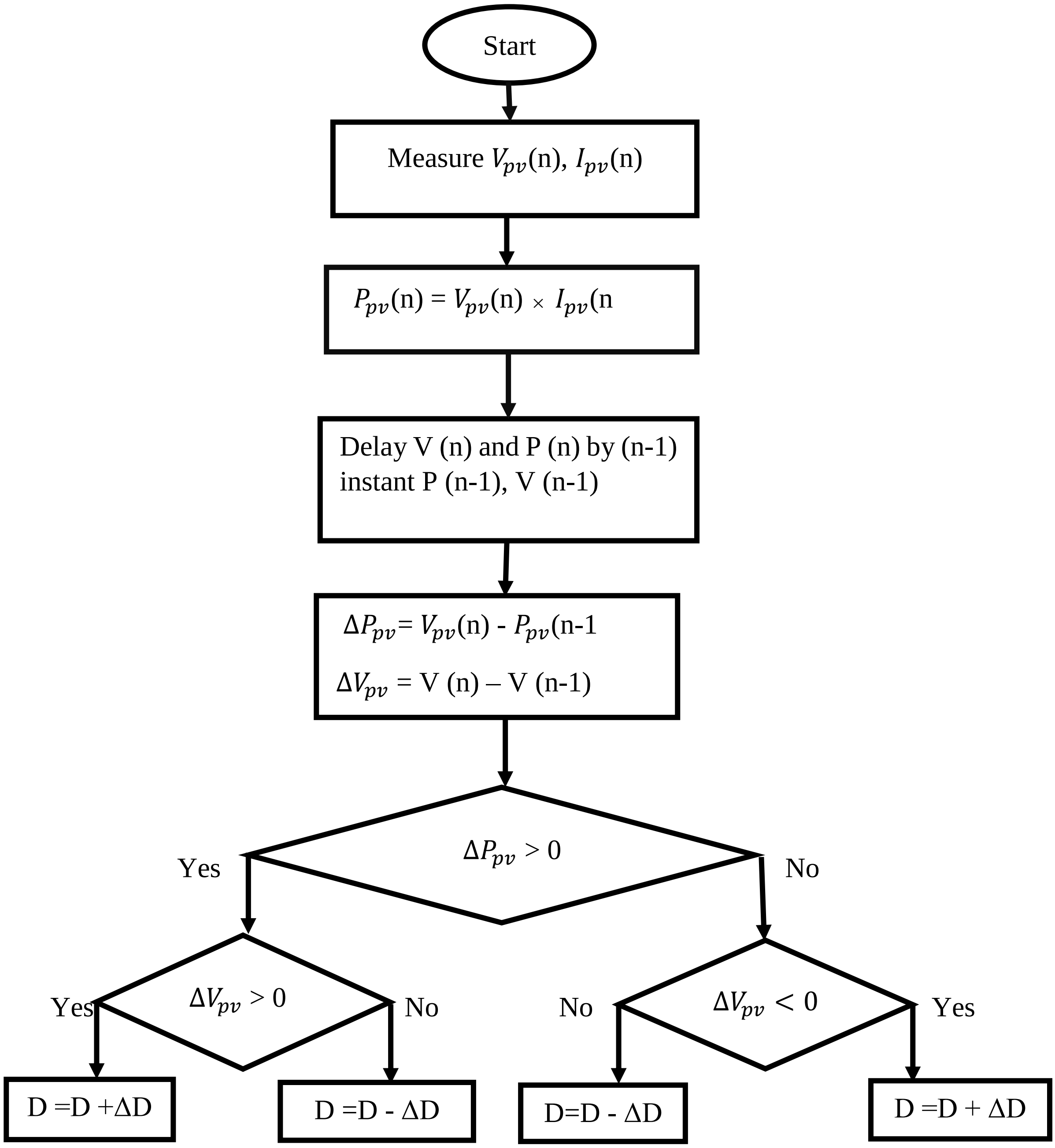

Figure 2.6 P&O MPPT flow chart

In this method, the first condition that must be checked is as the present power is the same as the previous reading. If there is no change in power (ΔP) we must be operating at the knee of the P-V curve and no change in operating voltage is needed. The second conditional statement compares the power of the previous values to the current values. Then the voltage is compared to the previous values and from these samples, it is possible to determine the direction of the maximum power point. The duty cycle is then perturbed in the direction that will increase the power[48]. The method continues its operating voltage of the PV module until the maximum power is obtained. The figure 2.6 Shows the flow chart of perturb and observe method.

2.4.3 Charge Controllers

Charge controllers are used to managing the flow of current from and to batteries in a microgrid system. They are used to protect the batteries and manage the Direct current bus voltage. In a microgrid standalone photovoltaic system, a charge controller will control a bidirectional converter by lowering the photovoltaic output voltage resulted in the level required by the batteries and when the photovoltaic output falls to zero the charge controller will activate the bidirectional converter to send the power produced from the batteries to the microgrid system.

It regulates the current and voltage that is coming from the photovoltaic panels and passing into the battery. If there is no charge control, the current from the photovoltaic module will flow to a battery proportional to the irradiance, whether the battery requires to be charging or not. If the battery is fully charged, unregulated charging will bring the risk of battery voltage to rise to extremely high levels which causing internal heating, severe gassing, accelerated grid corrosion, and electrolyte loss so the charge controller provides the health and increases the lifetime of the battery[49] .

2.5 Grid Integration

To simplify the control design method of a three-phase grid-connected system, two elementary transformations are used to reduce the dimensions of the mathematical model of the system and decouple the differential equations[50]. These transformations are:

- αβ transformation (Clarke transformation), and
- dq transformation (Park transformation)

Both of the above listed transformation is described in Appendix (E). With the synchronous framework control method (dq0), the control system must know the amplitude and phase of the grid voltage; this data is essential for the current and voltage control loops in order to stabilize the system and force it to work at its optimal point where the system generates and delivers maximum power[51]. To obtain this important information, a synchronization method must be used to synchronize the inverter power and the utility grid. There are several methods of extracting phase information from a given signal. Some of these approaches are:

- Zero-Crossing Method
- αβ and dq Filtering Algorithm
- Phase-Locked-Loop (PLL)

2.5.1 Zero-Crossing Method

In the zero-crossing method, the phase angle of the grid is set in line with the time distinction between two zero-crossing points of the grid voltage. Since the zero-crossing points are solely updated at each half cycle of the utility voltage frequency, the dynamic performance of this method is low. Other than zero-crossing delay, extra filtering needs to be applied to detect nominal frequency, which introduces an extra delay to the system. Filtering delay is improved by applying special high order predictive filters without delay, but these filters add a lot of complexness to the system.

2.5.2 αβ and dq Filtering Algorithm

The grid phase angle can be obtained by filtering the grid voltage in stationary (αβ) or synchronous (dq) frames. Figure 2.7 shows the schematic of these methods of synchronization [52]. As it is seen, the phase of the grid is extracted using filtering in either stationary or synchronous frame. In stationary frame, the arc-tangent function is directly applied to the frame however in synchronous frame, the dq signal should be remodeled back to the stationary frame before applying the arc-tangent function. The disadvantage of this methodology is that the use of filtering, which introduces a delay to the system, and thus the calculated phase angle will lag the real phase angle.

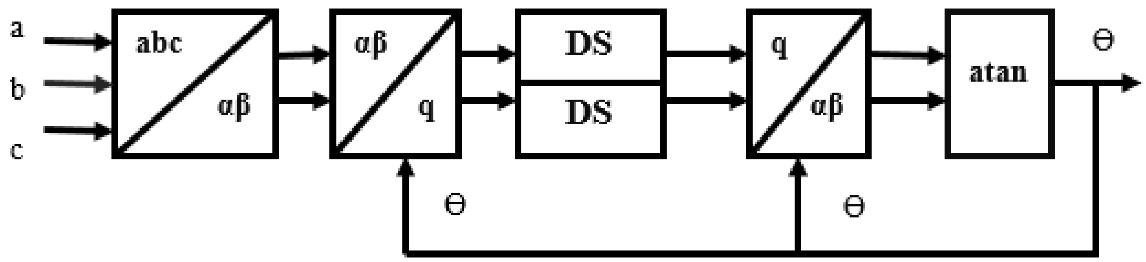

Figure 2.7 αβ and dq filtering algorithm[53]

2.5.3 Phase-Locked-Loop (PLL)

The third synchronization method is the phase-locked loop synchronization method[51]. A basic PLL circuit often consists of three essential components: a phase detector, a loop filter, and a Voltage Controlled Oscillator (VCO). Using a negative feedback loop, PLL minimizes the phase and frequency errors between the input and output signals. The schematic of PLL is depicted in figure 2.9 below. This algorithm has better harmonic and disturbance rejection compared to zero-crossing and αβ-dq transformation, but during grid unbalance conditions, this algorithm requires further improvements.

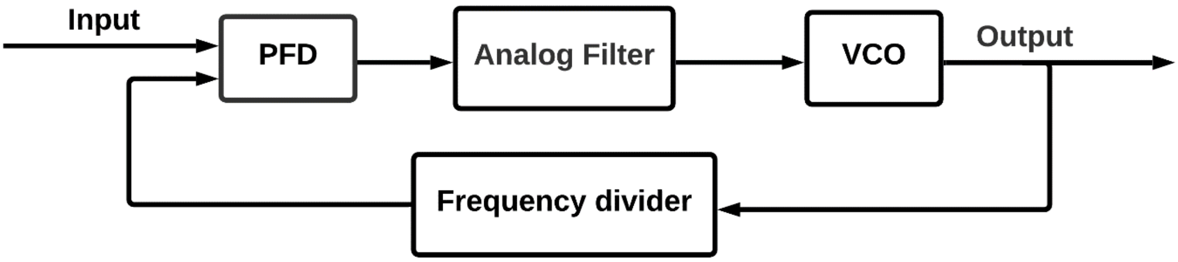

Figure 2.8 PLL components block[54]

Due to its benefits and its extensive realistic use, PLL is used in the simulation of the control system of this work.

Conditions for Grid interface

There are some conditions that must be fulfilled to integrate micro grid to the utility beside grid Codes[52]. If proper synchronization is not done then the micro grid power cannot couple to the grid. Those conditions must be fulfilled to integrate microgrid with utility grids are:

- ❖ Phase sequence must be the same
- ❖ Frequency should be match
- ❖ Voltage level should be the same
- ❖ Fulfill the grid codes
- ❖ Requires feed-in tariff policies

2.6 Grid codes and Feed-in tariff Policy for grid integration

Microgrids can trade electricity with grids. The surplus produced power of the PV arrays after charging batteries is traded to the grid. If the overall produced power of the microgrid can't fulfill the demand, power might be purchased from the grid. [55]. The growing grid-tied RESs would possibly threaten the protection and balance of the power systems. Therefore, the grid code is evolved for the PV power stations to ensure the security of PV integrated power systems. Photovoltaic power integration with national grid in a different grid code is investigated and summarized by table 2.3.

The Institute of Electrical and Electronics Engineers (IEEE) has written a standard that deals with all grid-tied decentralized generation systems, including renewable energy systems. IEEE 1547-2003 provides technical requirements and tests for grid-tied operation[29].

Table 2.3 Summary of grid codes of different countries

Grid Codes	Requirements in a grid code
National Standard and standard grid codes of china enterprise grid codes (China)	Be ready to control the active power in line with the commands issued by the dispatch center (if PCC rated voltage >=10KV)
National Grid (UK)	capable of manipulating the Active power for frequency regulation (Installed capacity >=50MW
Germany	Can perform with reduced output power (if the nominal voltage of the PCC is > = 10KV)
ENTSO-E(Europe)	Be ready to manage the active power for frequency control (Installed capacity>=0.8KW or determined by local TSO)
Ethiopian Electricity agency draft interface code (Drafted)(Ethiopia)	System operating is responsible for maintaining frequency with ±0.5HZ within ±10 seconds

Grid connected micro grid have another opportunity which is selling excess power to the grid. But, to sell excess energy to the main grid the operating micro grid requires feed-in tariff policies.

Feed-in Tariffs were initial introduced in Federal Republic of Germany within the 1990s and next applied to another European countries to promote micro scale wind and solar generation [56]. As of 2011, feed-in tariff policies are enacted in over fifty countries. underneath this kind of tariff, as it may also be the case of the other schemes explained herein, the money paid to the producer doesn't come from the government, however from the energy market i.e., the utilities. This incentive policy provides three main monetary benefits: (a) a payment for all the electricity produced, even though it's utilized by the producer itself, (b) an extra bonus payment for the electricity exported into the grid, (c) a discount on the producer's customary electricity bill, for using the energy made by itself. If a little power producer injects the electricity produced to identical utility from that it receives energy, the utility may even prefer to net off the energy quantity and simply pay a check or a bill for the energy difference which will result. comprehensive details and characteristics of this kind of tariff will be found in[57].

The micro grid tariff should establish a feed-in tariff to facilitate the exchange of electricity between micro grid operators and utilities. A feed-in tariff is a long-term contract that establishes a wholesale rate for owners of small renewable energy projects like micro grids to sell power to the local utility. Ethiopia has no national Feed-in tariff policies but in the late 2019 Ethiopian energy authority had drafted tariff guidelines and methodology for off-grid system suggests for grid connected micro grid its recommended that the tariff for sales to the main grid operators should be determined in accordance with a revenue[56]. It is a standard that needs from the renewable energy producer a minimum fixed proportion of generation sold-out or capacity installed. Several utilities are needed to make sure that the target is met. So far, some countries have already imposed a quota policy among those are USA, Australia, Italy, Japan, Poland, Romania, Sweden, UK, and Chile.

2.7 Pulse width modulation

A typical three phase VSI, an inverter is consist of insulated gate bipolar transistors (IGBTs) provides variable frequency output depending upon the applied reference voltage and switching techniques. There are many techniques that perform switching's. From available pulse width modulation techniques Space vector and sinusoidal PWM are the most used types. In this research only sinusoidal pulse width modulation is reviewed.

2.7.1 Sinusoidal PWM

Sinusoidal PWM is generally used to generate the switching signal for the inverter. A triangular carrier signal Vtri with high frequency fswt is compared with a sinusoidal modulating signal Vcontrol with desired frequency f1 as shown in Figure 2.9.

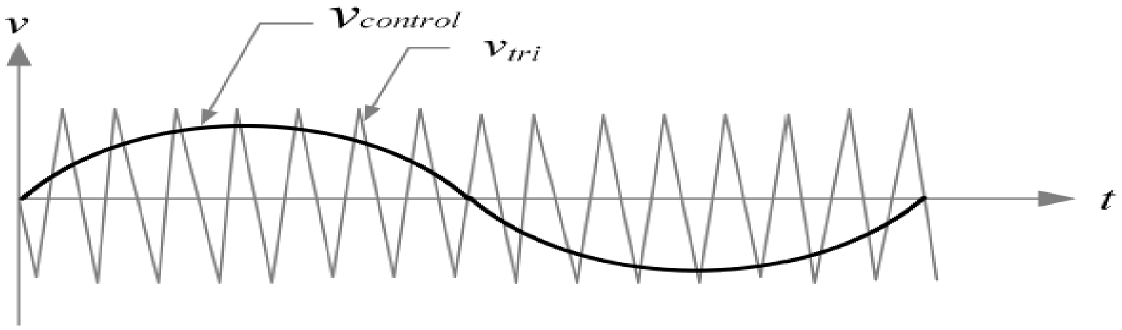

Figure 2.9 Sinewave modulation signal with its fundamental component[58]

The comparison between these two signals determines the switching signal. When sinusoidal signal has a higher magnitude than triangular wave the switching signal is high, otherwise it is low. The frequency of sinusoidal modulating signal determines the frequency of the fundamental component of the inverter output voltage and frequency of the triangular carrier wave determines the switching frequency of the switching signal.

The sinusoidal modulating signal is used to modulate the switch duty ratio. The ratio of the magnitude of sinusoidal modulating voltage (Vcontrol) to the magnitude of the carrier voltage (Vtri) is defined as amplitude modulation ratio, given as:-

$$ma = \frac{|V_{control}|}{|V_{tri}|} \qquad (2.3)$$

The magnitude of the Vtri is generally kept constant, so it can be said that amplitude modulation ratio can be controlled by controlling the magnitude of the sinusoidal modulating signal. In same way, the frequency modulation ratio mf is defined as:

$$mf = \frac{|f_{swt}|}{|f_1|} \qquad (2.4)$$

Where fswt is a switching frequency, which establishes the frequency with which inverter switches are switched and f1 is a desired fundamental frequency. A three phase pulse width modulated inverter consists of three legs in each phase and each leg includes two power switches as shown in Figure 2.10. Each power switch is transistor or IGBT with antiparallel diode. The switching signal is generated by comparing the triangular career voltage with the three sinusoidal modulating voltages that are $120°$ out of phase, as shown in figure 2.11.

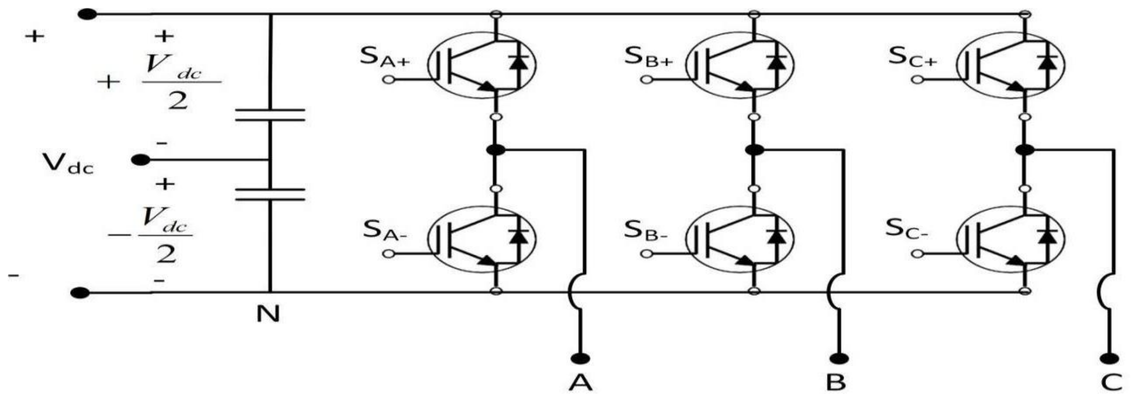

Figure 2.10 Three phase pulse width modulated inverter[59]

Thus, the balanced three phase voltages is produced in which each phase is displaced from one another by 120°. The output voltage of each leg of three phase inverter depends on the amplitude modulation ratio ma and DC voltage Vdc. The peak value of the fundamental-frequency component of the output voltage for one of the inverter leg with respect to neutral is given by:

$$V_{AN} = m_a\left(\frac{V_{dc}}{2}\right) \tag{2.5}$$

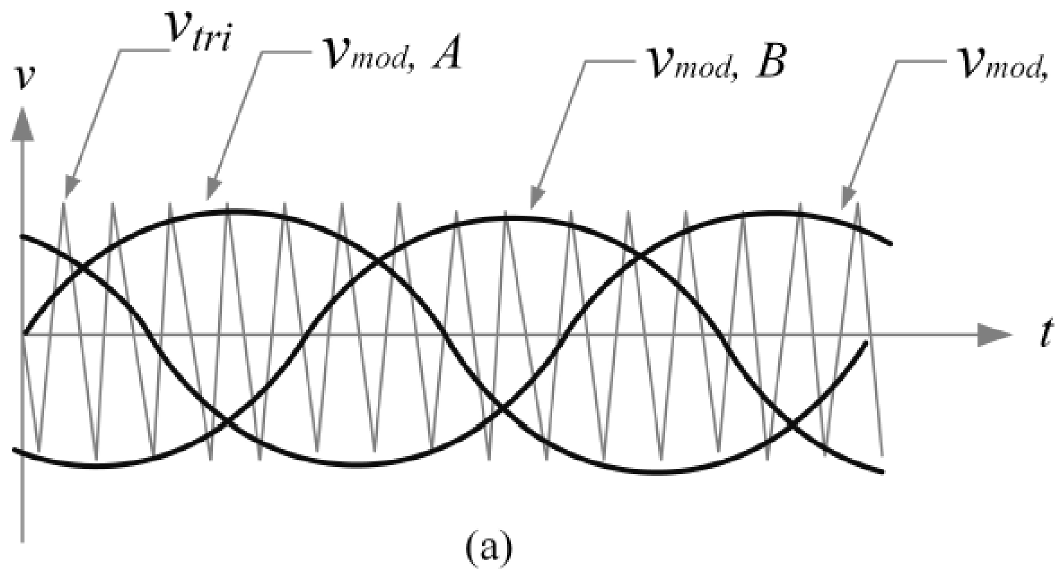

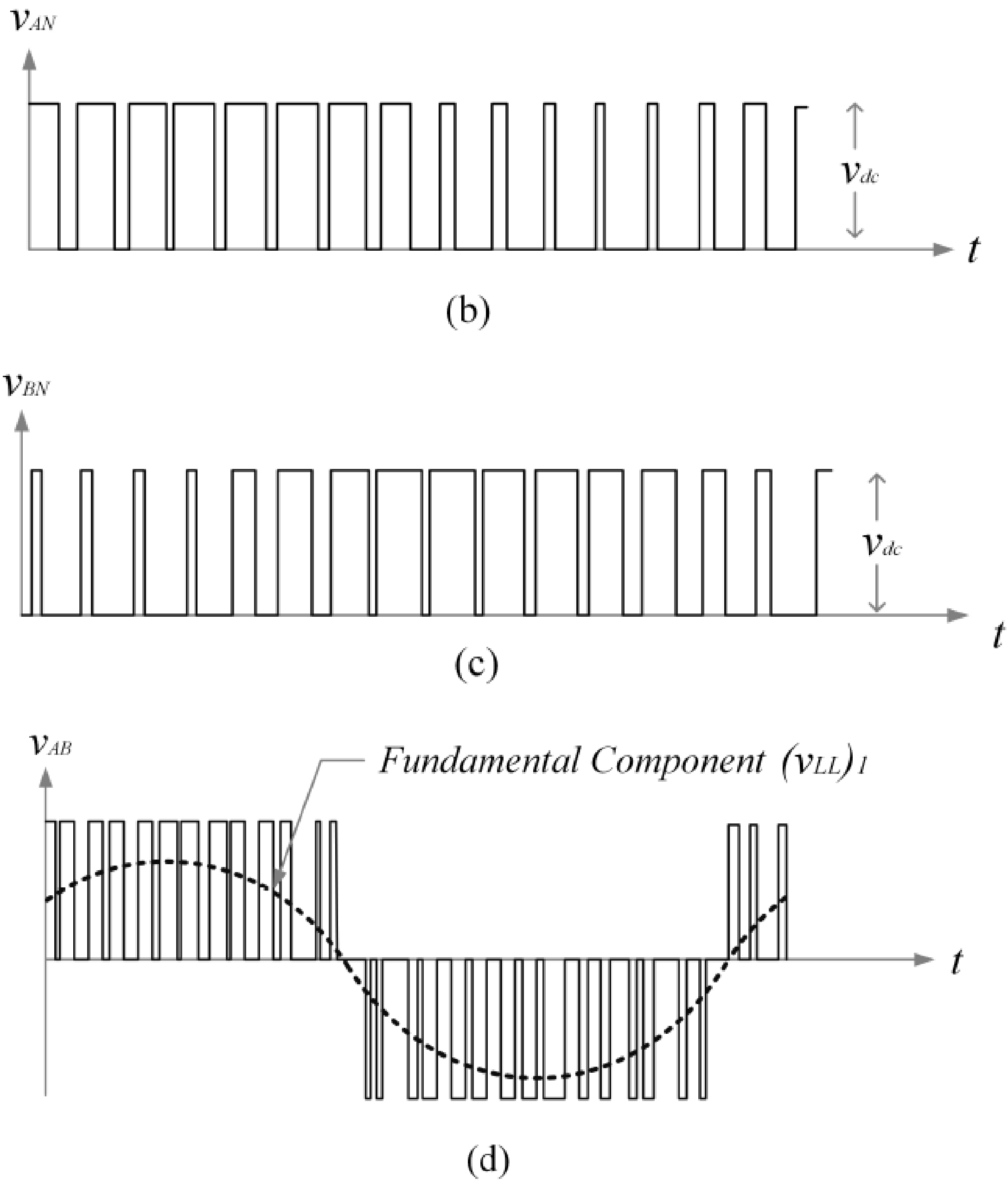

Figure 2.11 a,b,c,d three phase inverter transform waveforms[60].

From equation 2.5, it can be said that the output voltage of the three phase inverter can be controlled by controlling amplitude modulation ratio. The output phase voltages VAN and VBN measured with respect to neutral point N is shown in Figure 2.11 b,c. The line to line voltage can be obtained by subtracting VBN from VAN. The line to line voltage VAB with its fundamental component is shown in Figure 2.11 d.

2.8 Related Works

Several research papers and literatures presented on grid connected Microgrid using different methodology and control techniques. The closely related works to the proposed research work with their corresponding methodology merits and demerits are discussed. Literatures are analyzed and research gaps are identified.

Author in [1] deals with MPPT in a grid-connected photovoltaic system using MPC (Predictive Control Model) with various prediction steps taking into account two-stage voltage inverter and three-stage voltage inverter topologies. To eliminate the current sensor required by some well-known techniques such as the Perturb and Observe (PandO) technique. In addition, the proposed control method leads to a faster response and less power ripple in a steady state scheme under rapidly changing atmospheric conditions for both one and two steps. However, this controller has a model-based controller and is therefore very sensitive to parameter deviations, uncertainties, inaccuracies and delays. The selected controller requires an additional controller, which is another disadvantage of the selected controller in this work. The limitation of the paper is: it does not take into account the island operation and the dynamic operation of the photovoltaic system. Even if it does not use network integration techniques. Grid codes are not required in this document.

Author in [61] addresses a solar photovoltaic system with maximum power point tracking (MPPT) integrated with battery storage in an exceedingly grid-connected system with the assistance of an improved three-level Neutral Point Clamped (NPC) electrical converter. The equalization of voltages of capacitors within the NPC inverter of three-phase three-level is completed by higher studying of the vector space consisting of capacitor voltages switch patterns effects in space vector pulse width modulation(SVPWM) applications. The system uses a typical PI controller for the inner current loop and external voltage loop control. The system modeling in the dq-frame decides the Kp and Ki values. The matter of conventional PI controller is that saturation is not considered whereas there is a high point modification within the model. The control of a solar photovoltaic system with an electric battery energy storage system in sending power into ac grid is achieved with success by the planned topology. The limitations of this paper is that: there are no grid codes, islanding and transient operative scenario are not dictated in this paper.

Author in [58], proposed layout of the energy and manage subsystems of a 3-phase photovoltaic grid-linked system in an clean and complete way, as an integrative technique. In this paper, a zero crossing detector is employed. The d–q control technique is a totally reasonably-priced linear controller and employs PI regulators which results in a non-zero steady state error when dc variables are used, being now no longer capable of compensating the dead-time impact of the inverter. Its foremost drawbacks of the controllers used on this paper are its decrease dynamic response and the non-zero steady state error while ac variables are used. Limitation on this paper is: there are no grid codes and saturation of the system is not considered.

Author in [11] presents a parametric study conducted to improve the performance of the photovoltaic system connected to the grid with lead-acid battery model (BESS) battery energy storage systems. MPPT and PLL are applied during this paper. Normally used control for the VSC-based electrical converter is that the decoupled PQ control and SVPWM technique in this paper. The effectiveness of the controller improvement strategy has been evaluated by comparing the DC bus voltage fluctuations at completely different simulation situations subjected to the disturbances like abrupt changes in solar irradiation and faults. The aim of this work is to minimize the voltage fluctuations under difficult operating conditions. The limitation of this research work is that it is applicable in the only grid tied mode of operation and the grid connection does not apply grid codes.

Author in [62]proposes battery energy storage systems (BESS) providing frequency compensation techniques similar to virtual inertia response (VIR) are often an answer to tackle the frequency volatility. However, the electrical converter connecting the BESS could suffer performance and stability problems because of an occasional short circuit ratio (SCR). The inverter phase-locked loop (PLL) and also the grid impedance negatively interact. Each the robust-PI and the traditionally tuned PI controllers are used and compared. Finally, the robust-PI is shown to be superior to the conventional PI because it was capable of maintaining the benchmarked transient performance throughout the SCR variation. Limitation of this paper is that it does not acquired grid codes and the operation of the microgrid under study is analyzed only grid connected operation.

The author[63] addresses the problem of designing a robust and fully distributed secondary control scheme for voltage and frequency restoration of microgrids on islands along with the actual exchange of power. The scheme takes into account the effects of model uncertainty, parameter variation and unmodeled dynamics and therefore offers a certain degree of robustness against all these factors. The proposed secondary control framework facilitates the exchange of active and reactive power between the DG units and counteracts deviations in the voltage and frequency of the individual connections. This paper limited to islanded operation of microgrid, voltage and frequency control. No battery energy storage system in case of emergency.

The author in [64] proposed power management of the microgrid is achieved through energy storage application. The energy storage capacity varies and increases between voltage limits, current limits, and stability across power limits. These changes occur both on the demand side and where higher energy availability and efficiency are desired, and from the supply side, where the integration of technologies for the decentralized generation and peak reduction must be taken into account. Inverters provide the control and flexibility required for plug and play. The microgrid controls must ensure this; new micro-sources can be added to the system without changing existing equipment, the micro-grid can be quickly and smoothly connected to the grid or disconnected from the grid, reactive and active power can be controlled independently and can meet the dynamic requirements of the grid. This paper is limited to active and reactive power compensation. It does not take into account voltage and frequency regulation.

This author [65] addresses the design and analysis of a controller for multi bus microgrid system. The controller proposed for use with each distributed generation (DG) system in the microgrid contains inner voltage and current loops for regulating the three-phase grid-interfacing inverter, and external power control loops for controlling real and reactive power flow and for facilitating power sharing between the paralleled DG systems when a utility fault occurs and the microgrid islands. The controller also incorporates synchronization algorithms for ensuring smooth and safe reconnection of the micro and utility grids when the fault is cleared.This paper limited to active and reactive power compensation while Microgrid transit from islanding to grid connected mode of operation.Voltage and frequency deviation during transient operation of Microgrid is not discussed.

Author [4] Proposed the voltage-based droop control for islanded low-voltage microgrids with a high share of renewable energy sources. The primary control of the DG units is generally performed by droop-based control algorithms that avoid communication. With voltage based droop control, both dispatch able and less-dispatch able units will contribute in the power sharing and balancing. The priority for power changes is automatically set dependent on the terminal voltages. In this way, the renewables change their output power in more extreme voltage conditions compared to the dispatch able units, hence, only when necessary for the reliability of the network. This facilitates the integration of renewable units and improves the reliability of the network. This paper focusses on modifying the voltage based droop control strategy to enable a smooth transition between the islanded and the grid-connected mode of the microgrid. The islanding does not require additional measures as the control strategy does not need to be altered. For transition from islanded to grid-connected mode, which is a planned event, communication is used to announce the mode transition. This paper limited to voltage droop control and the power back up in emergency case is not considered.

This paper [15]presents the power management scheme for a power electronics based low voltage microgrid in islanding operation. The proposed real and reactive power control is based effectively decouple the real and reactive power flows and improve on the virtual frequency and voltage frame, which can the system transient and stability performance. Detailed analysis of the virtual frame operation range is presented, and a control strategy to guarantee that the microgrid can be operated within the predetermined voltage and frequency variation limits is also pro- posed. Moreover, a reactive power control with adaptive voltage droop method is proposed, which automatically updates the maximum reactive power limit of a DG unit based on its current rating and actual real power output and features enlarged power output range and further improved system stability. This paper limited to droop control strategy. It does not considered grid integration techniques, no grid codes is applied also.

The author [66] proposed a particle Swarm optimization-based DC-link voltage control method for two stage grid connected PV inverters. A two-stage grid connected Photovoltaic Generator (PVG) is used to test the performance of artificial intelligence based controller. The system test consists of PVG, a boost converter, a DC-link, an inverter, a LCL filter and the external grid. The objectives of the system controllers are three-fold. The first objective is to regulate PVG output voltage for Maximum Power Point Tracking (MPPT). The second objective is to keep the DC-link voltage of inverter constant. The third objective is to maximize the power factor of the inverter i.e. close to unity. To solve the first problem, a conventional MPPT technique known as Perturb & Observe (P&O) method is used which generates the best voltage reference for PVG. To track the reference voltage, back stepping control technique is used to regulate PV panel output voltage. The regulation of DC-link voltage of the inverter is realized with PI controllers, the parameters of which are optimized by Particle Swarm Optimization method. The third objective, power factor regulation, is also tackled using back- stepping control. Conventional PI control is compared to the proposed artificial intelligence-based controller, and the proposed technique for optimizing parameters of PI has reduced the ripple factor of DC-link voltage from 6.0193% to 3.3218% compared to a simple PI control with manually chosen parameters. This paper presents a controller which reduces transient peak injection to the grid consequently improving the transient dynamics of the complete system. The limitation of this paper is that it does not considered active power variation which causes frequency deviation in microgrid operation. Operation of microcrogrid is not considered.

After analyzing, existing related works it is observed that researchers proposed different techniques for the problem. Even if there is still a research gap to be covered by this study. Although, the researcher's proposed different approaches for the microgrid transient operation with integrating non dispatchable energy resources, integrating battery energy storage system with fuzzy logic based PI anti windup controller to control and manage frequent integration of distributed generation in utility grid is an open problem.

CHAPTER THREE

METHODOLOGY

3.1 Introduction

This chapter deals with data collection and analysis, mathematical modeling of microgrid components and design and control of microgrid is performed. Finally, the system is simulated by using MATLAB/2019b software both in Simulink and in script.

3.2 Tools

In this research work, software such as MATLAB/2019b, Microsoft office 2019, and Math type 6.0 equation are used. MATLAB is the computing software which consists of technical toolboxes and Simulink. Microsoft office is used for editing the thesis documentation. Math Type 6.0 is used for writing mathematical formulas and equations in Microsoft offices word and power point presentation tools.

3.3 Methods

The method used in this thesis is to accomplish the required objectives as shown in figure 3.1. The closely related papers and literatures are reviewed related to grid connected microgrid dynamic operation. Then the necessary data used throughout this research are collected and analyzed. Some of the specifications value of microgrid components like cafeteria load demand has taken from ASTU student cafeteria and some other data is taken from others secondary source like NASA. Then the collected data is analyzed for the purpose of understanding and developing the system modeling /code. The proposed microgrid system should meet the load demand of ASTU student cafeteria. Microgrid modelling with grid-tied and droop control is developed. The main components of microgrid considered in this thesis are solar PV system, battery energy storage system, and other power electronic converter like inverter, boost converter and connected to the main grid and loads at the point of common coupling. Microgrid transient operation like switching from grid connected mode of operation mode to islanded mode of operation while the voltage and frequency at the point of common coupling kept in the minimum variation as it is dictated in the drafted grid codes of Ethiopian energy authority is used throughout this thesis. Solar PV and converter are components that vary in size. Then the system is simulated by using MATLAB/Simulink.

In general, the method followed throughout the research study can be summarized as the following block diagram.

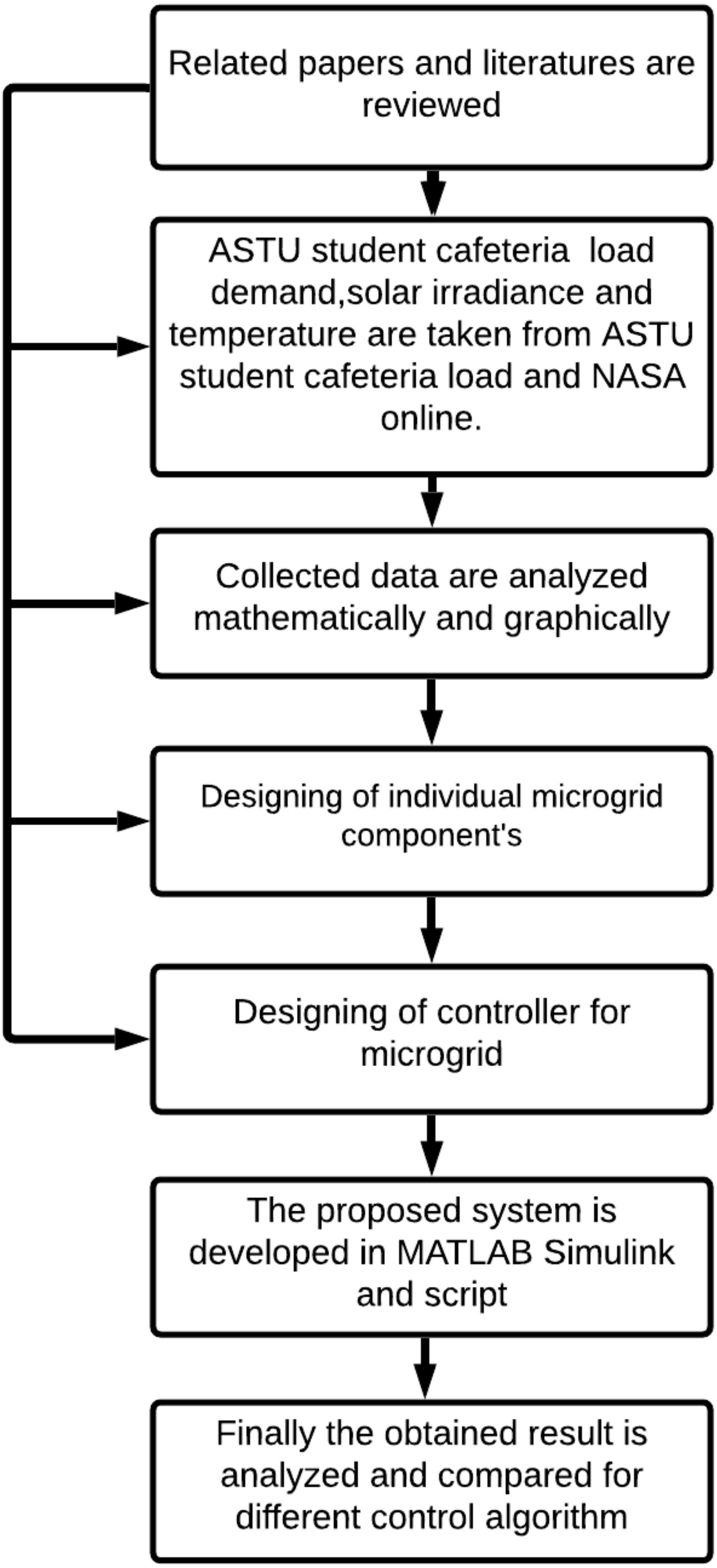

Figure 3.1 Block diagram of the research methodology

3.4 Proposed block diagram of microgrid

Figure 3.2 shows a block diagram of the proposed microgrid system, which is connected to the grid and which also operates autonomously.

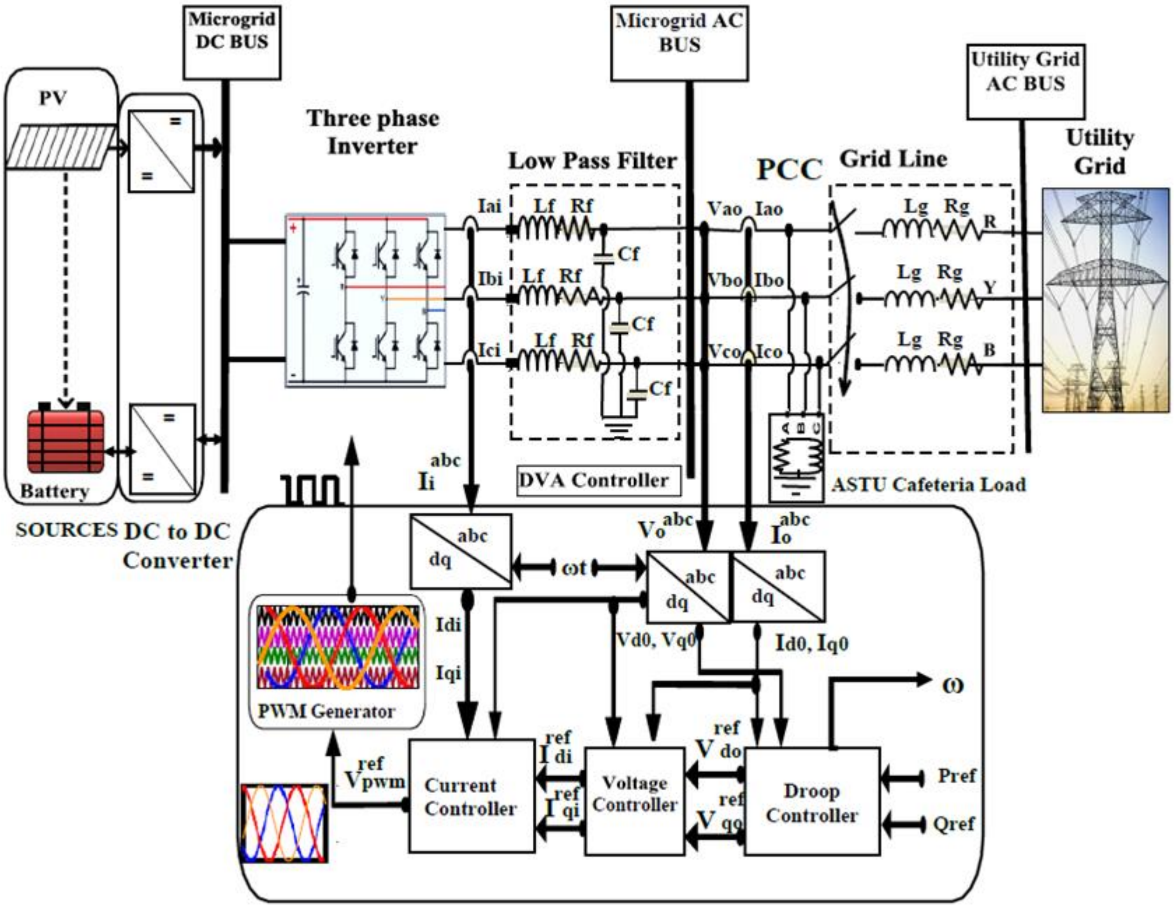

Figure 3.2 Proposed schematic diagram of the microgrid plant

In a grid connected mode the utility grid supports both voltage and frequency at the point of common coupling (PCC).But, in islanded mode of operation the microgrid controls voltage and frequency at the point of common coupling. If excess power is generated by solar array while the microgrid is operating autonomously power curtailment technique is used to reduce excess power generated by solar PV power since the utility is switched off to deliver excess power generated.

Three phase boost converter is a DC-to-DC converter that is controlled by MPPT (maximum power point tracking) that steps ups voltage from its input solar array and delivers stepped up voltage to three phase inverter. The three-phase instantaneous voltage and current taken from point of common coupling side filter is transformed into rotating reference frame dq0 by using Park-Clarke transform to make computation much easier. Furthermore, the proposed fuzzy logic control with anti-windup PI (Proportional- Integral) controller with conditional integration and feedforward implemented on voltage and current controller cascaded block respectively to generate voltage reference that converted for pulse width modulation which generates proper gate signal for switching inverter which converts DC to AC. In this study is three phase three level NPC (neutral point clamped) inverter converter is used for solar PV system regulation.

3.5 Energy consumption and power demand of ASTU student cafeteria

ASTU Student cafeteria is located at 8.5632402°N (latitude) and 39.2908869°E (longitude) in Adama, Oromia and Ethiopia which is taken from NASA. The collected data from NASA for ASTU student cafeteria location is in the Appendix (A).The table 3.1 shows the ASTU student cafeteria, which calculates the average daily solar radiation and temperature.

Table 3.1 Monthly average solar irradiation and temperature

Month	Monthly solar Irradiance (KWh/m2/day)	Monthly solar temperature (˚C)
January	7.6	26
February	7.7	27.5
March	6.75	28
April	6	27
May	6.4	27.5
June	5.6	27.25
July	4.5	24.75
August	4.5	24
September	5.4	24.5
October	6.8	25
November	7.7	25.2
December	8	25

The ASTU student cafeteria receive enough sun radiation and temperature and are suitable for generating solar power generation. As it is describing in the figure 3.4 the maximum available temperature at student cafeteria taken from NASA gives 28°C in January and minimum temperature of 24°C in August.

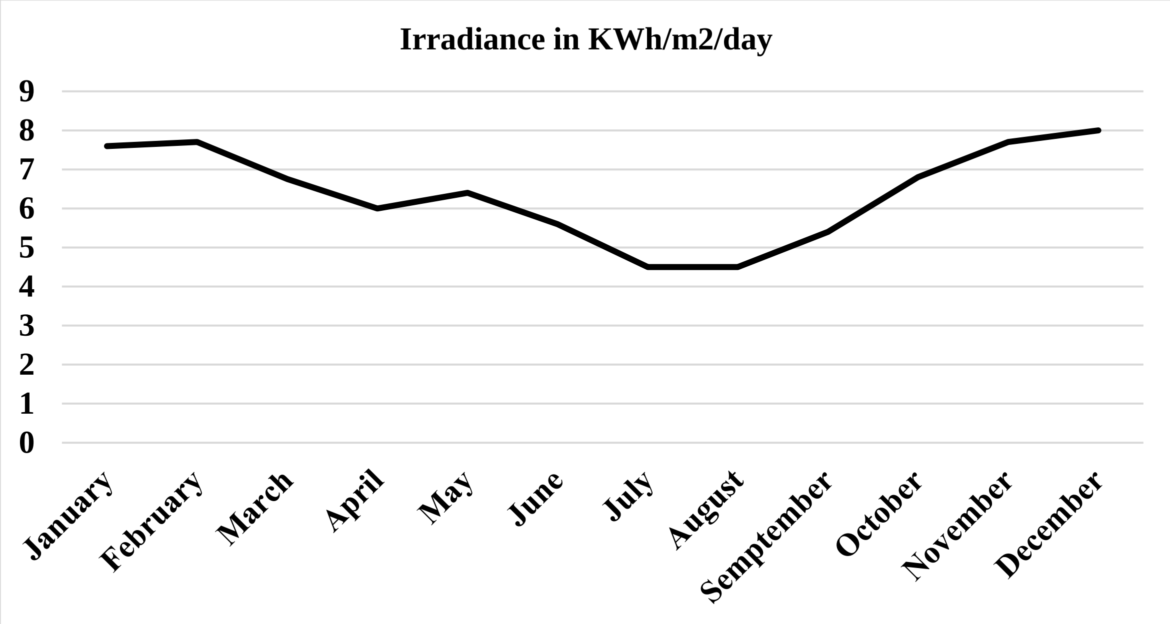

Figure 3.3 Monthly radiation curve at ASTU student cafeteria taken from NASA

The table 3.1 gives the minimum irradiation of 4.5 kWh / m2 / day in July and the maximum average irradiation of 8 kWh / m2 / day in December. So, both available solar radiation and temperature at the area is suitable for solar power generation which support ASTU student cafeteria load. The first step in determining the size of the microgrid system is to determine the loads it will support. Therefore, the load estimation was carried out based on the information from the student cafeteria of Adama Science and Technology University (ASTU).The microgrid which is the subject of this study are intended to be that of Photovoltaics (PV), and battery storage system which have been connected to grid with the help of inverter at the point of common coupling[2].

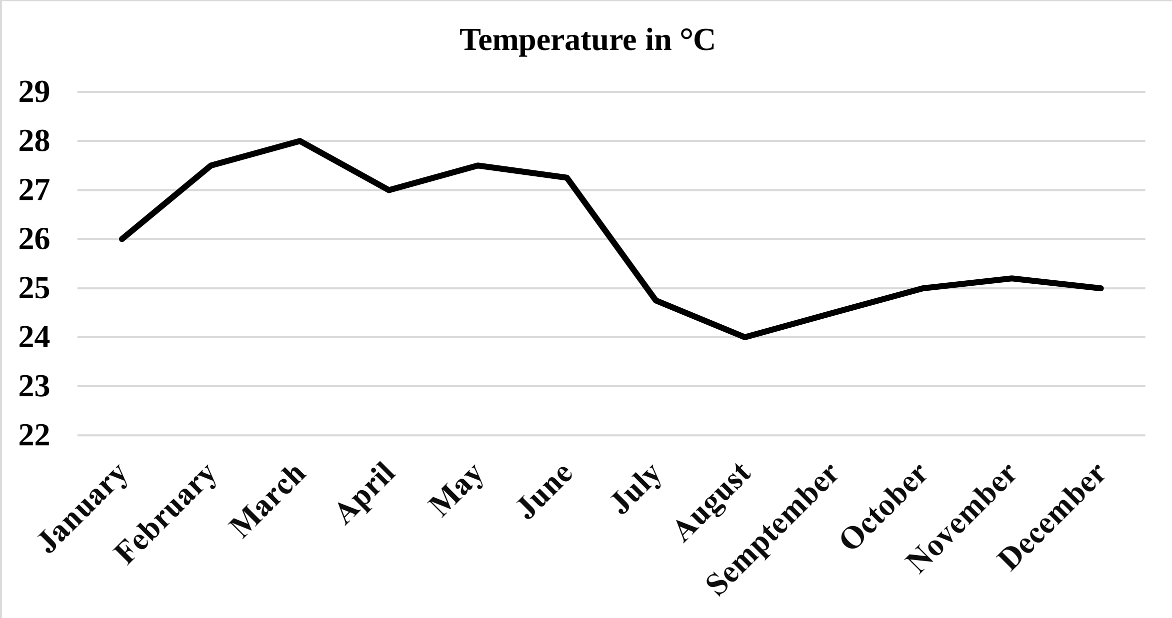

Figure 3.4 Monthly temperature at ASTU student cafeteria

The ASTU student cafeteria has contained general loads, sensitive loads, and other infrastructures.

General loads: general loads are the main parts of cafeteria appliances such as boilers, peeling machine, stove, meat mincer and exhaust fan.

Sensitive loads: They are an electronic load that is commonly used for reading students meal card barcode like computers and lighting appliances.

Table 3.2 DC load assessment of ASTU student cafeteria

Appliances	Quantity	Power (KW)	Daily usage		Maximum power demand(KW)
			Hrs./day (h)	Energy (KWh/day)	
Light	600	0.036	8	172.8	21.6
Computer	4	0.045	5	0.9	0.18
Daily D.C load energy demand (KWh/day)			-	137.7	-
Maximum D.C load power demand(KW)			-	-	21.78

Table 3.3 AC load assessment of ASTU student cafeteria

Appliances	Quantity	Power (KW)	Daily usage		Power factor	Maximum demand (KVA)	Surge factor	Surge demand (KVA)
			Hr/day	KWh				
Boiler	8	36	6	1728	0.8	360	2	720
Frying pan	7	12	4	336	0.8	105	2	210
Electric Peeling machine (5kg/min)	5	11	3	165	0.8	68.75	2	137.5
Electric peeling machine (3kg/min)	3	6.6	3	59.4	0.8	24.75	2	49.5
Electric Stove	2	24	6	288	0.8	60	2	120
Exhaust fan	1	2.2	12	26.4	0.8	2.75	1	2.75
Meat mincer	3	5.5	4	66	0.8	20.625	3	61.875
Daily maximum AC load power demand(KVA)					-	641.875	-	-
Daily maximum Surge demand(KVA)					-	-	-	1301.625

Different kinds of loads are taken from the selected area in the ASTU student cafeteria such as boilers, electric peeling machine, electric stove, and electric meat mincer and exhaust fan.

Surge factor: The overload factor refers to the instantaneous overload capacity of an uninterruptible power supply and is a measure of the ability of the uninterruptible power supply to initiate loads that temporarily require additional power at start-up[67].

Based on the table 3.2 and table 3.3, the total energy consumption of the electrical service for the ASTU student cafeteria has been calculated as:

Minimum load power (KW) =min AC load power (KW) +max DC load power (3.1)

Minimum load power (KW) = (641.875*0.8) KW+21.78KW=535.28KW

Maximum load power = max AC power (KW) +max DC load power (3.2)

Maximum load power= (1301.625*0.8) +21.78KW=1063.08KW

Total energy demand = AC load consumption +DC load consumption (3.3)

$$Wh_{dc} + Wh_{ac} = 173.7KWh + 2668.8KWh$$

$$=2.8425MWh$$

3.6 Mathematical modelling of the proposed microgrid

The first step to start sizing the photovoltaic system connected to the grid is to determine the load consumption to be supplied. Therefore, load estimates were made based on the information taken from the ASTU student cafeteria, the most important points to be assessed first were[68]:.

- Estimation of the building load,
- Sizing and specification of the photovoltaic system
- Sizing of the battery,
- Sizing of the inverter,
- Sizing of the battery charge controller
- Sizing of the system cable

3.6.1 Sizing of the PV array

Calculate total Watt-hours per day for each appliance used: add the Watt-hours required for all appliances to get total Watt-hours per day[34].

Calculate the total number of watts per day that the PV modules will need: multiply the total number of watts per day from the devices by 1.2 to get the total number of watts per day that the modules must deliver, where 1.2 is the correct factor for the energy loss in the system.

Calculate the total peak power in watts required for the PV modules: divide the total watt hours per day required by the PV modules by the average solar irradiation to get the total peak power. Finally, the number of modules in parallel and in series can be determined according to the following formula[69].

$$\text{Total DC Current} = \frac{\text{Peak power}}{\text{System DC voltage}} \tag{3.4}$$

$$\text{Number of series modules}(N_s) = \frac{\text{System DC voltage}}{\text{module rated voltage}} \tag{3.5}$$

$$\text{Number of parallel modules}(N_p) = \frac{\text{Whole module current}}{\text{Rated current of one module}} \tag{3.6}$$

$$\text{The total number of modules: } N_t = N_p \times N_s \tag{3.7}$$

In this thesis work the system DC voltage is assumed to be 600V at the ASTU student cafeteria bus bar.

PV array of AC sizing

By following the above formula, we can size the P_v array as:

Step 1: Multiply AC Watt-hours per day by 1.2 for correct factor or energy lost in the system.

Since, AC load energy consumption from table 3.3 is 2.6688MWh/day

$$= 2.6688\text{MWh/day} \times 1.2 = 3.20256\text{MWh/day}$$

Step 2: Divide AC load energy in consumption in step one by inverter DC input voltage.

$$I_{total} = \frac{3.20256\text{ MWh/day}}{600\text{V}} = 5337.6\text{Ah}$$

Step 3: Multiply total amp-hours per day by 1.2 to compensate for loss from battery charge/discharge.

$$=1.2\times5685A=6405.12Ah$$

Step 4: Divide Amp-hours in step-3 by average sun hours per day around ASTU cafeteria was 5(five) hours.

$$\frac{6405.12Ah}{5h} = 1281.024A$$

Step 5: To determine the total number of solar modules in parallel required- divide step 4 by peak amps of solar modules from PV specifications.

$$N_P = \frac{1281.024}{8.18A} = 156.6 \approx 157$$

Step 6: To get the number of modules in series divides the nominal system voltage by individual array voltage.

$$N_S = \frac{600}{43.4} = 13.825 \approx 14$$

PV array of DC sizing

Load demand estimation of a typical DC- sizing of student cafeteria (Ed) =173.7KWh/day.

Watt-hour from PV system (combined efficiencies = 0.6)

$$\text{Energy of PV}(E_{PV}) = \frac{\text{Energy demand}}{0.6} = \frac{173.7\text{KWh/day}}{0.6} = 289.5\text{KWh/day}$$

By taking the lowest average daily insolation taking minimum generation (Gmin) = 4500Wh/m^2/d.

Step1: PV array sizing:

$$P_{PV} = \frac{E_{pv}}{G_{min}} \times 1000W/m^2 \tag{3.8}$$

Where: P_{pv} is the total power of PV array in watts

E_{pv} is the total energy required from PV array.

G_{min} is the minimum solar radiation of a month that occurred in a year.

Therefore, using equation (3.8)

$$P_{pv} = \frac{289.5\times10^{3}\text{Wh/day}}{4500\text{Wh/m}^{2}\text{/day}}\times1000\text{W/m}^{2} = 64.3334\text{KW} = 64.34\text{KW}$$

Step 2: Load current.

$$I_{PV} = \frac{64.34\text{KW}}{600\text{V}} = 107.2\text{A}$$

The number of PV modules:

Step 3: Number of PV module in Parallel (N_p) = $\frac{\text{Whole module current}}{\text{Rated current of one module}}$

$$\frac{107.2A}{8.18A} = 13.105 \approx 13 \text{ mod}ules$$

Step 4: Number of series modules (N_s) = $\frac{\text{System DC voltage}}{\text{module rated voltage}} = \frac{600}{43.4} = 14$ modules

Step 5: Total number of modules = $N_p \times N_S = 23\times19 = 437$ modules

Step 6: To get total modules number of series modules add number of series modules for AC sizing and number of series modules of DC sizing.

$$N_T = N_{acS} + N_{dcS}$$

$$N_T = 157+13 = 170 \text{ modules}$$

Step 7: To determine the total number of solar modules required, multiply the number of series modules by the number of parallel modules.

$$N_T = N_{sT}\times N_p = 170\times14 = 2380$$

Step 8: To get Total PV power it is calculated as follow:

$$\text{PV Panel Power(KW)} = \frac{\text{Total energy demand}}{\text{PSH*efficiency}} = \frac{2842.3\text{KW}}{5\text{h*0.8}} = 710.575\text{KW}$$

Total area of solar panels design (A)

Sizing of the area covered by the solar module is very necessary during the design of the PV system so, considering the PV module length and width: L= 1640mm w = 990mm

$$A = L \times W \tag{3.9}$$

$$A_{total} = (1640mm \times 170) \times (990mm \times 14)$$

$$A_{total} = 3864168000\ mm^2 = 3864.168m^2$$

3.6.2 Battery sizing

Total energy consumption (E_c) = 3.411MWh/day

Days of autonomy (N) = 2

State of charge = 0.65

Step 1: Energy consumption of battery: $$(E_b) = \frac{N \times E_c}{0.65} \tag{3.10}$$

$$\frac{\left(3.411 \times 10^6 MWh/day\ x\ 2\right)}{0.65} = 10.495MWh/day$$

Step 2: Battery Ampere hour capacity:

$$C_{bat} = \frac{E_b}{V_{nominal}} = \frac{10.495 \times 10^6 Wh/day}{600V} = 17491.67Ah \approx 17492Ah$$

Select the battery, which are any kind, 12.8V nominal and 200Ah rating from specification of the microgrid understudy.

Step 3: Battery required for parallel: $$B_{parallel} = \frac{C_{bat}}{Ah_{rating\ of\ battery}} \tag{3.11}$$

$$= \frac{17492}{200} = 87.46 \approx 87$$

Step 4: Battery required for Series $$(B_S) = \frac{Vsystem}{V_{bnominal}} = \frac{600V}{12.8V} = 46.875 \approx 47$$

Step 5: The total number of batteries required = $B_{series} \times B_{parallel}$

$$= 87 \times 47 = 4089$$

Therefore, the total batteries required is 4089 batteries

3.6.3 Charge controller sizing

The sizing of charge controllers is depending on the maximum charging current from the photovoltaic (PV) array and the current rating of the charge controller[70].

$$\text{current controller rating} = 1.25 \times I_{sc} \times N_p \tag{3.12}$$

$$\text{Number of charge controller} = \frac{I_{\text{controller rating}}}{\text{Ampere of control from specification}} \tag{3.13}$$

Where: 1.25 is the safety factor for sizing PV system

I_{sc} the short circuit current of the PV module.

N_p is the number of solar modules connected in parallel

Therefore the charge controller current $= 1.25 \times 8.68 \times 125 = 1356.25A$

Select 12V, 60Ah from peak energy PK12V60H rechargeable sealed lead acid (VRLA) battery specification.

$$\text{Number of charge controller} = \frac{\text{total current controller rating}}{\text{controller rating of from specification}} \tag{3.14}$$

$$\frac{1356.25A}{60A} = 22.6 \approx 23$$

Therefore, the number of charge controller is 23.

3.6.4 Inverter Sizing

To sizing the inverter, it must be able to handle the maximum expected power of AC loads. From the load (energy) assessment on the above Tables 3.2 and 3.3, the selected inverter must be capable of supplying 641.875 VA continuously with a surge capability of 1301.625 VA for a short period of time-typically only a few seconds. So, it should be considered 25-30% bigger than the total AC rated power[68]. Therefore, the rated power of the inverter becomes 802.125KW + (0.26 ×802.125) KW = 1.0106775MW. Therefore, the 34 inverter selected is three phase string CSI-30KTL-GI-FL inverter which has 30KW and it can be handle continuous power rating is desirable for the PV system.

3.6.5 Cable Sizing

Cable sizes are particularly necessary for low voltage batteries, solar panels cables, and load cables. It must be properly sizing otherwise if it is far too small, so it can be dangerous and leads to heat up and potentially cause a fire and waste energy. The following steps are followed to determine the cable size[70].

Cables must cause less than 3% voltage loss between PV modules and battery charge regulator calculated as:

Length of cable = 10m

Conductivity of the copper = 58×10^{-6}S/m

Resistivity of the copper = $1.72\times10^{-8}\Omega$

The maximum controller DC current is defined as 125% times the rated short-circuit current I_{sc} from PV specification.

$$I_{max} = 1.25 \times 8.68 \times 125 = 1356.25A$$

Generally, the cross-sectional area (A) of the cable is given by the following equation.

$$A_{cross\_sectional} = \frac{2\times L\times I}{Conductivity \times V_{drop}} \qquad (3.15)$$

Where: ρ is the resistivity of copper wire which is 1.724×10^{-8} Ωm

$V_d =$ is the maximum allowable voltage drop,

L = is the length of the cable and

I = is the maximum current that can be carried by the cable or the conductor.

$$A = \frac{2 \times 10 \times 1356.25}{58x10^{6}\ \frac{s}{m}\ x\ 0.03 \times\ 600} = 26mm^2$$

Therefore $35mm^2$ single-core 90°C thermosetting Insulated Cables, Non-Armored, with or without Sheath is chosen from cable standard for cable is free in the air depending on their current carrying capacity[71].

The maximum charge controller to load current = $\frac{\text{total load power}}{\text{system voltage}} = \frac{418000}{600V} = 696.67A$

To calculate the cable size between loads and charge controller, the given voltage losses are 5%, length 10m, and 90A.

$A = \frac{2 \times 10 \times 697}{58 \times 10^6 \times 0.05 \times 600}$ = 8mm^2 thus the chosen cable is 10mm^2 with single-core 90°C thermosetting insulated cables, non-armored, with or without sheath from cable standard depending on their current carrying capacity[72].

The cross-sectional area of cable, between the charge controller and battery the voltage losses, is 0.02, length 10m and 160A.

$$A = \frac{2 \times L \times I}{58 \times 10^6 \times V_{drop} \times 600} \tag{3.16}$$

$A = \frac{2 \times 10 \times 90}{58 \times 10^6 \times 0.02 \times 600}$ = 3.88mm^2 so, from cable standard chosen 4mm^2 Cable.

To determine the cable size between load and inverter:

Let us assume that the length of the cable for powering the load from the inverter is 10m and the voltage drop is 0.04. So, the maximum current is given by [70].

$$I_{max} = \frac{P_{inverter\,(KVA)}}{\sqrt{3} \times V_{out}} \text{ (in case of 3 phase inverter)} \tag{3.17}$$

$$I_{max} = \frac{P_{inverter(KVA)}}{V_{out}} \text{ (in case of one phase inverter)} \tag{3.18}$$

Using equations 3.15 the maximum current for three phase is calculated as the following.

$$I_{max} = \frac{30000}{\sqrt{3} \times 500} = 34.64A$$

$$I = 1.25 \times I_{max} = 1.25 \times 34.64 = 43.3A.$$

Therefore, the cross-sectional area of the cable between load and inverter calculated as follows.

$$A = \frac{2 \times 15 \times 130}{58 \times 10^6 \times 600 \times 0.04} = 2.2413mm2$$ So, from cable standard chosen cable is $2.5mm^2$ cable.

3.7 Modeling of microgrid components

3.7.1 Photovoltaic model

A PV module contains a kind of many photovoltaic cells connected in series and parallel to provide high output voltage, and to increase the PV current, respectively. The DC of photovoltaic, generated by the PV module depends on temperature, solar irradiance, and load current. The PV model with a single diode circuit, series resistance, and parallel is the most commonly used in PV modeling and to predict energy production in photovoltaic cells[73]. The parameters of the selected PV array (1Soltech 1STH-350 WH) are given in table 3.4 which is important to model the PV array.

Table 3.4 Electrical characteristics for PV array specification.

Description	Value	Description	Value
Peak Power (P_{max})	349.59W	Power Tolerance	±3W
The voltage at P_{max} (V_{mp})	43V	Series fuse rating (A)	15
Current at P_{max} (I_{mp})	8.13A	Parallel resistance of PV model (ohms)	47.9694
Open-circuit voltage (V_{oc})	51.5V	Series resistance of PV model (ohms)	0.22828
Short-circuit current (I_{sc})	9.4A	Cell Efficiency	16.7%
Current Temperature coefficients $\alpha(I_{sc})$	0.03%/°C	Power Temperature coefficients	-0.42%/°C
Voltage temperature coefficients	-0.32%/°C		

$$P_{total\_array} = 170*14*350 = 833KW$$

$$I_{dc} = \frac{P_{mpp}}{V_{dc}} = \frac{833KW}{600} = 1388.33\ A$$

The PV array is simulated with different temperatures and irradiances. With a variety of temperatures and irradiances, the relationship between the current and power of the PV module can be found. By fixing the temperature at 25℃, and with varies of irradiance the I-V and P-V characteristic curves are plotted with G = 400W/m^2, 600W/m^2, 800W/m^{2,} and 1000W/m^2 respectively. The curve is nonlinear and which is depends on the temperature along with the solar irradiation. As the irradiation increases, the current increases more than the voltage, and the maximum power point also increase as shown in figure 3.5.

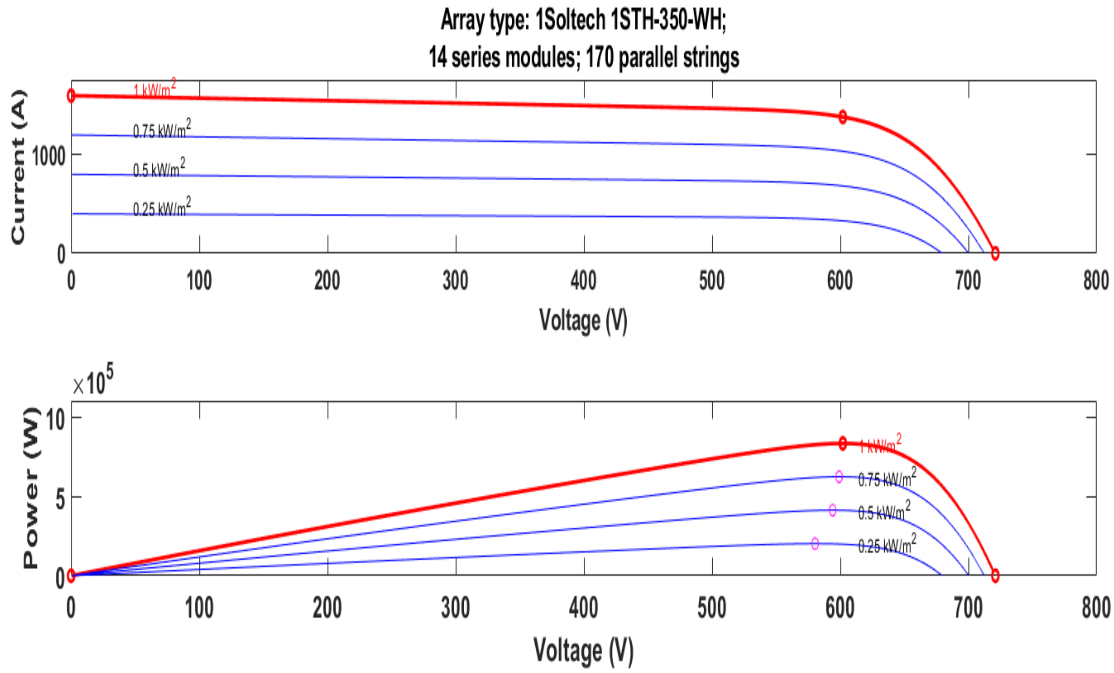

Figure 3.5 V-I and P-V characteristic with variable solar radiation[74]

Based on Figure 3.5, describes that the maximum power output of the Photovoltaic array increases with the increasing irradiance at a fixed temperature. The response of a PV array at different values of solar radiation and fixed temperature (25°C) has a significant effect on the short circuit current however exceedingly small effect on the open-circuit voltage. Therefore, when the solar radiation is increasing, the PV array generates more power.

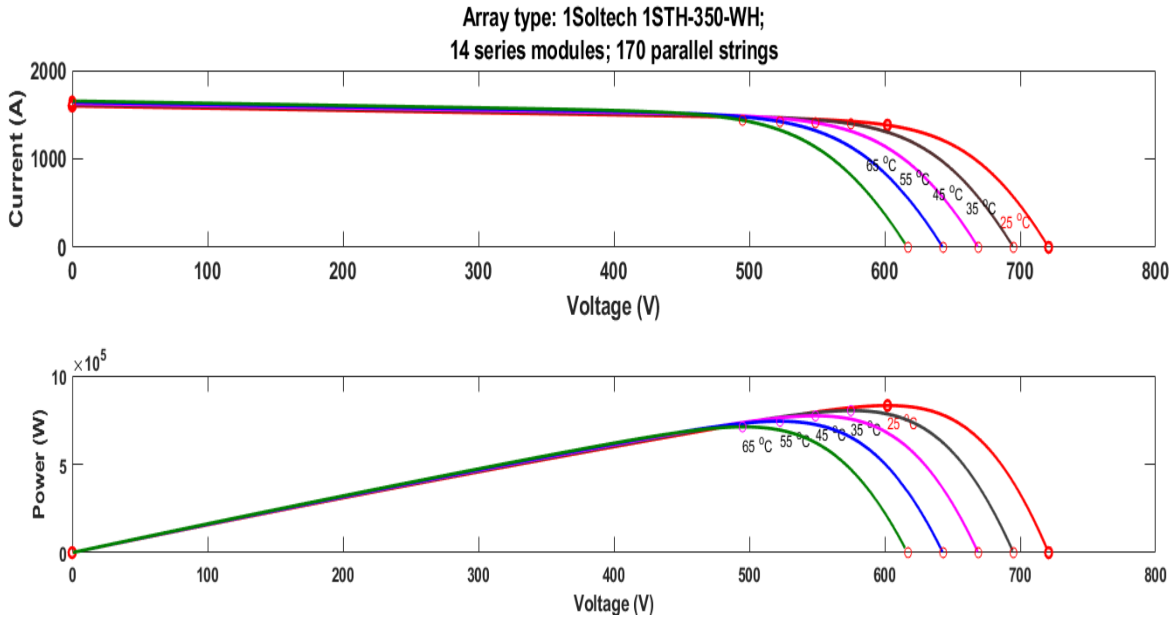

Figure 3.6. I-V and P-V characteristic with variable temperature[75]

The figure 3.6 graph shows that the temperature has a significant effect on the open-circuit voltage and has no effects on both power and current. However, when the temperature is decreased, the PV array generates more power.

3.7.2 DC-DC Boost Converter Model

There are three main types of DC-to-DC converters that are used: Boost Converter, the Buck Converter, and Buck-Boost Converter as mentioned in the literature review[62]. Their mathematical equations are described as follow. The buck converter decreases the input voltage; the boost converter increases the input voltage and they are described in figure 3.7.

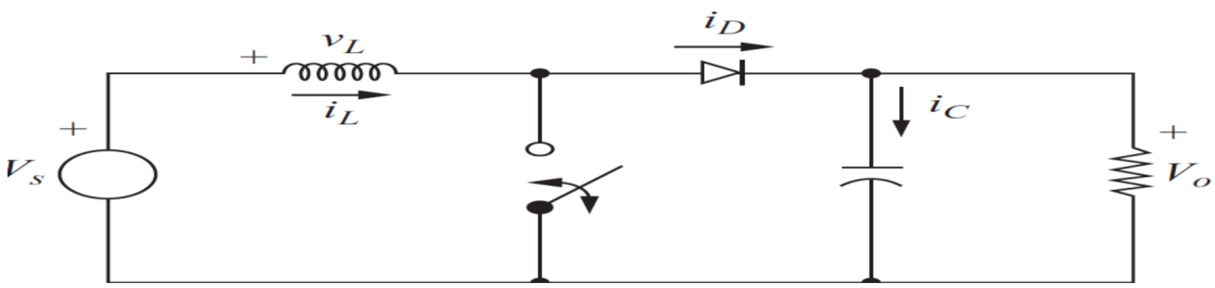

Figure 3.7. DC-DC boost converter circuit[76]

The mathematical equations for the parameter boost converter were determined using the following equations. The outputs of buck-boost converters are determined by the following equations.

$$V_{out} = \frac{V_s}{1\text{-}D} \quad \text{Or} \quad D = 1\text{-}\frac{V_{in}}{V_{dc}} \tag{3.19}$$

$$V_{out} = DV_s \tag{3.20}$$

$$V_{out} = -Vs\left(\frac{D}{1\text{-}D}\right) \tag{3.21}$$

Rearranging equation 3.21, $D = 1\text{-}\frac{Vs}{V_{OUT}}$

$$L_{critical} = \frac{(1\text{-}D)\times D\times R}{2f_s} \tag{3.22}$$

$$C_{critical} = \frac{D\times V_{out}}{R\times f_s\times V_r} \tag{3.23}$$

where: $V_r = \frac{\Delta V_{out}}{V_{out}}$, and $R = \frac{Vout^2}{P_{in}}$

In this thesis, the reference DC link voltage V_{dc} is 1000V, the DC link voltage ripple is taken as 1% of DC link voltage, so 1% of 600V is 6V and the switching frequency is 10 kHz and 5% deviation from the nominal output voltage to get the duty cycle[70].

The main parameter used such as inductance, capacitance, diode and resistor were designed[10]. The diode D is used to protect the PV array against the negative current. Capacitor C is placed here to limit the high-frequency harmonics.

$$V_r = \frac{564V}{600} = 0.094V$$

$$L_{min} = \frac{(1\text{-}0.05)\times 0.05\times 1.89}{2\times 10000} = 4.5\mu H$$

$$C_{min} = \frac{600\times 0.05}{1.89\times 10000\times 0.94} = 1.16mF$$

3.7.3 DC to AC Converter (Inverters) Modeling

DC to AC converter (inverters) is used to change the DC output voltage of the photovoltaic array into AC voltage. It is composed of a resistor and six power switching blocks. The pulse with Modulation (PWM) is used in the modeling of the inverter to get proper gating signals for switches, to control output voltage amplitude and frequency. Capacitor is used to filter the noise on the DC bus link[77].

In this thesis work, three phase three level neutral point clamped inverter is used for solar and two level three phase is inverter is used for battery energy storage system (BESS) to support load and deliver accurate voltage and frequency at the point of common coupling (PCC). This is the DC-AC converts the DC power from PV and BESS into AC power at desired output voltage and frequency. In this thesis 1000V DC output voltage is converted to the 600V AC at 50 Hz frequency[61].

Modelling of a three-phase voltage Source inverter (VSI) will be presented, which involves the representation of physical inverter system with the help of mathematical equations or transfer function. The mathematical models of the inverters can be used for the controller's design for three phase voltage source inverters. The Park-Clarke transformation theory is used to design the controllers for a three-phase voltage source inverter. Three single phase half bridge inverters are connected in parallel to form a three-phase inverter. The VSIs is divided into pulse width modulated (PWM) inverters and square wave inverters. PWM inverters are among the most used power-electronics circuits in practical application. These inverters are capable of producing AC output voltage of variable magnitude and variable frequency[78]. Thus, the aim of a PWM inverter is to generate good quality sinusoidal voltage waveform of desired fundamental frequency and magnitude. Generally, Cascaded control structure is popularly used for VSC control. The inner loop realizes current control and the outer loop realizes power control or voltage/frequency control. The reason to have an inner current control is that VSCs are sensitive to large currents. With current control, VSCs can be protected against overcurrent's. The inner loop control and the outer loop control are usually designed separately due to their distinct bandwidth requirements. The inner current controls require a fast response and a high bandwidth. The outer controls require a much slower response and a lower bandwidth[1]. Design of both outer and inner control loop is presented below. And also, low pass filters are provided at the output of the pulse width modulated inverter to achieve good quality sinusoidal waveforms with low harmonics content. Power electronics switches like BJTs, IGBTs, MOSFETs and SITs are used to design inverters. A three phase pulse width modulated inverter consists of three legs in each phase and each leg includes two power switches as shown in Figure 3.8. Each power switch is transistor or IGBT with antiparallel diode.

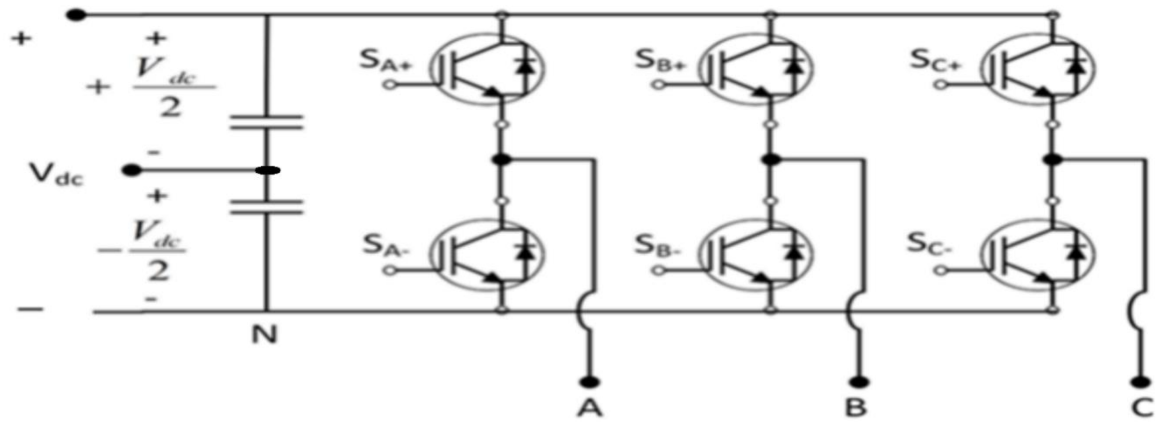

Figure 3.8 Three phase three level NPC inverter[42]

Three phase transformations are mathematical transformations employed to simplify the analysis of three phase circuit[26]. They are often used to decouple variables in order to facilitate the solution of difficult equations with time varying variables. Moreover, the complexity of differential equations is often reduced due to change of variable[2]. They are generally used to design and model the control system for power system application. Clarke and Park are generally used transformation techniques. Both Clarke and Park transformation is used in this thesis are in the Appendix (E).

3.7.4 Filter Design

Filter is connected to the output of voltage source inverter (VSI) to eliminate the current ripples caused by switching of the inverter[79]. The control system for VSI consists of inner current, voltage control loop and external droop control loop. The main purpose of current control loop is to regulate the output current. This is the loop around the filter inductor and VSI, which builds a controlled current source. The voltage control loop is around the filter capacitor and VSI, which behaves like a controlled voltage source. The droop control loop generates voltage magnitude and frequency reference set points for generation of the reference three-phase voltage.

The value of equivalent resistance can be calculated using following formula:

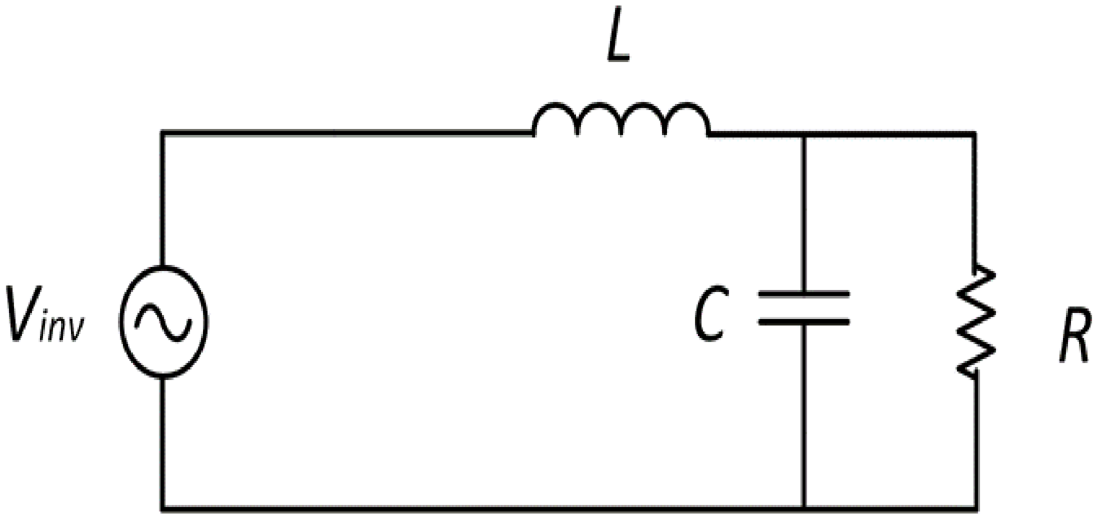

Figure 3.9 Simplified filter circuit

$$R = \frac{V^2}{\frac{P}{3}} = \frac{(600v^2)}{(875KW/3)} = 0.13714\Omega$$

Where, V is the rated voltage and P is the rated power of the inverter. The transfer function of the LC filter can be derived from circuit diagram by writing KVL equations[12]. The second order transfer function is obtained as:

$$G_{Filter} = \frac{V_C(s)}{V_{Inv}(s)} = \frac{\frac{1}{LC}}{s^2 + \frac{1}{CR}s + \frac{1}{LC}} \tag{3.24}$$

Where VC is the voltage across the capacitor. Now, the general form of a second order transfer function, G-second order(s), using. Where, ωn is the natural frequency, ξ is the damping ratio of the second order system. Switching frequency of inverter is 10 KHz.

$$G_{Second\_order}(S) = \frac{\omega n^2}{s^2 + 2\xi\omega ns + \omega n^2} \tag{3.25}$$

The value of capacitance (C), inductance (L) of the LC filter can be calculated by comparing equation (3.24) and (3.25) yields in:

$$C = \frac{1}{2\xi\omega nR} = \frac{1}{2 \times 0.707 \times 8769.45 \times 0.13714} = 5.88\times10^{-4}\ F$$

$$L = \frac{1}{\omega n^2 C} = \frac{1}{(8796.5\text{rad/sec})^2 \times 5.86\times10^{-4}} = 2.219\times10^{-5}\ \text{H}$$

The natural frequency is ωn taken to be 1.4 kHz (= 8796.45 rad/s) for inductance and capacitance calculation. The natural frequency is chosen to be one decade below the switching frequency of the inverter that ensures adequate attenuation to high frequency noises produced at the inverter output[3]. Similarly, the value of damping ratio (ξ) is selected to be 0.707, which provides an acceptable tradeoff between the system overshoot and speed response of the designed filter system.

3.7.5 Inner Current Control Loop Design

The inner current controls for the vector control should be designed to be much faster than the outer control loops[80]. The converter voltage in (abc) frame is notated as v and the current is notated as i. The voltage at the point of the common coupling (PCC) is notated as v1. An RL circuit is considered between the converter and the PCC as shown in Figure 3.10.

Therefore:

$$L\frac{d\vec{i}}{dt} + R\vec{i} = \vec{v} - \vec{v}_1 \tag{3.26}$$

Where $\vec{x}$: is the space vector.

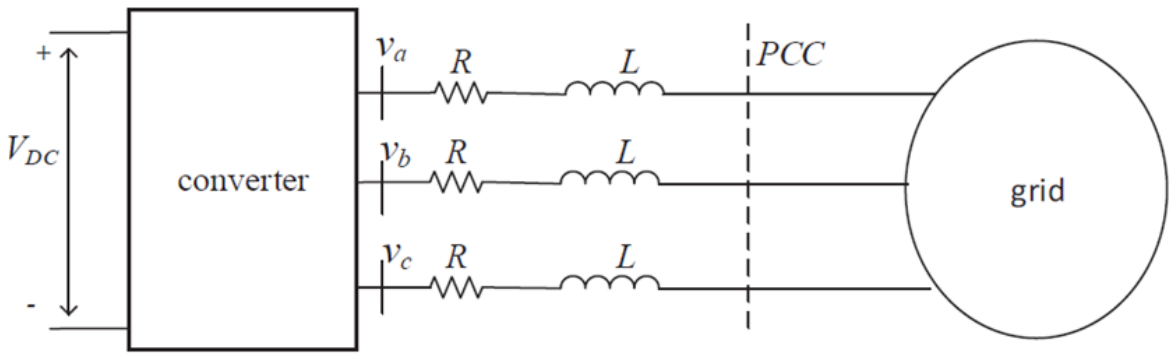

Figure 3.10 Point of common coupling

The dq-reference frame is now utilized. It is assumed that the d-axis is aligned with the space vector of the PCC voltage.

$$L\frac{d(i_q + ji_q)}{dt} + (j\omega L + R)(i_q + ji_q) = V_d + jV_q - (V1_d + jV1_q) \tag{3.27}$$

Where ω is the grid's frequency, v1q = 0 since the PCC voltage is aligned with the d-axis.

Separating equation (3.26) into dq-axes, the plant model for the current control design is derived:

$$L\frac{di_d}{dt} + Ri_d = \underbrace{v_d - v1_d + \omega L i_d}_{ud} \tag{3.28}$$

$$L\frac{di_q}{dt} + Ri_q = \underbrace{v_q - v1_q + \omega L i_q}_{uq} \tag{3.29}$$

The plant model for the current controller is assumed as 1=(R + sL) for both d and q axes. The inputs are ud and uq while the outputs are id and iq. The feedback controls are designed for the dq-axis currents to track the reference signals[58]. In addition, to generate the dq components of the converter voltage, the cross coupling and feed-forward voltage terms should be added after ud and uq are obtained from the controllers.

The inner current loop simplified as below.

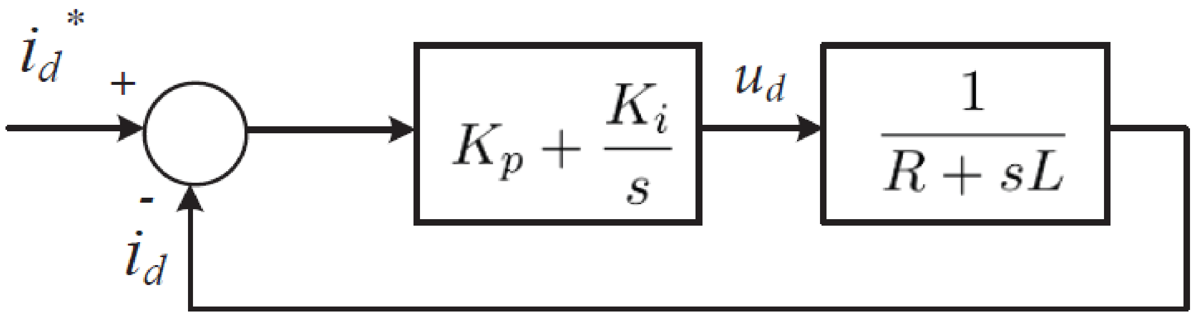

Figure 3.11. Inner current loop with PI controller

The closed loop transfer function of inner current control loop derived as below.

$$Ti(S) = \frac{Kp}{sL}\left(\frac{s + \frac{Kp}{Ki}}{s + \frac{R}{L}}\right) \tag{3.30}$$

Assume, the plant pole is fairly close to the origin. Therefore, this plant pole is canceled by the compensator's zero $\left(\frac{K_i}{K_p} = \frac{R}{L}\right)$ and the loop gain becomes:

$$l(s) = \frac{K_p}{sL} \tag{3.31}$$

The closed-loop transfer function can be represented as:

$$G_{Inner}(s) = \frac{l(s)}{1 + l(s)} = \frac{1}{\tau s + 1} \tag{3.32}$$

where: $\tau = \frac{L}{K_p}$ and $K_i = \frac{R}{\tau}$.

If R = 0.13714 and $y_{max} > y > y_{min}$ the inner loop with Ki = 15, Kp = 0.2 will lead to a bandwidth around 2500 rad/s (τ = 0.4 ms).The frequency response of the inner closed loop transfer function is as below.

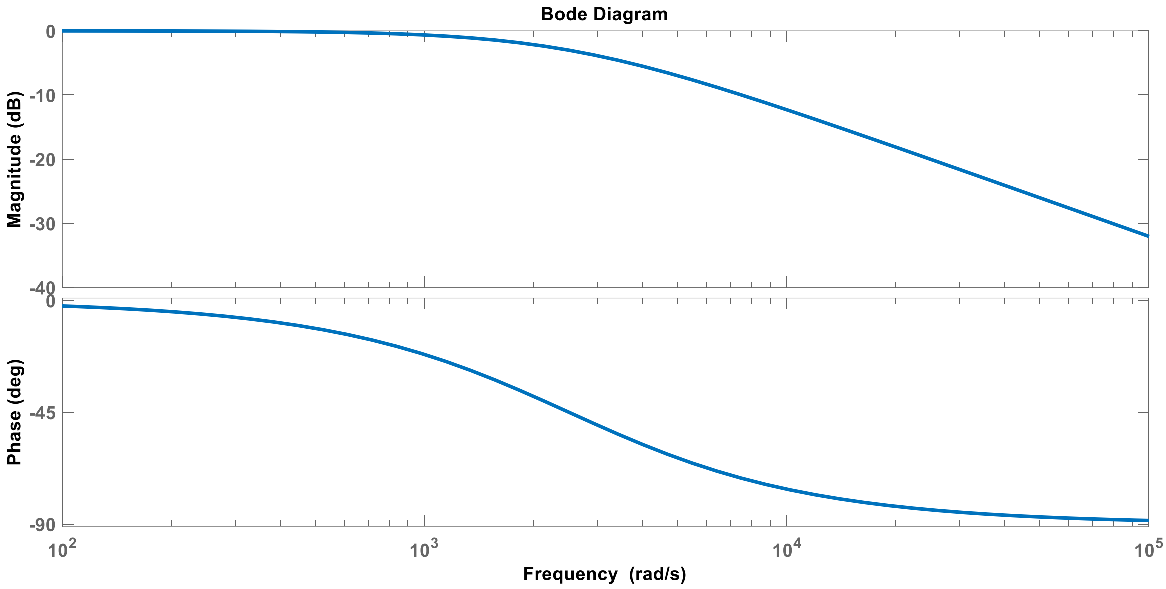

Figure 3.12 Inner current loop Frequency response

3.7.6 Phase Locked Loop

A phase-locked loop or phase-locked loop (PLL) is a control system that provides an output signal whose phase is related to the phase of the input signal[13]. There are several different types; the simplest is an electronic circuit consisting of a variable frequency generator and a phase divider in the feedback circuit.

The oscillator generates a periodic signal, and a phase detector compares the phase of that signal to the phase of the periodic input signal, adjusting the oscillator to maintain phase matching.

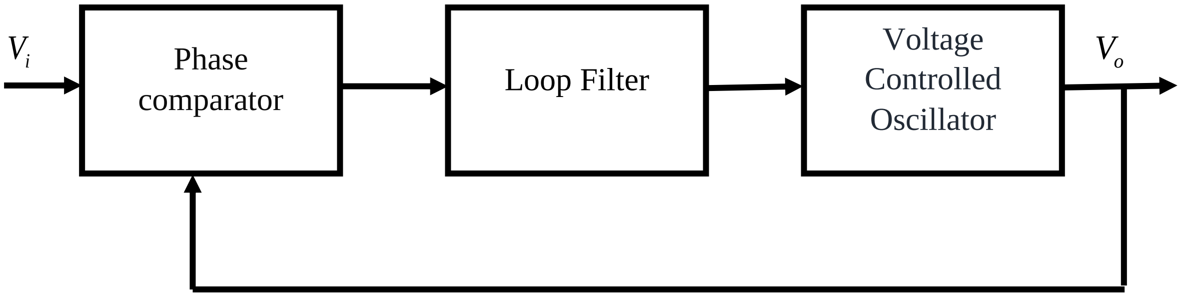

Figure 3.13 Simple analog single phase PLL [79]

Keeping the input and output phase in lock step also implies keeping the input and output frequencies the same[81]. Consequently, in addition to synchronizing signals, a phase-locked loop can track an input frequency, or it can generate a frequency that is a multiple of the input frequency.

With the inner current controller, ud and uq will be produced. The converter dq-axis reference voltage v_d and v_q can then be computed as

$$v_d^* = u_d + v1_d - \omega L i_d \tag{3.33}$$

$$v_q^* = u_q + v1_q - \omega L i_q \tag{3.34}$$

Note that the generation of v_ d and v_ q requires the feedforward units (v1d and v1q) from the PCC voltage and the cross coupling terms ($-\omega L i_q$ in d-axis and $\omega L i_q$ in the q-axis). Further, since the inputs of the PWM of a VSC are abc voltages, the dq-axis voltages need to be converted to vabc. Note that the dq-reference frame is based on the space vector of the PCC voltage and the d-axis is aligned with the PCC voltage space vector.

Therefore, the space vector of the converter voltage will be

$$\vec{v} = (u_d + j u_q) e^{j\theta} \tag{3.35}$$

Where θ is the PCC voltage space vector's angle relative to the static reference frame. va, vb, and vc can be found from the space vector.

$$v_a = R(\vec{v}) = v_d \cos\theta - v_q \sin\theta \tag{3.36}$$

$$v_b = R(\vec{v} e^{-j\frac{2\pi}{3}}) = v_d \cos(\theta - \frac{2\pi}{3}) - v_q \sin(\theta - \frac{2\pi}{3}) \tag{3.37}$$

$$v_c = R(\vec{v}e^{j\frac{2\pi}{3}}) = v_d\cos(\theta+\frac{2\pi}{3}) - v_q\sin(\theta+\frac{2\pi}{3}) \quad (3.38)$$

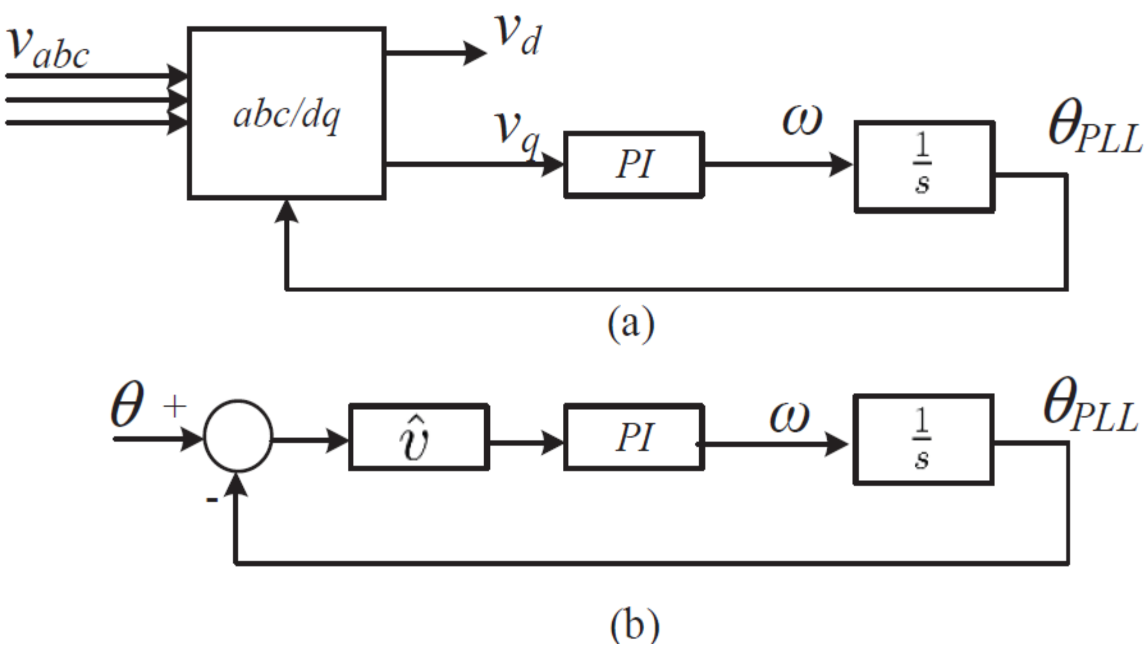

Figure 3.14 a) Block diagram of PLL and b) simplified block diagram of PLL[82]

The angle for the space vector $\vec{v1}$ will be obtained by a PLL. Figure 3.13 presents the control diagram for a simple PLL. The inputs to a PLL are three-phase voltages. For the application of a grid-connected VSC, the voltages are the PCC voltages v1a, v1b and v1c.

The voltages will be converted to dq-axis voltages based on an angle θ_{PLL}. A feedback loop equipped with integral controls now tries to make the q-axis voltage zero[83]. This way, the input voltages space vector is now aligned to the d-axis of a reference frame based on θ_{PLL}. Using the space vector concept, it can yield to show that the first block abc to dq is in fact the following input-output relationship:

$$v_d + jv_q = \vec{v}e^{-j\theta_{PLL}} = \hat{v}e^{j\theta}e^{-j\theta_{PLL}} = \hat{v}e^{j(\theta - \theta_{PLL})} \quad (3.39)$$

Therefore,

$$\begin{cases} v_d = \hat{v}\cos(\theta - \theta_{PLL}) \\ v_q = \hat{v}\sin(\theta - \theta_{PLL}) \end{cases} \quad (3.40)$$

The abc coordinate voltage and current has phase difference of $\theta=\frac{2\pi}{3}=120^{\circ}$. The abc/dq block is built based on the following V_d and V_q can be found from V_{abc} .The space vector $\vec{v}$ will be expressed by V_a , V_b and V_c .

$$v_d + jv_q = \vec{v}e^{j(\theta-\theta_{PLL})} = (v_a + v_b e^{j\frac{2\pi}{3}} + v_b e^{-j\frac{2\pi}{3}})e^{-j\theta_{PLL}} \quad (3.41)$$

Therefore,

$$v_d = \frac{2}{3}(v_a\cos(\theta_{PLL}) + v_b\cos(\theta_{PLL} - \frac{2\pi}{3}) + v_c\cos(\theta_{PLL} + \frac{2\pi}{3})) \quad (3.42)$$

$$v_q = -\frac{2}{3}(v_a\sin(\theta_{PLL}) + v_b\sin(\theta_{PLL} - \frac{2\pi}{3}) + v_c\sin(\theta_{PLL} + \frac{2\pi}{3}) \quad (3.43)$$

3.7.7 Outer Voltage Control loop

The block diagram of the outer voltage control loop for PV and BESS is designed as the

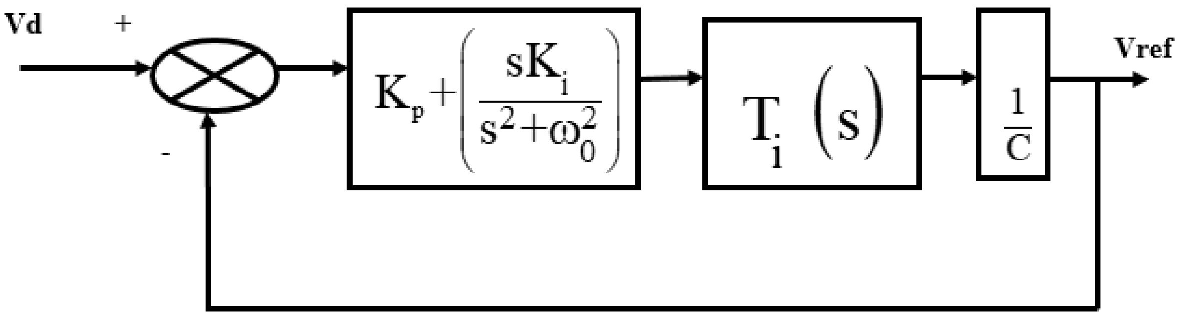

Figure 3.15 Outer Voltage control loop

Where, Kp is the proportional gain, Ki is the integral gain of the Proportional Integral controller, Ti(s) is the transfer function of current control loop, ω_0 is the system frequency and C is the filter capacitor. The closed loop transfer function of outer voltage loop is obtained by using following equation.

$$Tv(S) = \frac{G(S)}{1 + G(S)H(S)} \quad (3.44)$$

Where G(s) is the open loop transfer function. G(s) of voltage control loop of the above figure. $Ti(S)=\frac{1}{1+\tau s}$ while $\tau=0.4\times10^{-4}$.

$$G(S) = \frac{1(s^2Kp + SKi + Kp\omega 0^2)}{(s^2 + \omega 0^2)(s\tau + 1)sC} \tag{3.45}$$

H(S)=1.

In this case, the bandwidth of outer voltage control loop must be smaller than the current control loop. Hence, the bandwidth of voltage control loop is chosen to be 312.5 Hz, which is approximately one eighth of the current control loop[84]. Therefore, closed loop transfer function of outer voltage loop is found to be

$$Tv(S) = \frac{G(S)}{1 + G(S)H(S)}$$

$$Tv(s) = \frac{s^2Kp + sKi + Kp\omega_0{}^2}{s^4\tau C + s^3C + s^2X2 + sx1}$$

$$x2 = \tau\omega_0^2 C$$

$$x1 = \omega_0^2 C$$

The values of Kp and Ki can be obtained by plotting root locus of for the open loop transfer function of G(S) voltage loop controller. The fundamental frequency of the system is 50Hz.

Assume the ratio of Ki and Kp is 1250.Substituting values of Kp, Ki, τ, ω_0 , L,C the open loop transfer function becomes

$$G(S) = \frac{(S^2Kp + 1250SKp + 98696.04401Kp)}{2.344e - 8S^4 + 5.86e - 4S^3 + 2.314e - 3S^2 + 57.8358S}$$

The value of Kp is obtained by plotting root locus.The root locus of G(S)

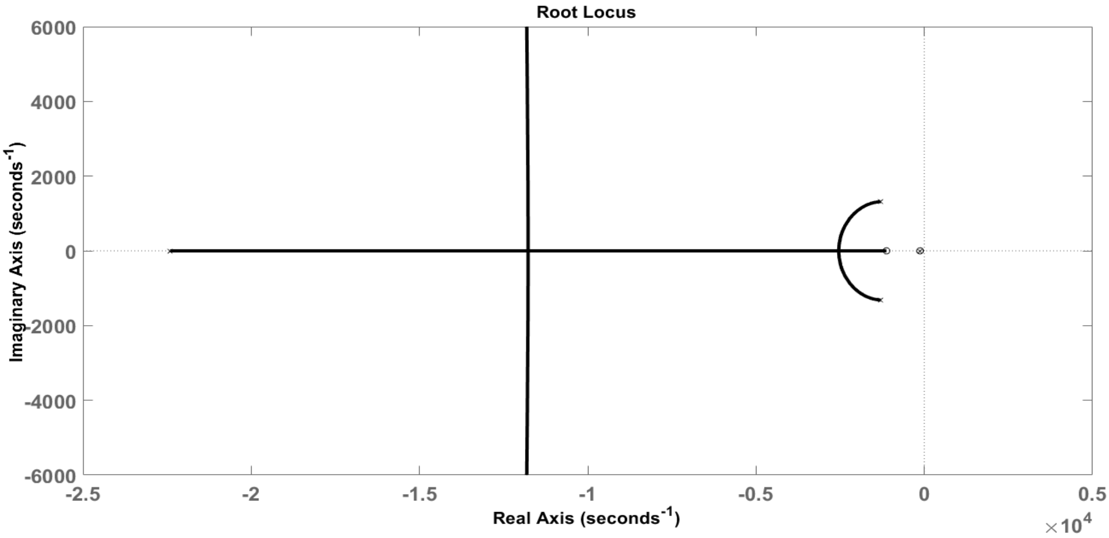

Figure 3.16. Outer voltage loop root locus

From the root locus plot, the gain at the value of ξ =0.707 is found to be 0.143.Thus the value of Kp and Ki are obtained as 0.143 and 178.75.

The closed loop transfer function of the outer Voltage Control loop is obtained as,

$$Tv(S) = \frac{0.143S^2 + 178.75S + 14113.53429}{2.344e\text{-}8S^4 + 5.86e\text{-}4S^3 + 0.83556s^2 + 2.314e\text{-}3S}$$

The Routh-Hurwitz (RH) criterion is applied to examine the stability of voltage control loop. The characteristic equation is 1+ G(S)H(S) provides the pole of closed loop transfer function can be written as,

$$2.344e\text{-}8S^4 + 5.86e\text{-}4S^3 + 0.83556s^2 + 2.314e\text{-}3S$$

Now applying Routh Hurwitz Criterion

S^4	2.344e-8	0.83556	0
S^3	5.86e-4	2.314e-3	0
S^2	0.8355	0	0
S	2.314e-3		
S^0	0		

From the above analysis it is found that the number of sign change is zero, therefore the number of pole on the right hand side of S-plane is zero. Thus, this closed loop system is said to be stable.

3.7.8 Droop Control loop Design

In this thesis it is assumed that maximum active power deviation delivered by voltage source inverter (VSI) is assumed to be 30KW and maximum reactive power is assumed to be 30KVAr.the maximum permissible frequency change and voltage magnitude change is also assumed to be 2% and 5% respectively[41]. Therefore, change in voltage magnitude 2% change in frequency per 30 kW active power is set as a frequency droop whereas 5% change in voltage magnitude per 30 KVar reactive power is set as a voltage droop shown in equation below:

$$m = \frac{\Delta\omega}{\Delta P} = \frac{2\times\pi\times 50\times 0.02}{30000} = 2.09\times 10^{-4}$$

$$n = \frac{\Delta V}{\Delta Q} = \frac{600\times 0.1\times 0.05}{30000} = 1\times 10^{-4}$$

Where m and n are frequency and voltage droop coefficient respectively.

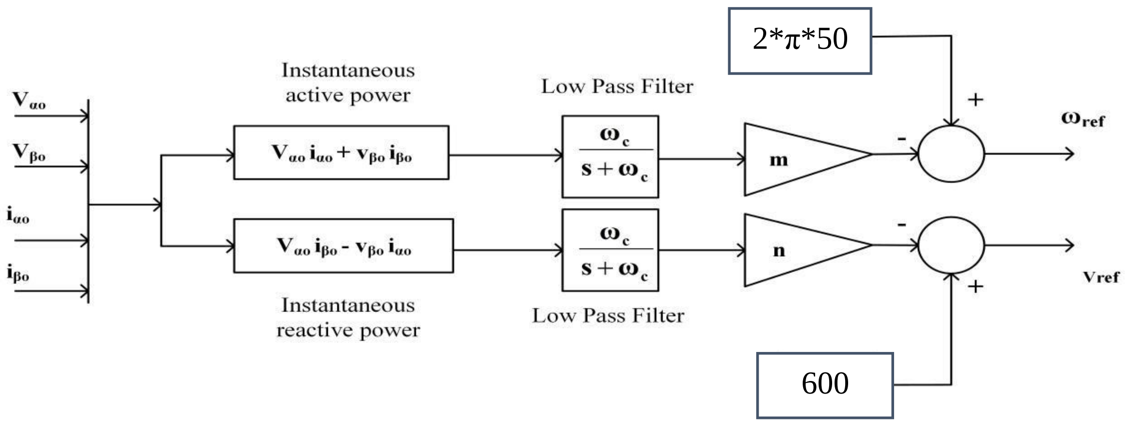

Figure 3.17 Droop Control

From the droop controller block diagram shown in Figure 3.17, the average active and reactive power can be obtained with the help of low pass filter form equations:

$$P = \frac{\omega_C}{S + \omega_C} p \qquad (3.46)$$

$$Q = \frac{\omega_C}{S + \omega_C} q \qquad (3.44)$$

For design of low pass filter, the cut off frequency is chosen to be 90 Hz. Now, the transfer function of low pass filter become $\frac{2\times\pi\times90}{S+(2\times\pi\times90)}$.Then the frequency response of the designed low pass filter is:

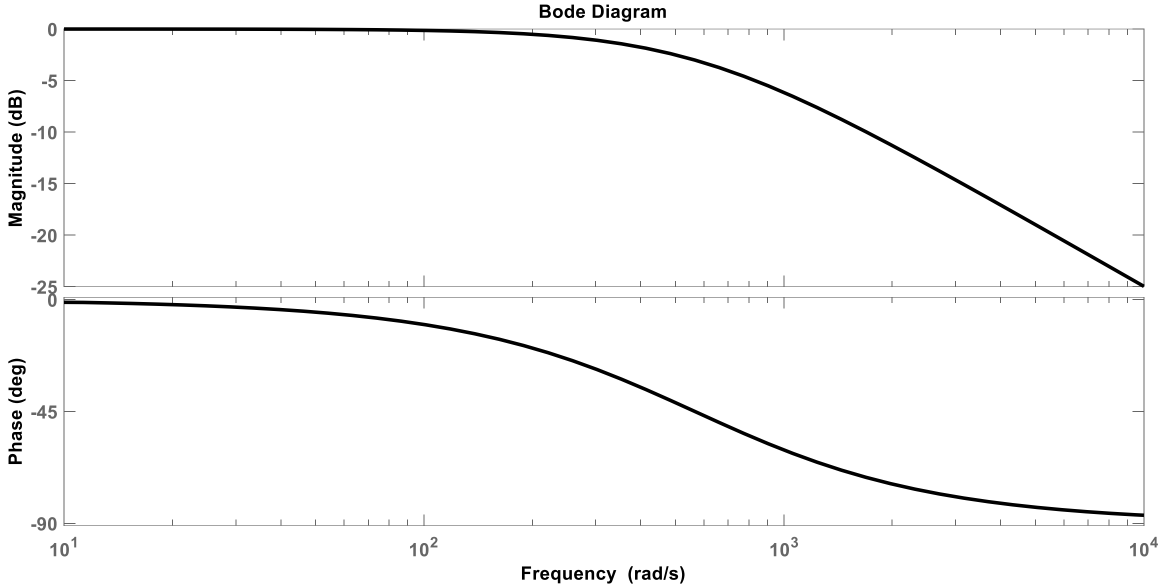

Figure 3.18 Droop control transfer function bode plot

3.7.9 Battery Modeling

The battery is an essential element for a microgrid grid tied consisting of PV system because of the fluctuating nature of the photovoltaic array[85]. A simple equivalent circuit of rechargeable battery modeling is shown in figure 3.16,

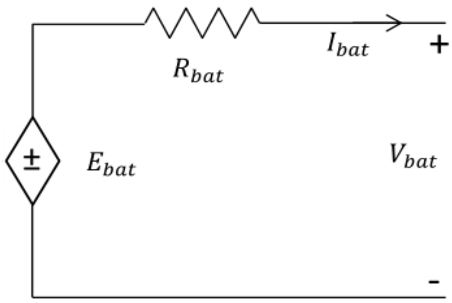

Figure 3.19 Simple equivalent circuit of rechargeable battery modeling[40]

Applying the law of KVL, the voltage at the battery storage can be found as the following.

$$V_{bat} = E_{bat} - R_{bat}I_{bat} \tag{3.45}$$

$$P_{bat} = V_{bat}I_{bat} \tag{3.46}$$

It is necessary to use a control strategy battery or energy storage to provide its lifespan. So, the State of Charge (SOC) is a basic parameter used in battery charging and discharging. SOC is the criterion for determining the charging or discharging of the battery. SOC is shown in equation 3.44.

$$SOC=\frac{Q_c}{Q_r}\times 100\% \tag{3.47}$$

Where: P_{bat} = Battery power delivered to the load

R_{bat} = Internal resistance of the battery bank

I_{bat} = Battery current to the load

Q_c = remain capacity of the battery (Ah)

Q_r = rated capacity of the battery (Ah)

A battery or energy storage is modeled as a non-linear voltage source where its output voltage depends on the state of charge and current and the voltage and internal resistance also depends on the state of charge[86].

3.8 Proposed Controller Design for Microgrid Control

In designing microgrid controller, one major issue is microgrid consists of a group of interconnected loads and distributed generation resources that act as single controllable entity with respect to the grid and each components of microgrid requires different controllers and they work together for common goal[87]. A linear regulator is easy to implement and performance is good as long as the dynamics remain close to linear. However, it may have difficulty if there is a large change in the set point and the integral term accumulates a significant error during the increase (windup) direction which causes the controller to become non-linear. [88]. Nonlinear effects require caution, such as actuator saturation (always present); saturation phenomena, if neglected in the design phase, can lead to closed-loop instability, especially if the process is unstable.

This condition has the effect that the control loop is interrupted if the saturation is not taken into account by the regulator parameters[89]. This problem generally occurs when the input error for the controller is large or when the input error remains non-zero for an extended period of time. The controller output may saturate due to a large input error or a non-zero error, causing the integrator output to continue to accumulate. A low saturation controller can give a delayed response to any change in input, and that delay would be greater as the controller enters a deep saturation level[90]. There are many techniques to handle input saturation. so it becomes necessary to use anti-windup strategy to stop the controller from going into deep saturation and to see windup or change of controller output. PI controller with anti-windup

The transfer function of the PI controller is shown as

$$G_{PI}(s)=K_P+\frac{K_I}{s} \tag{3.48}$$

Here Kp is the proportional constant and Ki is the integral constant. The output from controller y can be expressed as:

$$y=K_P\times e+K_I\int edt \tag{3.49}$$

Here e is the input error. The block diagram for the implementation is shown in the figure 3.20.

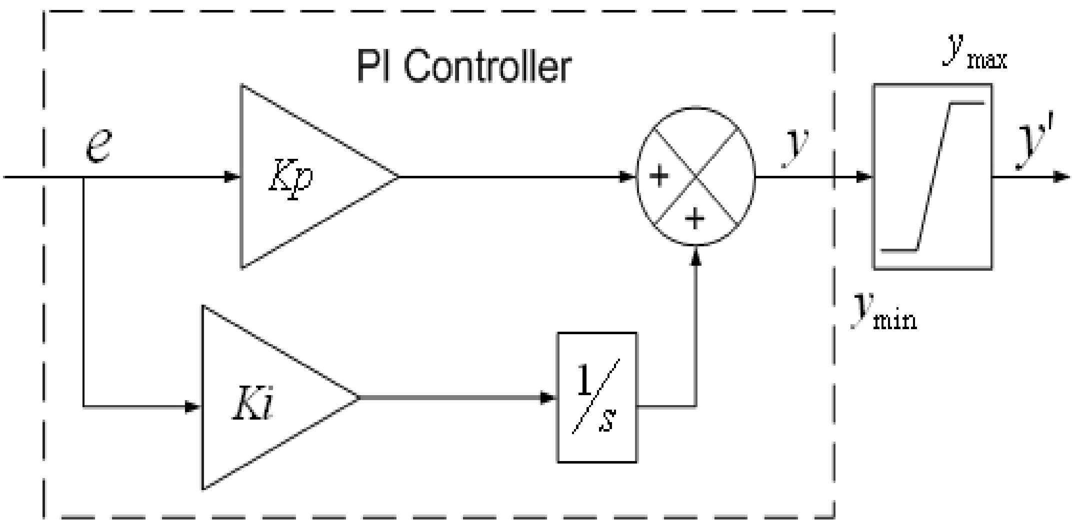

Figure 3.20 Block diagram representation of a PI controller with saturation.

Variables can therefore reach values between a certain finite range and any value outside this range leads to a roll over and the controller output (y) would show this as a sudden jump from positive to negative or vice versa[91]. Such an undesirable condition can occur if the error (e) is too large or if it remains non-zero for a long period of time during which the integrator causes the roll over. To limit the output, a saturation block can be used on the output connection as shown in figure 3.19 above. Here output (y′) can be expressed as:

$$y' = \begin{cases} y & \text{for } Y_{max} > y > Y_{min} \\ Y_{max} & \text{for } y > Y_{max} \\ Y_{min} & \text{for } y < Y_{min} \end{cases} \tag{3.50}$$

However, the above approach would lead to a problem if the input 'e' remains non-zero for a long time and the integrator output continues to accumulate during this time. This can lead to a delay in the response if the input error changes, or even to an update of the output. To avoid this, in such situations it is necessary to check the integration process commonly known as ant windup[92]. The good approach aims to prevent the controller state from growing too much during saturation and to give the controller good values of the state. One of the best approaches is the conditional integration method, which turns integration off under certain conditions. In this thesis, study carried out using Conditional integration and anti-windup tracking with feedforward control.The purpose of integrator is to remove steady state errors in the process output[90]. A simple approach to avoid integration windup is to switch off the integration when the controller is far from steady state. Error is the DC link voltage reference and DC link voltage difference.

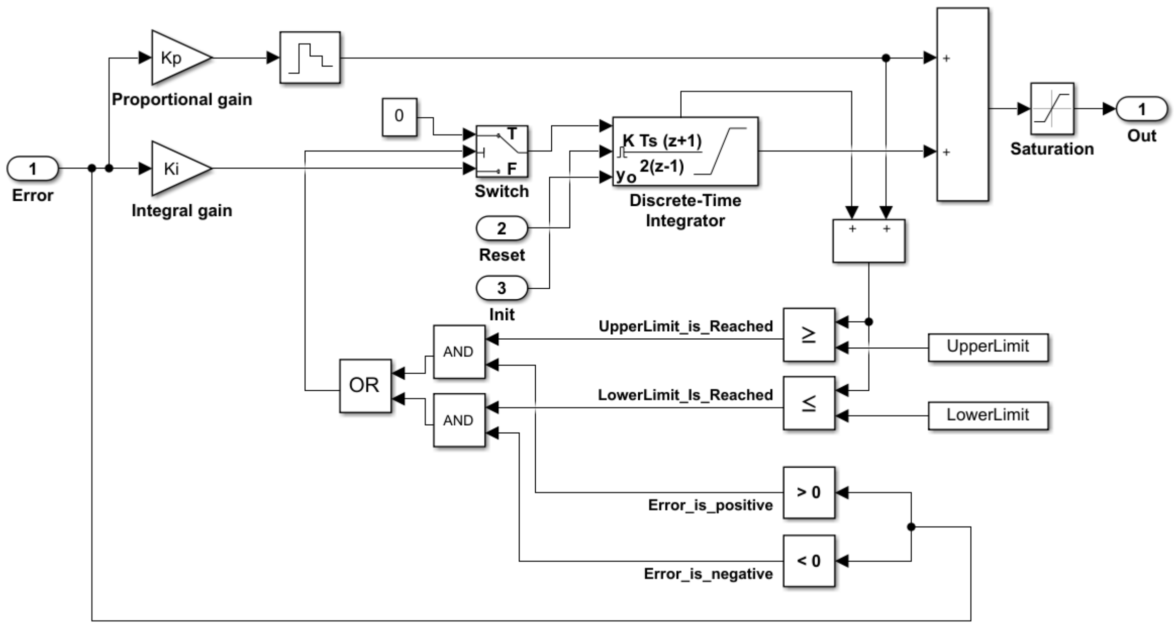

Figure 3.21 PI anti windup for voltage control loop in MATLAB/Simulink

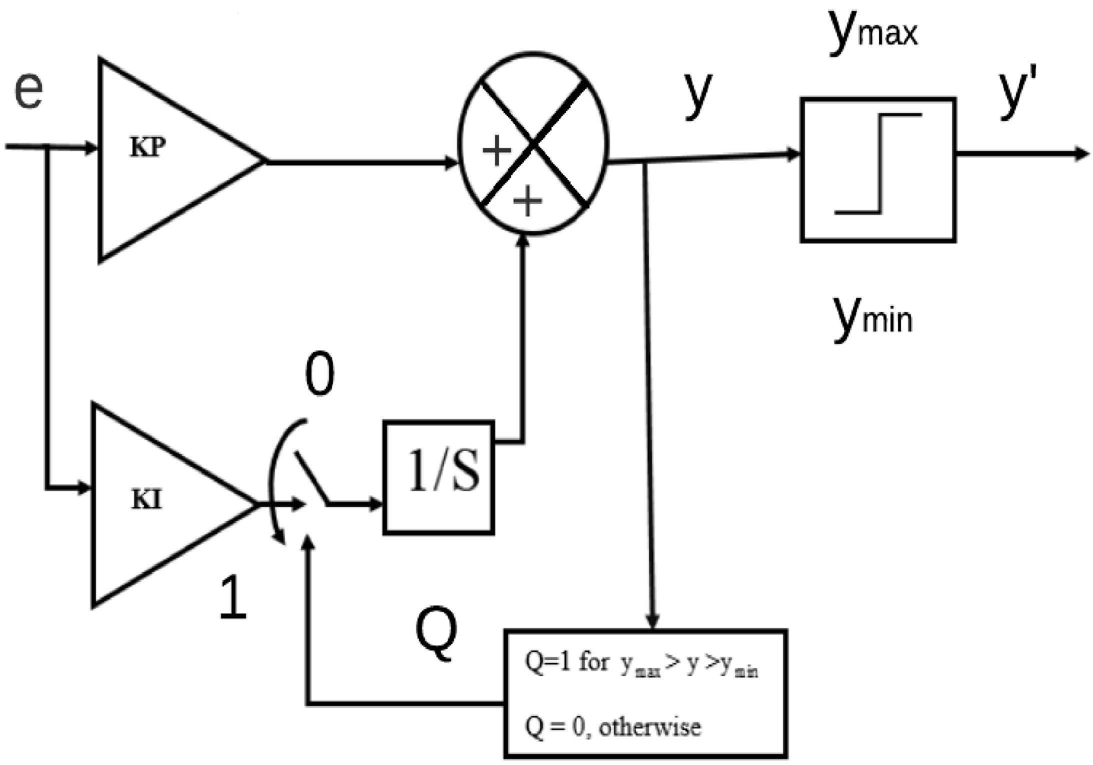

Figure 3.22 PI anti windup with conditional integration[93]

Five basic method for switching off integration depending on the above block could be[94]:

- ❖ Quit integrating when the control error is maximum. $|e(t)| > e$
- ❖ Quit integrating when the controller saturates. y > ymax and y < ymin
- ❖ Quit integrating when the controller saturates and the control error e has the same sign as the control signal.
- ❖ Limit the integrator I such that $|i(t)| \leq i_0$.
- ❖ Quit integrating and assign a predetermined or computed value to the integrator when a specified condition is true.

This method can also be considered as a variable structure PID control method.

This ensures that the value of output "y" does not increase any further while the controller is saturated. If the error falls below a certain value at which the output leaves saturation, the integrator starts to work again. For example: in a PV inverter, DC voltage regulator: Kp_Vreg=4, Ki_Vreg=25 while Vreg_Saturation limits is [1.5,-1.5] the result of the PI anti windup is as in the figure below.

Figure 3.23 PI anti windup saturation output

In this method the PI controller output never goes beyond the saturation limit and never goes below the saturation limit value.

3.8.1 Saturation

Saturation can be defined as static nonlinearity. The saturation block provides an output signal that the input signal is limited to the high and low saturation values[90]. The upper and lower limits are set by the parameters for the upper and lower limits. The summary of the conditional PI anti-windup integration used in the sub-block diagram of this thesis microgrid for the solar system and the battery energy storage system for each block used for the thesis. In Appendix (D) of the microgrid component script.

3.8.2 Fuzzy PI anti windup

In this thesis, the three-phase power converter circuit topology uses a three-phase three-phase level neutral point clamped (NPC) circuit.

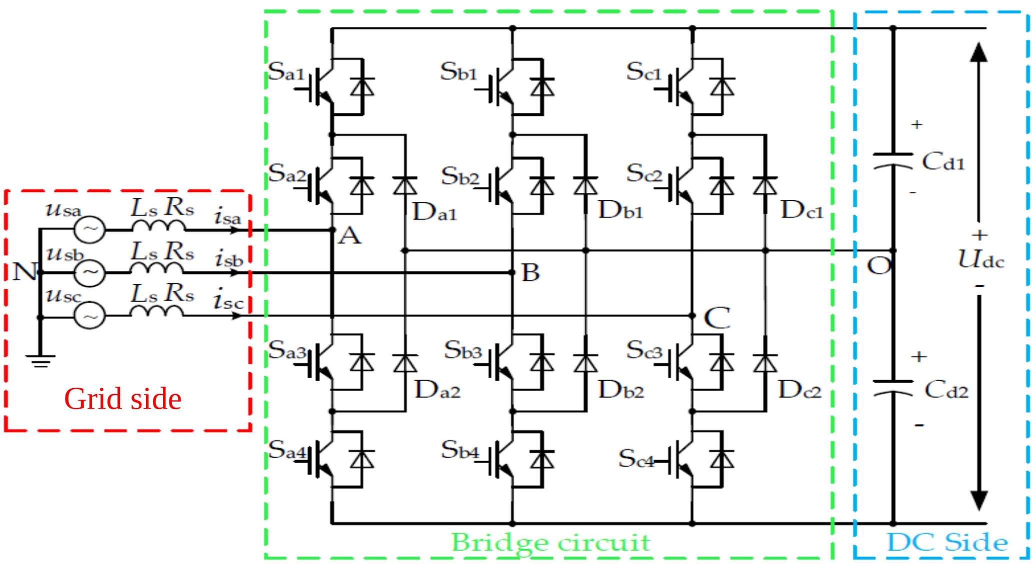

Figure 3.24 Three level three phase NPC[37]

Figure 3.23 shows three phase three level NPC, which mainly includes the three parts: AC grid side, bridge circuit, and DC side. usa, usb and usc are the phase voltages of the grid side with the center of N; Ls and Rs are the inductance and the equivalent resistance of the grid-side filter, respectively; isa, isb and isc are the currents on the gridside. Each phase of the three-phase bridge arm consists of four Si1 ~ Si4 (i = a, b, c) insulated gate bipolar transistor (IGBT) switches with free-wheeling diodes and two clamping diodes D_{i1}~D_{i2} (i = a,b,c). Two bus capacitors (C_{d1} and C_{d2}) of the same size are connected.

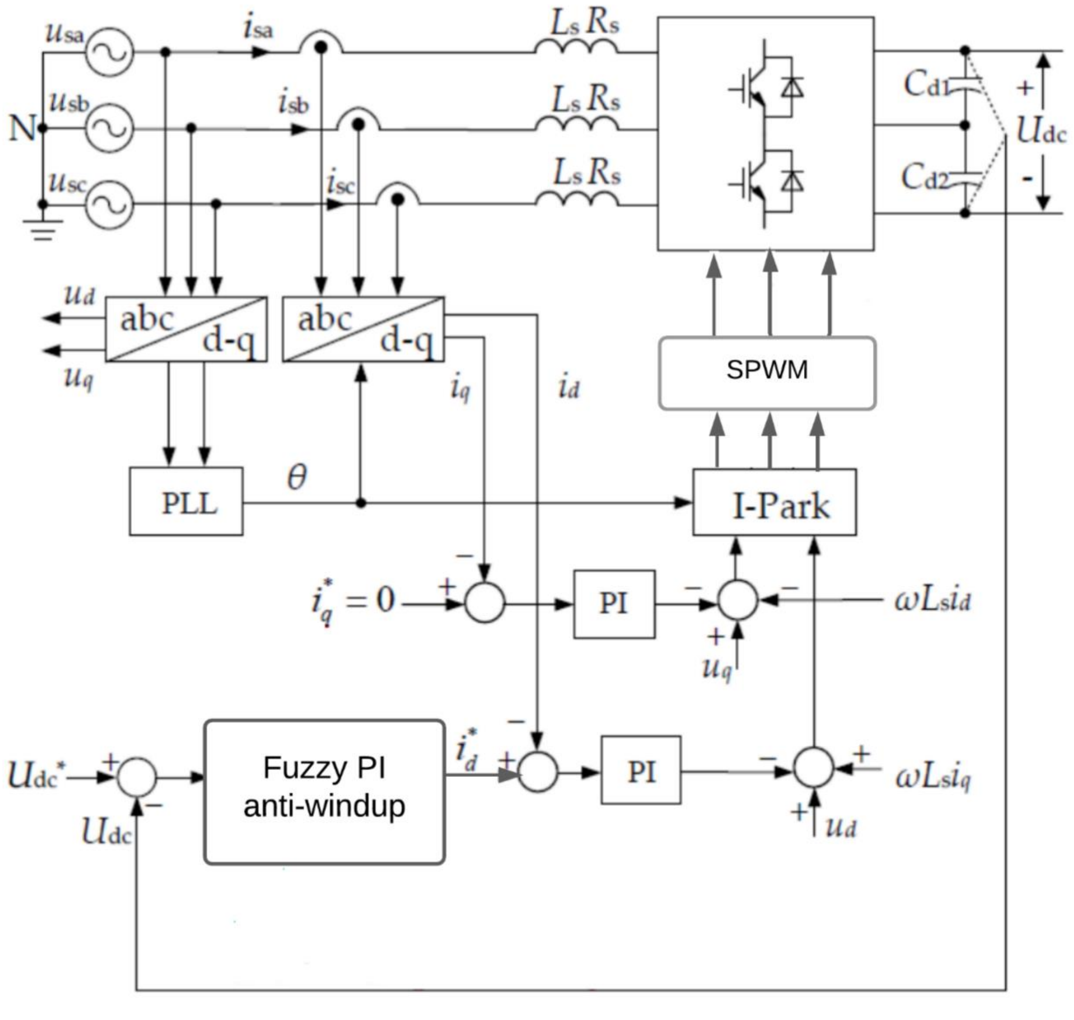

Figure 3.25 Inverter Fuzzy PI control

Two bus capacitors (C_{d1} and C_{d2}) of the same size are connected.

On the DC voltage side, two bus capacitors (Cd1 and Cd2) of the same size are connected in series. O is the midpoint of the capacitance and Udc is the DC bus voltage. The converter uses the double closed loop control structure. Voltage vector-oriented control, including the outer voltage loop and the inner current loop, is shown in Figure 3.25.

The modulation method uses a sinusoidal pulse width modulation (SPWM). The orientation angle calculated by the phase locked loop (PLL) is sent to the abc / dq transformation unit and the reverse park transformation unit (I-Park). The abc / dq transformation transforms the mathematical model of the system from a three-phase static abc coordinate system into a dq rotation coordinate system. ud and uq are the voltage components of the d-axis or q-axis and id and iq are current components of the d-axis and q-axis, respectively. The current components of the d-axis and q-axis are coupled to one another after the coordinate transformation. The feedforward decoupling control strategy is introduced, in which the components ωLsiq and ωLsid (feedforward coefficients) from q-axis and d-axis are implemented in the d-axis or q- axis.

3.8.3 Fuzzy PI Controller for Voltage Outer Loop

The fuzzy PI controller presented here generates the correction of the PI control parameters according to the DC voltage error and its error rate. Controller and auxiliary PI parameter correction. The output of the PI controller in the figure serves as the d-axis current for a given signal id * of the internal current loop, and G (s) is the transfer function of the d-axis current to the direct voltage Udc. The proposed fuzzy PI controller works as shown in figure 3.25 below.

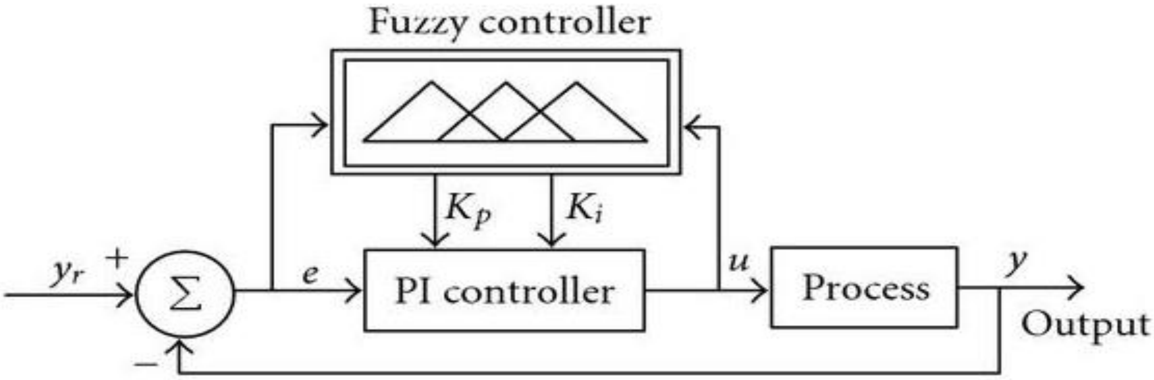

Figure 3.26 Fuzzy PI controller

The fuzzy controller inputs are the error e between the given DC bus voltage Udc * and the actual DC side voltage Udc, which is Yr, and the error rate ec. A group of correction values is obtained for the PI control parameters for the PI controller Δkp1 and Δki1.

3.8.4 Design of Fuzzy Controller

The structure of the main fuzzy controller is shown in the figure. The main design process has three parts: fuzzification, fuzzy rule justification, and defuzzification.

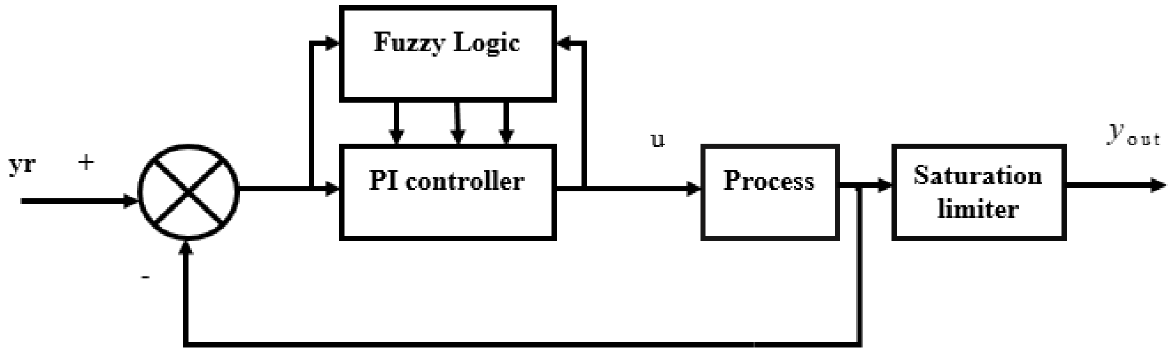

Figure 3.27 Block diagram of fuzzy PI anti windup

The output of fuzzy PI anti windup is the best regulator for voltage loop control, BESS active and reactive power control with voltage droop controller work better together to make the model run faster and have better dynamics and less saturation. Saturation limiter limits of the saturation input.

3.8.5 Fuzzification

Fuzzification consists of converting precise input and output values into fuzzy linguistic values. The concrete implementation steps are as follows:

The basic universe of error e between the given voltage of the DC side Udc * and the voltage DC link, and the basic universe of the corresponding error rate ec is can be obtained through simulation. Here, the error range e is [–600, +600] and the error rate of the change range e is [–200, +200]. Assuming that the fuzzy universe of the error e and the rate of change of the error ec is set as as [−3, 3], then the two intervals are discretized and the discrete set is {−3, −2, −1, 0 , 1, 2. 3}. The error e and the error rate of the change ec can be transformed from the basicuniverse into the fuzzy universe with the following quantization factor:

$$ke = 3/600 = 0.005$$

$$kec = 3/200 = 0.015.$$

The main outputs of the fuzzy controller are a group of correction values, Δkp1 or Δki1, which correspond to the proportional control parameters and the integral control parameters in the PI controller. The ranges of the two outputs are also obtained by simulation and experiment, here the range of Δk_{p1} is [−1.5, +1.5], while Δk_{i1} [−1.5 × 10−3, +1.5 × 10−3]. Assuming that the fuzzy universe of Δk_{p1} and Δk_{i1} is also set as [−3, 3], the discrete set is {−3, −2, −1, 0, 1, 2, 3}. The following scale factor can be gotten to transform Δk_{p1} and Δk_{i1} from basic universe to fuzzy universe:

$$k_{c1} = \frac{1.5}{3} = 0.5$$

$$k_{c2} = \frac{1.5\times10^{-3}}{3} = 5\times10^{-4}$$

Considering that the input voltage error e and error change rate ec, as well as the output Δk_{p1} and Δk_{i1} can change in positive and negative directions, the fuzzy universe is described by seven linguistic values: “Negative Big (NB),” “Negative Middle (NM),” “Negative Small (NS),” “Zero (ZE),” “Positive Small (PS),” “Positive Middle (PM),” and “Positive Big (PB).” Then, the quantized discrete set {−3, −2, −1, 0, 1, 2, 3} can be described as fuzzy language set {NB, NM, NS, ZE, PS, PM, PB}. The membership function of input and output is defined as a triangular membership function, as shown in figure 3.28.

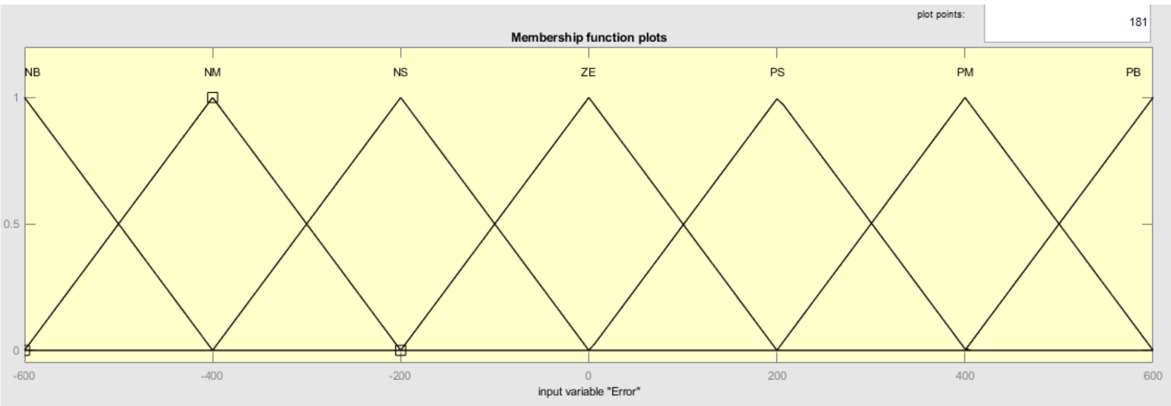

Figure 3.28 Triangular membership function of e,ec and kp1,ki1.

With the above two steps, the four correct input and output signals can be fuzzified and converted into a set of fuzzy language sets. The fuzzy rule circuit of the fuzzy controller directly affects the parameters of the PI controller, and then affects the dynamic and static characteristics of the inverter. First, the influence of PI parameters on the dynamic and static characteristics of the system is analyzed:

1. scaling factor kp: when kp is small, the response speed of the system is low, the adjustment time is long, the adjustment accuracy is low, the dynamic and static performance of the system is poor; As kp increases, the response speed of the system increases and the accuracy of the tuning system increases, but when kp is too large, the system will make a large overshoot and the oscillation time will increase, the adjustment time will be longer and in severe cases lead to system instability.

2. Integration coefficient ki: when ki is small, the static error of the system inference is

difficult to eliminate, resulting in poor system tuning accuracy; with an increase in ki, the rate of elimination of static errors in the system increases, but if ki is too large, the system will produce integral saturation in the initial period of the reaction, causing large emissions and even causing system fluctuations. This will affect the stability of the system. The saturation of the integral will be resolved by applying the conditional integral PI against winding.

In accordance with the influence of kp and ki on the dynamic and static characteristics of the system, a table of fuzzy controller rules has been developed. The transient response curve is shown in figure 3.28. According to the error range e and the rate of change of the error ec. The analysis looks like this:

i. part ab: if e and ec are large positives, larger kp and smaller ki will be required to achieve faster response rates and prevent large overshoot from occurring;
ii. part bc: if e is a positive medium, and ec is a large positive, then the higher kp, the medium ki is chosen to achieve a stable value as soon as possible;
iii. part cd: if e changes from a small positive value to 0, and ec has a large positive value, then large kp and ki should be chosen to ensure system stability;
iv. part de: if e changes from 0 to a small negative value and ec changes from a large positive value to 0, a larger kp and an average value of ki are required to suppress the overshoot;
v. part ef: if e is from a small negative value (or negative average) to 0 and ec is from 0 to a negative average, then the smallest kp should be chosen and ki is increased from a positive average to a positive large value to reduce or to suppress the secondary oscillation.
vi. part fg: if e is from 0 to a small positive value (or moderately positive), and ec is from a large negative value to a small negative value, then kp must be increased gradually and ki must be gradually decreased to increase the system response speed and avoid overshoot;
vii. Part gh : if e gradually decreases from a small positive value (or positive mean) to zero, and ec gradually decreases, then kp and ki must gradually increase for the system to have good stability.

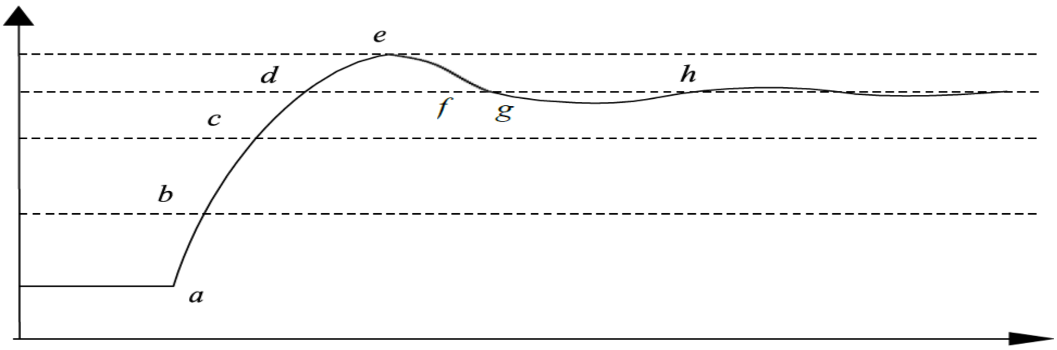

Figure 3.29 Step response curve

According to the above analysis, the fuzzy language rule tables of Δk_{p1} and Δk_{i1} are designed as shown in tables 3.5 and 3.6, respectively.

Table 3.5 Fuzzy rules for dkpi

e \ ec	NS	NM	NS	ZE	PS	PM	PB
NB	PB	PB	PB	PB	PS	ZE	NS
NM	PB	PM	PM	PM	ZE	NS	NM
NS	PM	PS	PM	PM	NS	ZE	NB
ZE	ZE	ZE	PS	PS	PS	ZE	ZE
PS	NB	NM	NS	PM	PM	PS	PM
PM	NM	NS	ZE	PM	PM	PM	PB
PB	NS	ZE	PS	PB	PB	PB	PB

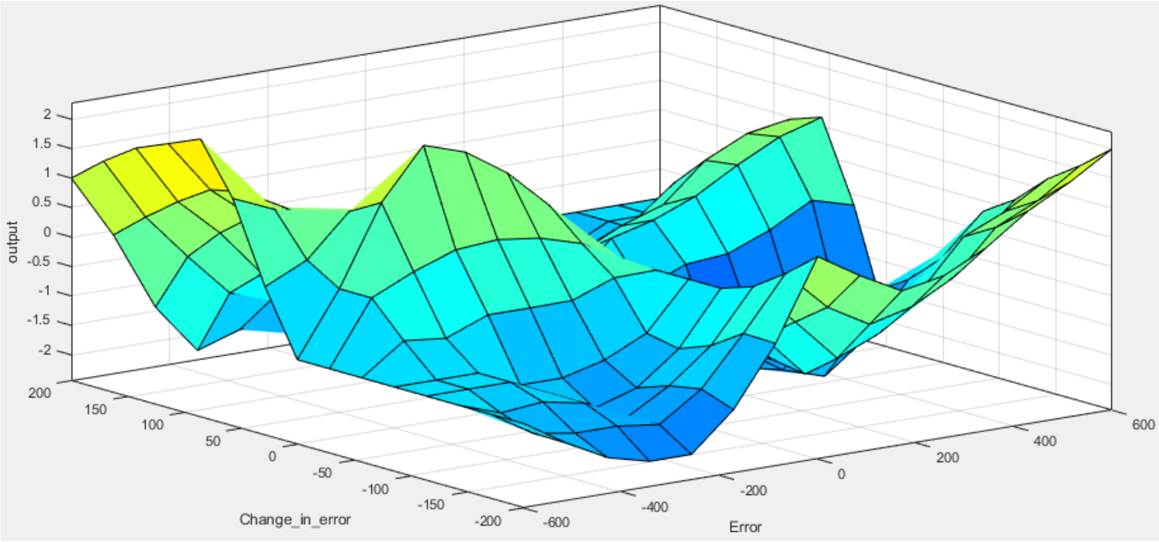

Figure 3.30 Fuzzy Ki rule surface

Table 3.6 Fuzzy rules for dki1

e \ ec	NB	NM	NS	ZE	PS	PM	PB
NB	NB	NB	NB	PB	PM	PS	ZE
NM	NB	NB	NM	PB	PS	ZE	NS
NS	NB	NM	NM	PM	ZE	NS	NM
ZE	ZE	ZE	PS	ZE	NS	NM	NM
PS	NM	NS	ZE	NS	ZE	NM	NB
PM	NS	ZE	PS	NM	PS	NB	NB
PB	ZE	PS	PM	NM	PM	NB	NB

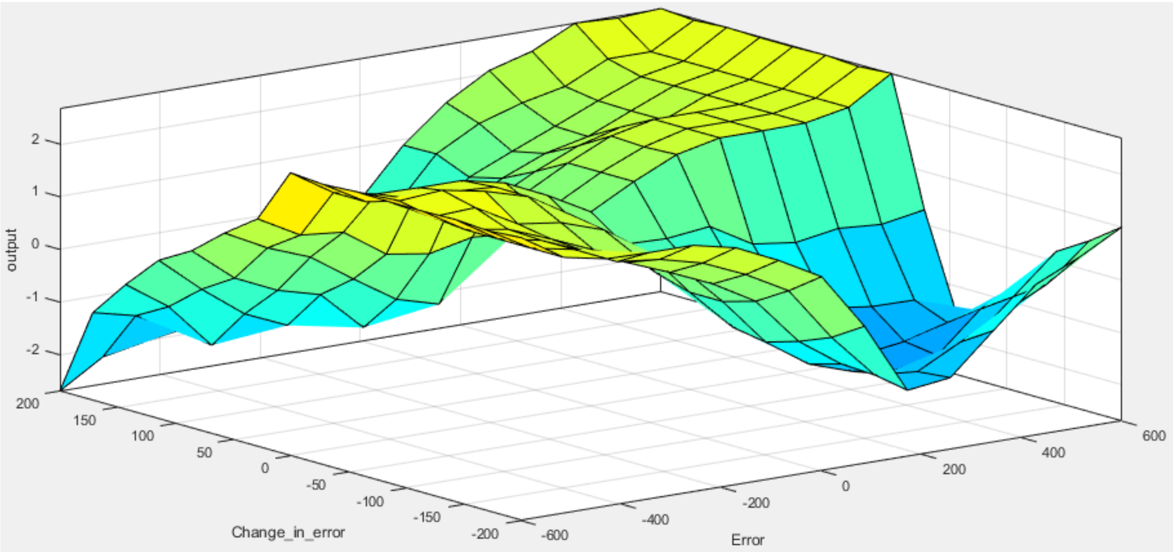

Figure 3.31 Fuzzy Rule surface for Kp

Any rule in the fuzzy rules table of Δk_{p1} and Δk_{i1} can be expressed in the form of "R_i: if *e* is A_i and *ec* is B_i then u is C_i." Then, the statement of fuzzy language rules table can be expressed as follows:

1)R_1: if *e* is NB and *ec* is NB then Δk_{p1} is PB and Δk_{i1} is NB 2)R_2: if *e* is NB and *ec* is NM then Δk_{p1} is PB and Δk_{i1} is NB 3)R_3: if *e* is NB and *ec* is NS then Δk_{p1} is PB and Δk_{i1} is NB . . .

49) R_{49}: if *e* is PB and *ec* is PB then Δk_{p1} is PB and Δk_{i1} is NB

For the membership function with seven linguistic values corresponding to the two inputs, the total number of the control rules is 7 × 7 = 49. Each fuzzy control rule can give a fuzzy implication relation R_i (i = 1, 2, . . . , 49). Then, the total fuzzy implication relations corresponding to fuzzy rules are as follows:

$R = R_1 \cup R_2 \cup \ldots R_{49}$

The result of fuzzification and fuzzy reasoning is the fuzzy set of Δk_{p1} and Δk_{i1}, so it is necessary to defuzzify the fuzzy set in order to get a clear and precise values of the correction. Here, the weighted average method is used to defuzzify. For each element x_i (i = 1, 2, . . . , n) in the universe, the membership degree $u(i)$ of the fuzzy set after fuzzification is taken as the weighting coefficient of the corresponding element, and the final decision value x_o can be obtained from the following equation

$$x_0 = \frac{\sum_{i=1}^{n} x_i . u(i)}{\sum_{i=1}^{n} u(i)} \tag{3.51}$$

After difuzzification, dki1 and dkp1 are transformed from fuzzy universe to basic universe through the scale factor and the final output value is obtained.

After applying all the methods used in this chapter, the result obtained and briefly explained under Result and discussion chapter.

CHAPTER FOUR

RESULT AND DISCUSSION

This chapter describes the result and the analysis of the proposed controller for grid connected microgrids under different operating scenario. The result of the research simulation is compared with the related works mentioned in the literature in order to achieve the specific research objectives. The simulation results explained in this chapter are carried out for the same values of the system parameter under study. In this research work, the MATLAB model of different operating modes of microgrid are modelled and simulated. The simulation with variation of parameters are divided into three major scenario for simplification and clarity of the research work. In a grid connected mode operation simulation are generally simulated to support voltage and frequency at the point of common coupling in the presence of grid under variation of solar irradiance variation. In a transient operation mode simulation the dynamic behavior of microgrid under study tested and battery energy storage system support is analyzed while fuzzy PI anti-windup and PI anti windup controller performances are compared.

4.1 Results

In this research work, Fuzzy-PI anti-windup control of grid tied microgrid which consists of solar PV power, battery energy storage system, load at the point of common coupling, utility power with three phase three level neutral point clamped inverter controlled are proposed .The results are explained thoroughly within the following sections.

4.1.1 Scenario 1: Grid Connected operation

In this scenario, the input parameters for solar PV array, solar irradiance are changing with time. The varying solar power is generated which have varying solar irradiation. Solar irradiation was assumed to be 500W/m2 between t=0hr (12 pm) and t= 5hr (6 am). Then solar irradiance increases to 700w/m2 between t=5hr(6 am) and t=18hr(6 pm) while eventually solar irradiance decrease to 500W/m2 between t = 18hr(6 Pm) and t=24hr(12 pm) which generates maximum solar power from solar array using MPPT and control boost converter to feed DC voltage to inverter while solar array temperature is kept constant to 25 °C. Generic 800KW solar power, 650KW load consumption which have a surge capability of 1301.625KW was connected at the point of common coupling with grid power of 630KVA utility transformer. The performance of the fuzzy PI anti-windup and PI anti wind-up are compared with each other which have better dynamic performance over conventional PI controller.

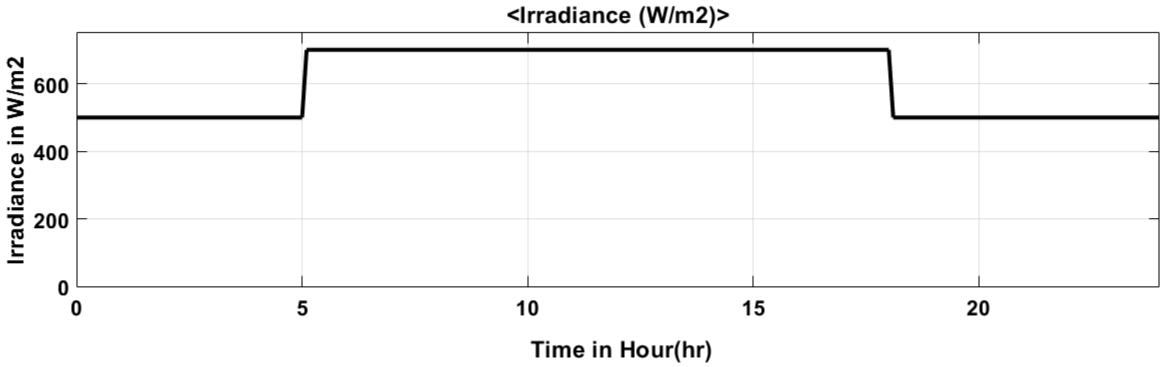

Figure 4.1 Simulink result of solar irradiance variation

As the input irradiance for solar are changing with time, battery output must supply variable power to compensate insufficient amount of power provided by solar PV. Utility grid is maintaining the voltage amplitude, frequency and phase. The main objective of this scenario, therefore, is to manage the active power injected and exported from and to the point of common coupling. Solar PV system operate under MPPT algorithm they can be modelled to generate optimal generation capacity of solar PV sources. The solar array MPPT using perturb and observe (P&O) algorithm control solar array to generate maximum available power in a specified solar irradiation. MPPT generates duty cycle in order to create switching signal for the boost converter. Solar PV system operate at optimum voltage of 500V DC in this thesis. The duty cycle for this scenario is as in figure 4.2.

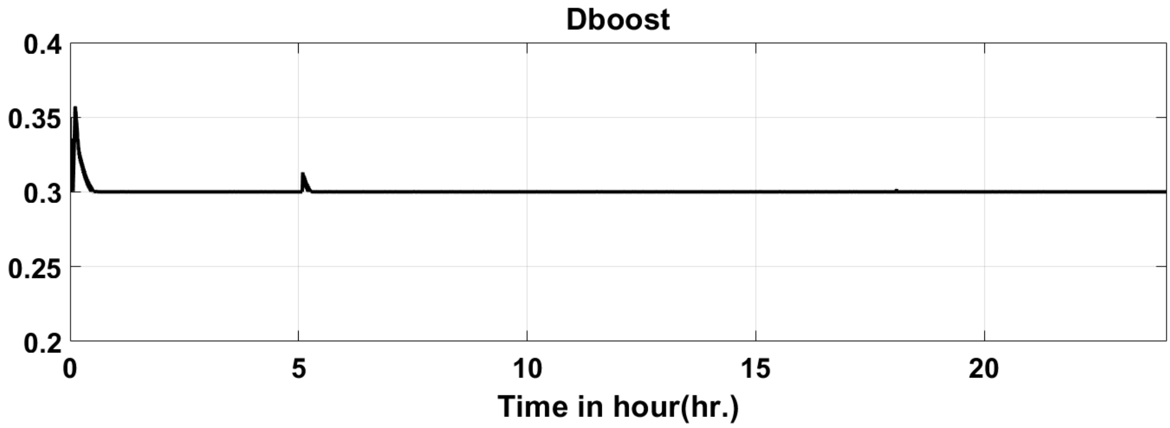

Figure 4.2 Boost duty cycle of solar PV boost converter

Within variation of solar irradiation solar PV system generates maximum power which feed into utility grid to support active power at the point of common coupling for continuous supply of load. The generated power and battery energy storage support at the point of common coupling for continuous supply of the load when solar PV system power reduces due to solar irradiance reduction is shown in figure 4.3.

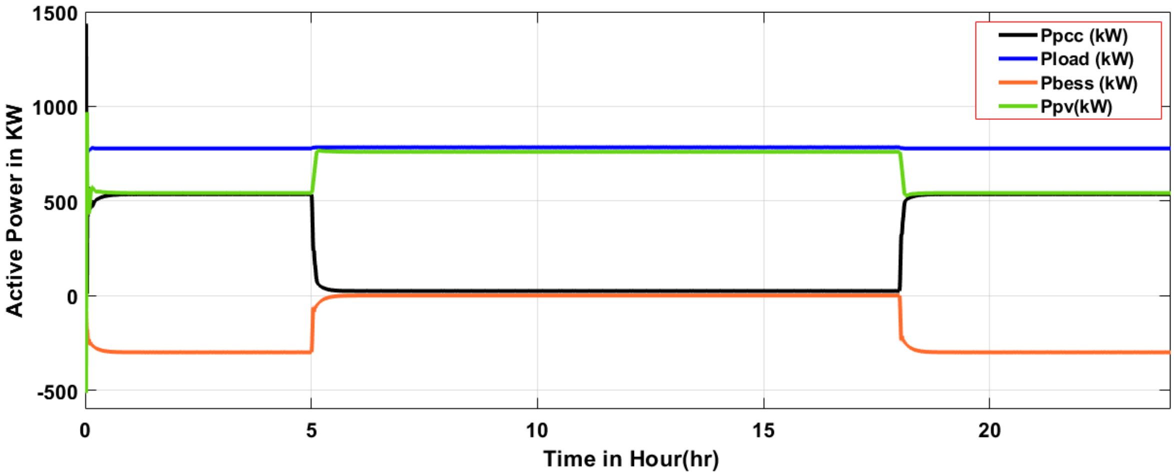

Figure 4.3 Variable power of microgrid

Figure 4.3 shows the variation of solar PV system power between t=12 pm and t=12pm hour while battery energy storage system injects active power to support the active power at the point of common coupling by injecting 300KW.The power at the point of common coupling increases as the power injected from battery energy storage system is greater than the reduced power due to solar irradiance reduction between t=0hr(12pm) to t=5hr(6 am), t= 5hr(6am) to t=18hr(6 pm) and t=18hr(6pm) to t=24hr(12 pm) . The battery energy storage system discharges to support constant load under varying irradiance.

Table 4.1 shows a frequency variation with solar irradiance variation which causes solar PV system power variation. The figure 4.3 shows variation of active power t=0hr and t=24hr which shows there are variation of active power at that point as the power of solar PV system decrease and increase respectively. The utility grid control voltage amplitude and frequency at the point of common coupling in a grid tied microgrid operation. The variation of frequency from nominal frequency 50Hz caused by variation of parameters is shown in table 4.1. Under varying parameters the frequency of the microgrid is the same as the frequency of utility grid in minimal variation due to parameter variation. Microgrid frequency vary between 50.1HZ and 50Hz due to solar PV system varies with small range.

Table 4.1 Frequency of grid connected microgrid

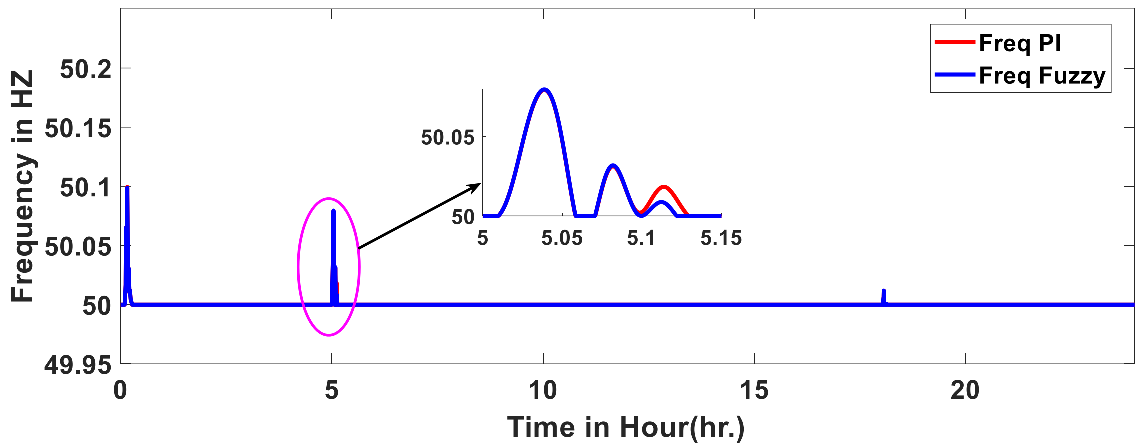

Fuzzy PI anti windup performance	PI anti windup performance

```
>> stepinfo(freq_fuzzy)

ans =

  struct with fields:

        RiseTime: 0
    SettlingTime: 4.5173e+04
     SettlingMin: 50
     SettlingMax: 50.0988
       Overshoot: 0.1976
      Undershoot: 0
```

```
>> stepinfo(freq_PI)

ans =

  struct with fields:

        RiseTime: 0
    SettlingTime: 4.5173e+04
     SettlingMin: 50
     SettlingMax: 50.0995
       Overshoot: 0.1991
      Undershoot: 0
```

Table 4.1 shows the result of MATLAB simulation for frequency deviation under varying irradiance and solar PV system while battery energy storage system is supplying active power to balance frequency deviation while comparing the controller robustness in which fuzzy PI anti-windup have less settling time and percentage overshoot over PI anti wind-up. For integration of microgrid with utility grid the phase difference must be with minimal phase angle. With small phase angle deviation keeping voltage amplitude and small frequency deviation microgrid connected to the grid. With the variation of variable power solar PV system voltage source inverter produces pure sinusoidal phase voltage signal.

The voltage deviation caused by the variation of solar irradiance are depicted in table 4.2. The nominal assumed voltage at the point of common coupling is 600V.The percentage of variation of voltage is in a small variation which have a dynamic performance using Fuzzy

PI ant-windup is the rise time of 0.2274 second, settling time of 240.6481 seconds (4.01 minutes) and percentage overshoot of 4.4634 per 600V.

Table 4.2 Phase voltage at the point of common coupling

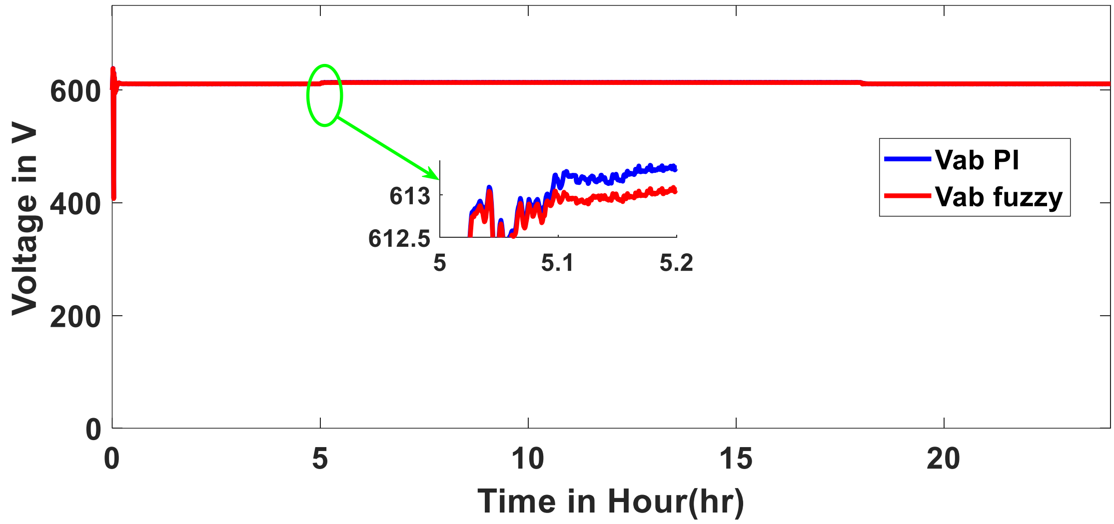

Fuzzy PI anti-windup performance

```
>> stepinfo(vab_fuzzy)

ans =

  struct with fields:

        RiseTime: 0.2274
    SettlingTime: 240.6481
     SettlingMin: 407.3346
     SettlingMax: 638.0889
       Overshoot: 4.4634
      Undershoot: 0
```

PI anti-windup performance

```
>> stepinfo(vab_PI)

ans =

  struct with fields:

        RiseTime: 0.2277
    SettlingTime: 240.7727
     SettlingMin: 407.8354
     SettlingMax: 638.2297
       Overshoot: 4.4766
      Undershoot: 0
```

The result from three phase three level neutral point clamped (NPC) inverter shows a perfect pattern of three phase sinusoidal voltage waveform with equal phase angle difference between each phase which is 120° at the point of common coupling as in the figure 4.4. The purpose of using the inverter was to get voltage wave form of

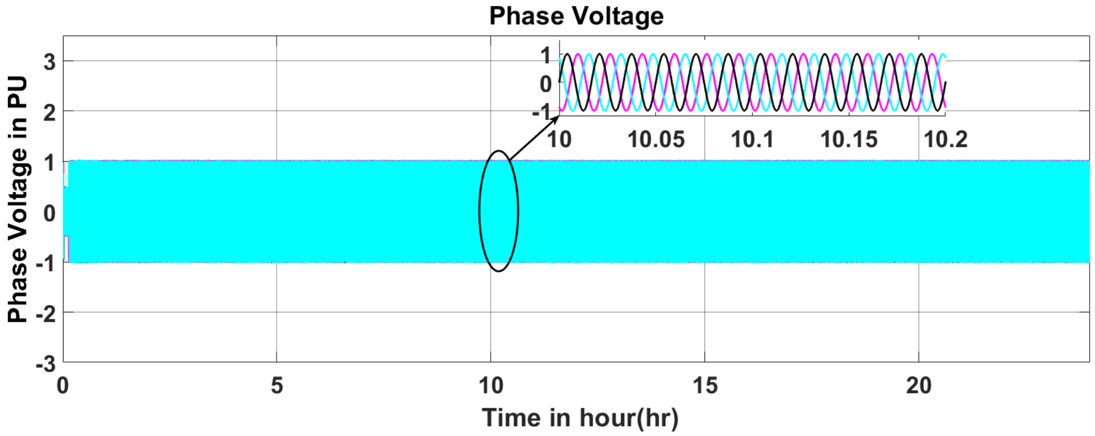

Figure 4.4 Three phase voltage at the point of common coupling.

4.1.2 Scenario 2: Microgrid Transient Operation

In this scenario solar irradiance assumed to be constant of 700W/m2 but the microgrid is islanded and reconnected to the utility grid between t=10 hr and t=15hr. The solar array is controlled with MPPT to generate constant maximum power at constant irradiance and temperature. In this transient operation microgrid supports voltage amplitude and frequency at the point of common coupling while the utility power is removed intentionally and resynchronized with microgrid. During transition from islanded system to resynchronization with utility grid the variation of voltage and frequency happen.

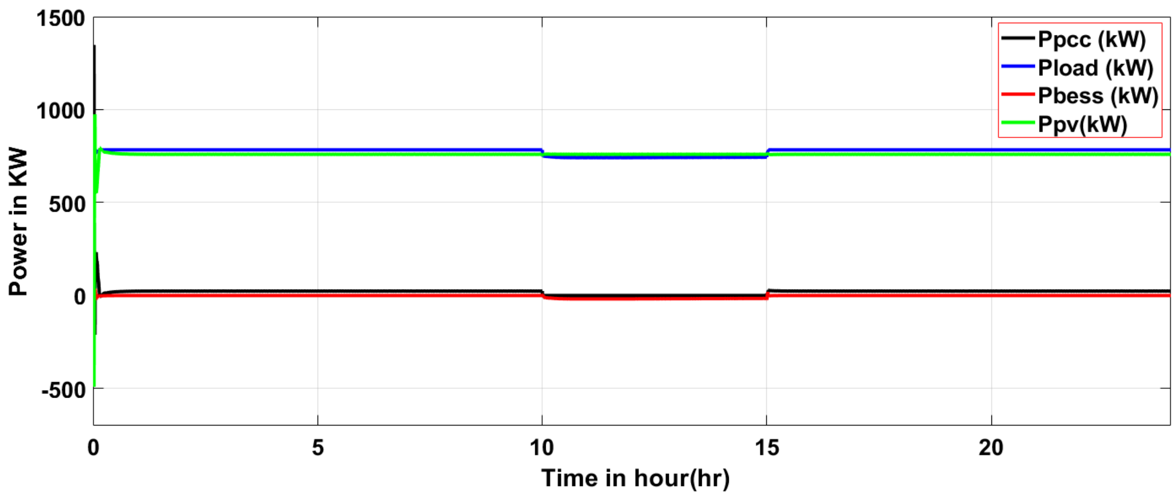

Figure 4.5 Power Variation in transient operation

The figure 4.5 describes the power change of components of microgrid under transient operation. The constant solar PV power is supplied to the grid. Between t=10 hr and t=15 hr microgrid control voltage, frequency and the load is completely supported with microgrid alone.After resynchronization microgrid again reconnect with utility grid with small variation in voltage level and frequency value.

Table 4.3 Frequency of transient operation

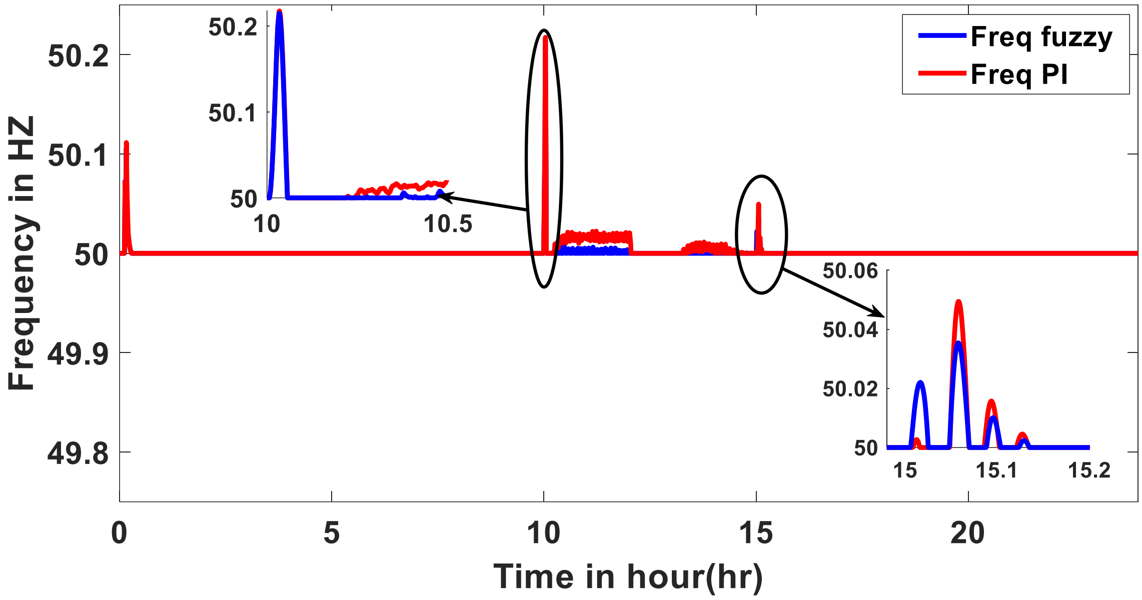

Fuzzy PI anti windup performance	PI anti windup performance
>> stepinfo(freq_fuzzy)	>> stepinfo(freq_PI)
ans =	ans =
struct with fields:	struct with fields:
RiseTime: 0	RiseTime: 0
SettlingTime: 3.7754e+04	SettlingTime: 3.7822e+04
SettlingMin: 50	SettlingMin: 50
SettlingMax: 50.2145	SettlingMax: 50.2173
Overshoot: 0.4290	Overshoot: 0.4346
Undershoot: 0	Undershoot: 0

Even if the generated power from solar PV system is constant changing from grid connected to isolated for t=5 hour between t= 10 hr and t=15hr causes voltage and frequency variation. The inverter and controllers work together to attain minimum acceptable variation range as shown in table 4.3 for frequency variation control in the transient operation mode of microgrid comparing fuzzy PI anti-windup and PI anti windup.

The fuzzy PI anti-windup dynamic frequency performance have a rise time of zero(0) seconds, settling time of 37754 seconds(10 hour) and percentage overshoot of 0.4290 per 50Hz fundamental frequency. Comparing with PI anti wind up have settling time of 37822 seconds (10:30 hour) and percentage overshoot of which is less than 13.88% less time comparing with fuzzy PI anti windup but have higher overshoot than fuzzy PI anti windup which have 0.4209 per 50Hz of fundamental frequency which have more overshoot percentage of 6.7429% compared with fuzzy PI ant windup. At the point of t=15 hr the PI anti windup have zero (0) overshoot comparing with PI anti windup as it is shown by ellipse and zoomed part seen clearly.

Table 4.4 Voltage At the point of common coupling

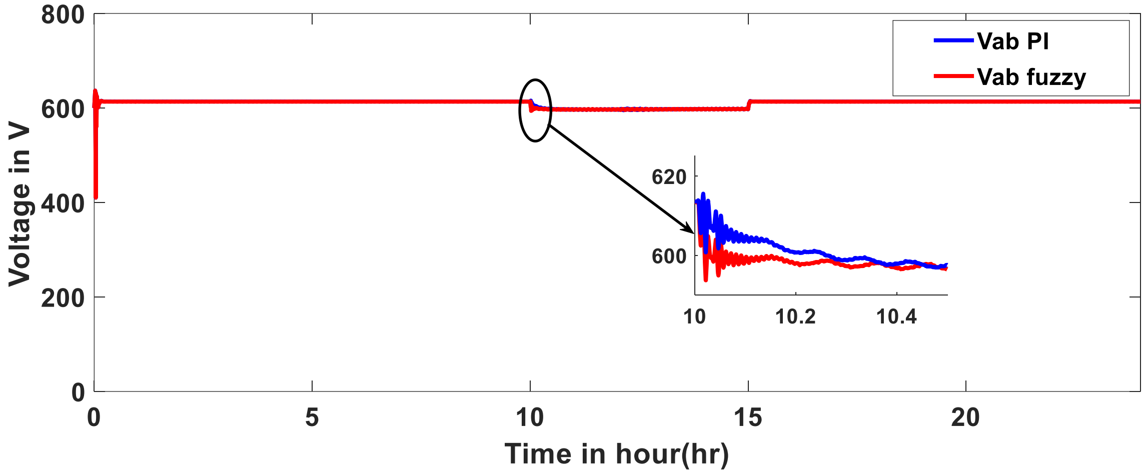

Fuzzy PI anti windup	PI anti windup
>> stepinfo(vab_fuzzy) ans = struct with fields: RiseTime: 0.2917 SettlingTime: 3.7568e+04 SettlingMin: 410.0812 SettlingMax: 636.7783 Overshoot: 3.8139 Undershoot: 0	>> stepinfo(vab_PI) ans = struct with fields: RiseTime: 0.2958 SettlingTime: 3.7571e+04 SettlingMin: 410.0812 SettlingMax: 636.7783 Overshoot: 3.7818 Undershoot: 0

The table 4.4 depicts the variation of voltage at the point of common coupling under transient operation of microgrid. Microgrid is islanded on t=10hr and seamlessly resynchronized to the utility grid on t=15 hr. The phase voltage at the point of common coupling depicts that the voltage phase amplitude and frequency was varied when the microgrid is islanded and the varied voltage stabilized to normal sinusoidal wave form after synchronization. This scenario describes this situation as its dynamic performance varied from normal operating mode with increase percentage overshoot to 3.81391% and the voltage phase angle is distributed equally after smooth resynchronization. The fuzzy PI anti windup have dynamic voltage performance have a rise time of 0.2917 second ,settling time of 37568 second(10:20 hour) and percentage overshoot of 3.8139 per 600V. But, PI anti windup results dynamic voltage performance have a rise time of 0.2958 second ,settling time of 37571 second(10:30 hour) and percentage overshoot of 3.7818 per 600V.

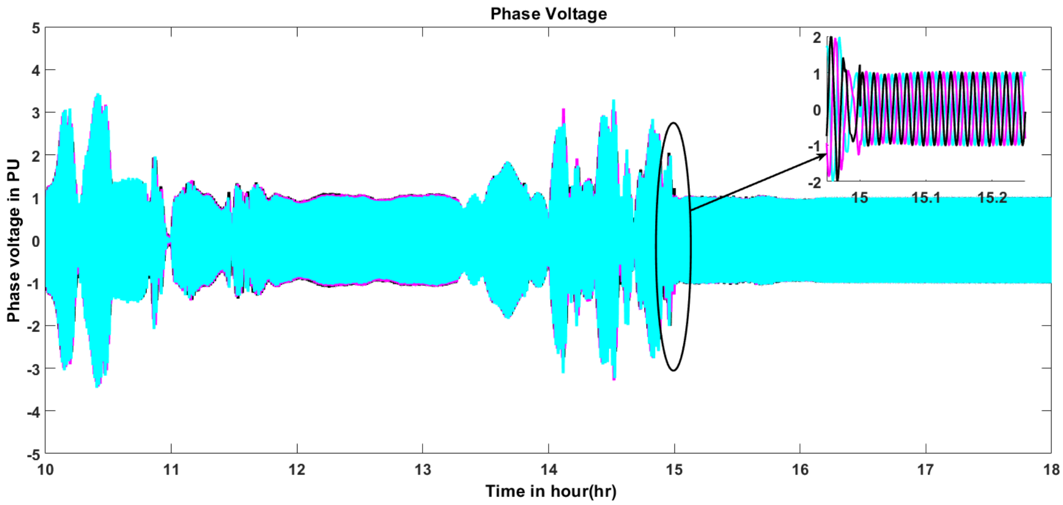

Figure 4.6 Three phase voltage at the point of common coupling

The figure 4.6 describes the (pu) variation of three phase voltage at the point of common coupling due to switching on and off of the existing utility grid. The transient operation have higher frequency dynamic performance than variation in scenario 1.

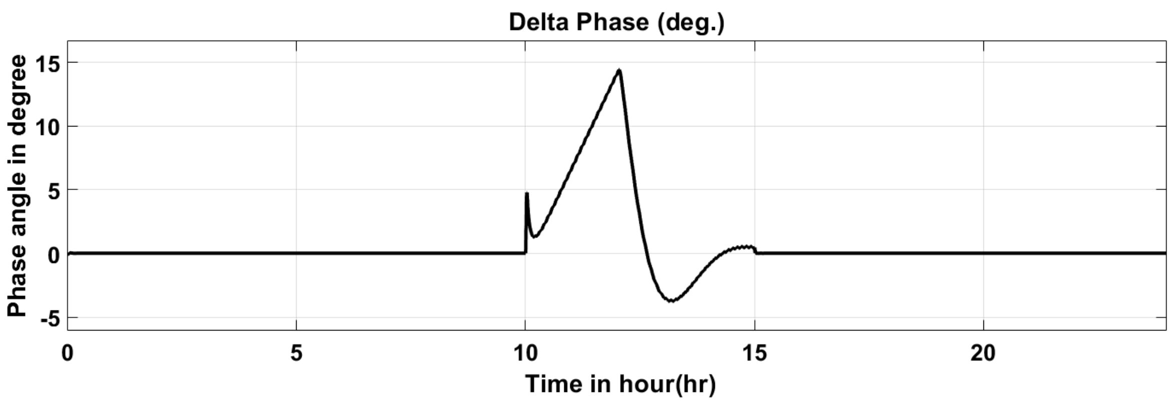

Figure 4.7 Phase difference

The minimum deviation of phase difference was due to microgrid tried to produce its own frequency and voltage in islanded operation but after synchronization the phase difference reduces to zero. The microgrid supports frequency deviation in islanded operation of microgrid as in the table 4.3 as it varies the frequency with a minimum of 0.2Hz in islanded situation and it forms its own frequency and the inverter acts as grid forming inverter while it follows grid in grid connected operation modes.

4.1.3 Scenario 3: Load Imbalance compensation

Load imbalance in this scenario is caused while the single phase load switched on at t=5hr.The solar PV system is generating constant power while the microgrid is connected to the grid. Battery energy storage system immediately injects active power to support load at the point of common coupling which increases active power at the point of common coupling.

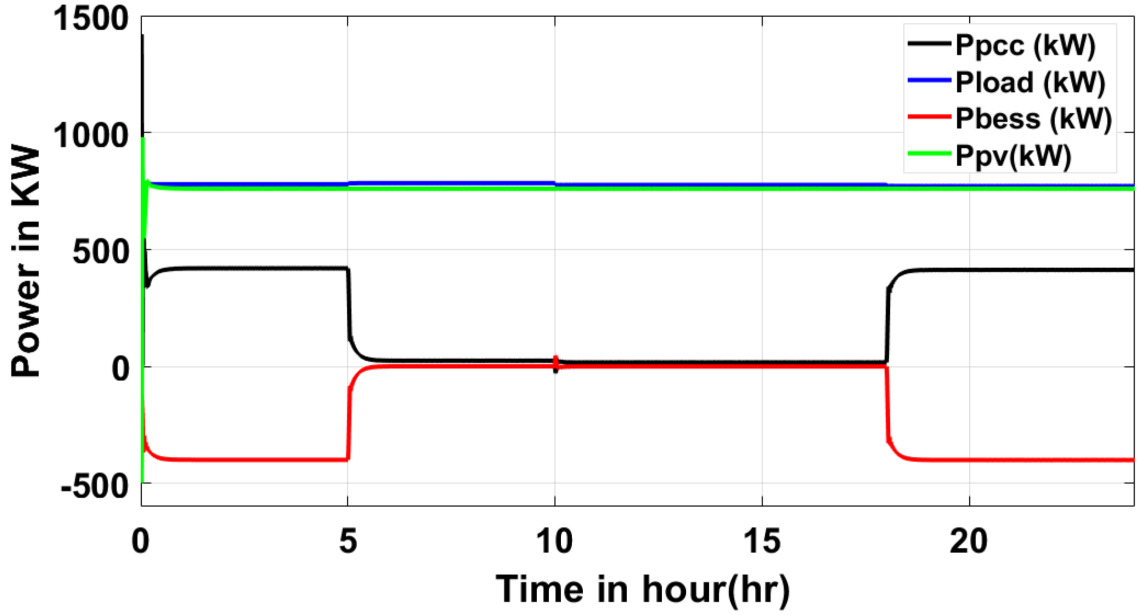

Figure 4.8 Power variation

Figure 4.8 shows load power decrease at the t=10 hour, battery energy storage system injects active power to compensate imbalance which increases active power at the point of common coupling. All the components of the microgrid works together and are stable after load is balanced on t=10 hour.

Table 4.5 Frequency Variation due to load imbalance

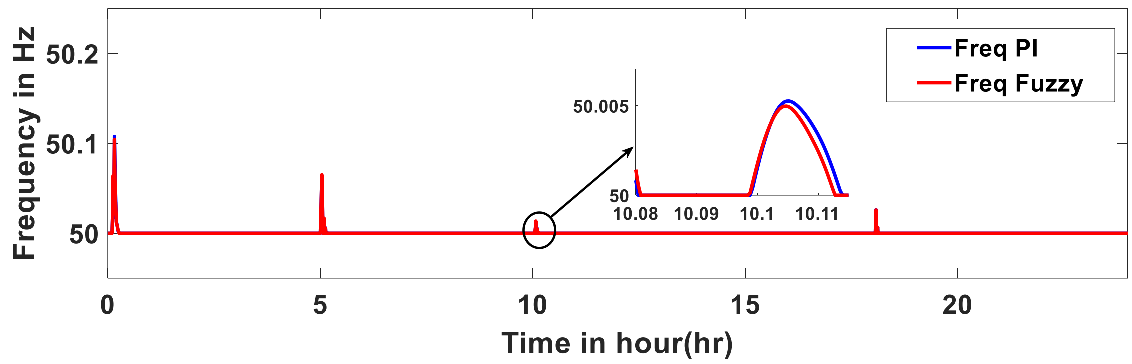

Fuzzy PI anti windup dynamic performance	PI anti wind up dynamic performance

`>> stepinfo(freq_fuzzy)`
`ans =`
`struct with fields:`
`RiseTime: 0`
`SettlingTime: 4.5302e+04`
`SettlingMin: 50`
`SettlingMax: 50.1044`
`Overshoot: 0.2088`
`Undershoot: 0`
	`>> stepinfo(freq_PI)`
	`ans =`
	`struct with fields:`
	`RiseTime: 0`
	`SettlingTime: 4.5302e+04`
	`SettlingMin: 50`
	`SettlingMax: 50.1077`
	`Overshoot: 0.2154`
	`Undershoot: 0`

Imbalance compensation applied immediately when microgrid single phase load switched on which resulted in imbalance of voltage and frequency. The immediate action of load balance kept frequency in acceptable range of 49.5Hz < f < 50.5Hz without causing great disturbance in a system.

The inverter and controllers work together to attain minimum acceptable variation range as shown in table 4.5 for frequency variation control for imbalance compensation of microgrid comparing fuzzy PI anti-windup and PI anti windup.

The fuzzy PI anti-windup dynamic frequency performance have a rise time of zero(0) seconds, settling time of 45302 seconds(12:30 hour) and percentage overshoot of 0.2088 per 50Hz fundamental frequency. Comparing with PI anti wind up dynamic frequency performance results in rise time of zero(0) second, settling time of 45302 seconds(12:30 hour) and percentage overshoot of 0.2154 per 50Hz. Comparing with fuzzy PI anti windup have better overshoot than PI anti windup.

Table 4.6 Phase Voltage at PCC imbalance compensation

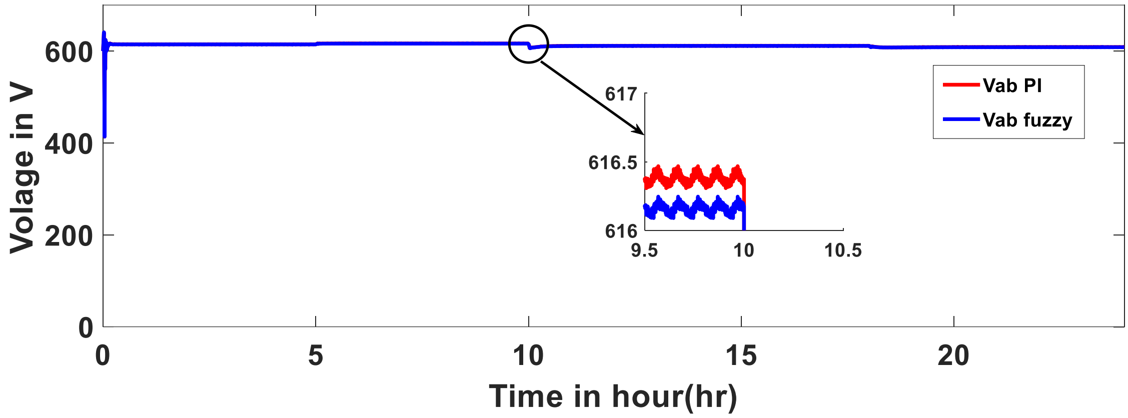

Fuzzy PI dynamic performance	PI anti windup dynamic performance
>> stepinfo(vab_fuzzy) ans = struct with fields: RiseTime: 0.1666 SettlingTime: 2.5021e+04 SettlingMin: 413.6697 SettlingMax: 640.5121 Overshoot: 5.2722 Undershoot: 0	>> stepinfo(vab_PI) ans = struct with fields: RiseTime: 0.1708 SettlingTime: 2.5021e+04 SettlingMin: 413.6697 SettlingMax: 640.5121 Overshoot: 5.2347 Undershoot: 0

The table 4.6 depicts the variation of voltage at the point of common coupling under imbalance of microgrid. Single phase load is switched on t = 10hr and imbalance compensator turned on t = 10hr to compensate imbalance. This scenario describes this situation as its dynamic performance varied from normal operation to imbalanced until it removed. Fuzzy PI anti windup have dynamic voltage performance have a rise time of 0.1666 second, settling time of 25021 seconds(7 hour) and percentage overshoot of 5.2722 per 600V.Also, PI anti windup results dynamic voltage performance have a rise time of 0.1708 second, settling time of 25021 second(7 hour) and percentage overshoot of 5.2347 per 600V.

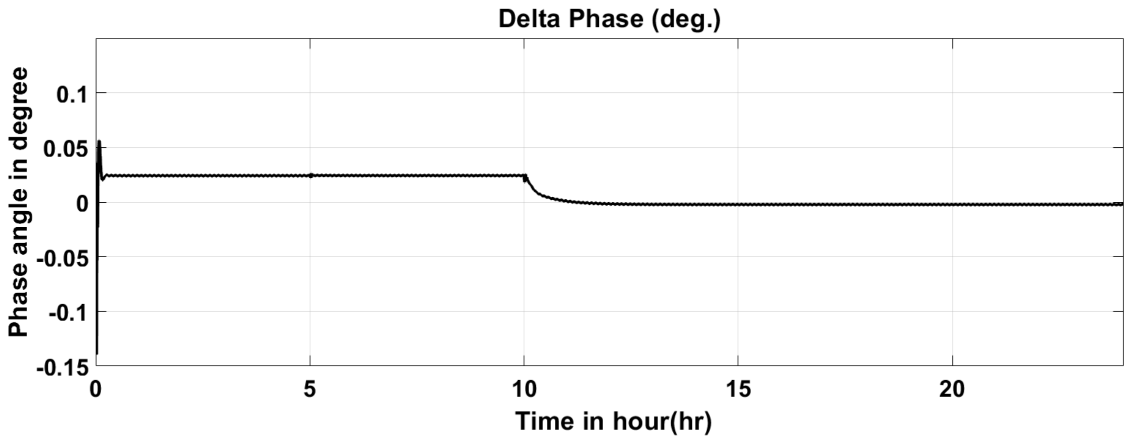

Figure 4.9 Phase difference

The minimum deviation of phase difference was due to load imbalance caused while single phase switched on which caused voltage and frequency variation and the phase difference reduces to zero after compensating the load imbalance. The microgrid supports frequency deviation in as well as the voltage amplitude variation after imbalance removed.

4.2 Discussion

4.2.1 Discussion of grid Connected mode of operation of microgrid

In the grid connected mode operation of microgrid the utility grid support voltage and frequency. The microgrid support active and reactive power at the point of common coupling. But, solar active power varies with irradiance variation which causes voltage and frequency deviation which supported by BESS active power. In this variation fuzzy PI anti windup shows better performance in reducing settling time, rise time and have less percentage overshoot compared to PI anti windup. The overall performance of both controller and their specific performance for irradiance variation checked on the frequency and voltage amplitude variation at the point of common coupling while the frequency and voltage is controlled by utility grid. The microgrid better works while utility exist by integrating all existing power at one common point of interconnection to fully and supply load without interruption. The battery energy storage system act as a master unit which is responsible for active power regulation, frequency and voltage support at the point of common coupling. Fuzzy Pi anti wind up have better dynamic performance over PI anti windup.

4.2.2 Discussion of microgrid transient Operation

In this operation mode of microgrid the irradiance is constant but the utility grid shut down for minimum of t=5 hr to check the voltage and frequency deviation because the microgrid will control and form its own voltage and frequency. The proposed fuzzy logic PI anti windup controller compared with conventional PI anti windup controller and again the fuzzy PI anti windup controller have a better dynamic properties. After the utility back up the utility grid again starts to control both frequency and voltage at the point of common coupling. The performance of the controller fuzzy PI anti windup controller and PI anti wind up the performance of the controller is tested on the frequency and voltage of Point of common coupling and utility grid bus.

4.2.3 Load Imbalance compensation in a grid connected mode of operation

Load imbalance compensation to balances the load power with available power at the point of common coupling causing small variation in voltage, frequency and active power regulation. But, the battery energy storage system which act as the master unit injects active power to support load balance. Voltage source inverter outer voltage loop and inner current loop controlled with fuzzy PI anti wind up and PI anti wind up for better dynamic performance of the varied parameter which was voltage amplitude and frequency. When compared with each other the fuzzy PI anti wind up have a better dynamic performance.

CHAPTER FIVE

CONCLUSIONS AND RECOMMENDATIONS

5.1 Conclusions

In order to reduce reliance on fossil fuel power generation, decentralized renewable energy technologies are becoming increasingly important, environmentally friendly, highly efficient and relatively inexpensive alternative energy sources in the world. The microgrid concept was developed for decentralized generation (DG) integration with energy from the grid to support local load with less interruption and power cut. A nonlinear model of microgrid for ASTU student cafeteria load is developed. Various significant aspects of the microgrid system, such as sizing, modeling, optimization, and analysis of system components were discussed. The different components and overall microgrid system were modeled using MATLAB/Simulink. The appropriate sizes of microgrid system elements were applied and the models are simulated based on the mathematical modeling. Also the design of micro source controller operating in grid-connected mode to control active power, and in transient mode to control voltage and frequency has been demonstrated in MATLAB/ SIMULINK.

In this work, the dynamic control of grid connected microgrid consisting of solar PV system and battery energy storage system was investigated. Maximum power point tracking using perturb and observe (P&O) algorithm have been used and the algorithm is the best algorithm supported solar array to produce maximum power. The voltage source inverter was designed and it was responsible to set up the microgrid voltage and frequency. The design of the solar PV plant, BESS and voltage source inverter was also validated. Solar power changes according to weather condition which causes fluctuation of frequency and voltage set-point according to the load change and change renewable power generations at the point of common coupling. However, the frequency and voltage can be maintained within the normal range of operation by setting the appropriate controller values without breaking grid codes. A flexible design of microgrid is capable of integrating different energy sources. The designed microgrid properly supply ASTU student cafeteria load and provide ancillary services to the utility grid. Power flow regulation, voltage and frequency stability are ensured under different operation of microgrid. Fuzzy PI anti-windup controller is designed such that operation of each device is guaranteed. The dynamic performance grid-tied microgrid frequency under grid connected operation with variation irradiance using proposed fuzzy PI anti windup controller have the rise time of zero (0) second, settling time of 45173 seconds (12:30 hour) and percentage overshoot of 0.1976 per 50Hz. Also, under varying irradiance of grid connected microgrid phase to phase voltage dynamic performance at point of common coupling using proposed fuzzy PI anti-windup have the rise time of 0.2274 second, settling time of 240.6481 seconds and overshoot of 4.4634 per 600V.The dynamic performance of frequency in transient operation of microgrid under constant solar irradiation but the microgrid islanded for 5 hour and resynchronized to utility grid using proposed fuzzy PI anti windup have the rise time of zero (0) ,settling time of 37754 seconds(10:30 hours) and percentage overshoot of 0.4290 per 50Hz.Also,under transient operation phase to phase voltage at the point of common coupling dynamic performance using proposed fuzzy PI anti-windup have the rise time of 0.2917 seconds, settling time of 37568 seconds(10:20 hours) and percentage overshoot of 3.8139 per 600V.The simulation result in all aspects validates the importance of voltage, frequency and active power control in a grid connected microgrid. The imbalanced system balanced with implementing imbalance compensation of negative sequence voltage in a minimal possible time for overall system stability.

5.2 Recommendations

The proposed microgrid, solar PV system with battery energy storage system, is investigated to be efficient and reliable in terms of enhanced dispatchablity and minimum parameter variation for ASTU student cafeteria load. These designed microgrid have been demonstrated using ASTU student cafeteria which demand continuous power needs to supply for its sensitive loads. Therefore this study would like to recommend for the application of the proposed microgrid with its designed PEVSIs and microgrid components controllers so that it can be used as a model to other microgrids to be developed for the intended purpose of reliable power supply to sensitive loads. It is also possible to develop other type of comprehensive microgrid with a different combination of microsources. Also it is possible to develop a microgrid to support all loads of a community whenever power from the utility is interrupted.

Implementation of load sharing between inverters could be future research direction. Also, future researchers can study and investigate the microgrid system for other areas with similar problems.

Acknowledgements: This research theses is was funded by Adama Science and Technology University under the grant number of **ASTU/SM-R/172/20**, Adama, Ethiopia.

REFERENCES

[1] B. Lekouaghet, A. Boukabou, N. Lourci, and K. Bedrine, "Control of PV grid connected systems using MPC technique and different inverter configuration models," *Electr. Power Syst. Res.*, vol. 154, pp. 287–298, 2018, doi: 10.1016/j.epsr.2017.08.027.

[2] T. Aydemir and D. A. G. Bu, "A simplified stability analysis method for LV inverter-based microgrids," vol. 7, pp. 612–620, 2019, doi: 10.1007/s40565-018-0478-1.

[3] W. Guo and L. Mu, "Control principles of micro-source inverters used in microgrid," *Prot. Control Mod. Power Syst.*, pp. 1–7, 2016, doi: 10.1186/s41601-016-0019-8.

[4] T. L. Vandoorn, S. Member, B. Meersman, S. Member, J. D. M. De Kooning, and S. Member, "Transition from Islanded to Grid-Connected Mode of Microgrids with Voltage-Based Droop Control," pp. 1–9.

[5] Y. V. P. Kumar, S. Member, and R. Bhimasingu, "Fuzzy Logic Based Adaptive Virtual Inertia in Droop Control Operation of the Microgrid for Improved Transient Response," 2017.

[6] A. H. Kasem Alaboudy, H. H. Zeineldin, and J. Kirtley, "Microgrid stability characterization subsequent to fault-triggered islanding incidents," *IEEE Trans. Power Deliv.*, vol. 27, no. 2, pp. 658–669, 2012, doi: 10.1109/TPWRD.2012.2183150.

[7] N. Soni, S. Member, and S. Doolla, "Improvement of Transient Response in Microgrids Using Virtual Inertia," vol. 28, no. 3, pp. 1830–1838, 2013.

[8] T. Nadu, "Safety Assured Reliable Microgrid," vol. 6, no. 14, pp. 81–90, 2017.

[9] K. C. Soni, A. S. Adesara, and D. B. Parmar, "Control Strategy of Microgrid during Grid-Connected Mode," vol. 2, no. 2, pp. 2018–2022, 2018.

[10] L. P. Sampaio, M. A. G. De Brito, G. De Azevedo E Melo, and C. A. Canesin, "Grid-tie three-phase inverter with active and reactive power flow control capability," *2013 Brazilian Power Electron. Conf. COBEP 2013 - Proc.*, no. Lmi, pp. 1039–1045, 2013, doi: 10.1109/COBEP.2013.6785243.

[11] M. Z. Daud, A. Mohamed, and M. A. Hannan, "Optimization of PI compensator parameters for grid-tied photovoltaic with energy storage systems using simplex

algorithm,” *Int. Rev. Model. Simulations*, vol. 5, no. 2, pp. 751–760, 2012.

[12] P. Piagi and R. H. Lasseter, “Autonomous control of microgrids,” *2006 IEEE Power Eng. Soc. Gen. Meet. PES*, 2006, doi: 10.1109/pes.2006.1708993.

[13] D. K. Dheer, N. Soni, and S. Doolla, “Improvement of small signal stability margin and transient response in inverter-dominated microgrids,” *Sustain. Energy, Grids Networks*, vol. 5, pp. 135–147, 2016, doi: 10.1016/j.segan.2015.12.005.

[14] S. Rivera, A. M. Farid, and K. Youcef-Toumi, “Coordination and Control of Multiple Microgrids Using Multi-Agent Systems,” *Energypath 2013 Our Glob. Sustain. Energy Futur.*, pp. 1–5, 2013, [Online]. Available: http://amfarid.scripts.mit.edu/resources/SPG-C14.pdf.

[15] F. Frame, “Power Management of Inverter Interfaced Autonomous Microgrid Based on Virtual,” vol. 2, no. 1, pp. 30–40, 2011.

[16] R. Lasseter, *Control and Design of Microgrid Components*. 1996.

[17] E. Villanueva, P. Correa, J. Rodriguez, and M. Pacas, “Control of a single-phase cascaded H-bridge multilevel inverter for grid-connected photovoltaic systems,” *IEEE Trans. Ind. Electron.*, vol. 56, no. 11, pp. 4399–4406, 2009, doi: 10.1109/TIE.2009.2029579.

[18] D. Kondoleon, L. Ten-Hope, T. Surles, and R. L. Therkelsen, “The CERTS MicroGrid Concept,” *Integr. Distrib. Energy Resour. – CERTS MicroGrid Concept*, no. October, p. 32, 2003, [Online]. Available: http://certs.lbl.gov/pdf/50829.pdf.

[19] M. Saleh *et al.*, “MPPT Design Using PSO Technique for Photovoltaic System Control Comparing to Fuzzy Logic and P&O Controllers,” *Energy Power Eng.*, vol. 8, no. 2, pp. 349–366, 2017, doi: 10.4236/epe.2016.811031.

[20] S. A. Roosa, “Introduction to Microgrids,” *Fundam. Microgrids*, pp. 1–16, 2020, doi: 10.1201/9781003082408-1.

[21] C. Loane, G. Roos, G. Hardy, and B. Dell, “Operation and Control of a Hybrid AC–DC,” *Core.Kmi.Open.Ac.Uk*, vol. 117, pp. 112–123, 2013, [Online]. Available: http://core.kmi.open.ac.uk/download/pdf/11243429.pdf.

[22] L. Ali and F. Shahnia, “Determination of an economically-suitable and sustainable

standalone power system for an off-grid town in Western Australia," *Renew. Energy*, vol. 106, pp. 243–254, 2017, doi: 10.1016/j.renene.2016.12.088.

[23] E. W. Prehoda, C. Schelly, and J. M. Pearce, "U.S. strategic solar photovoltaic-powered microgrid deployment for enhanced national security," *Renew. Sustain. Energy Rev.*, vol. 78, pp. 167–175, 2017, doi: 10.1016/j.rser.2017.04.094.

[24] T. P. To *et al.*, "Robust adaptive nonlinear control of microgrid frequency and voltage in the presence of renewable energy sources by," 2017.

[25] S. Chowdhury, S. P. Chowdhury, and P. Crossley, *Microgrids and active distribution networks*. 2009.

[26] R. P, R. I. Vais, S. Yadav, and P. Swarup, "A Modified PI Control for Grid-tied Inverters to Improve Grid Injected Current Quality," *Int. J. Eng. Technol.*, vol. 9, no. 3S, pp. 529–534, 2017, doi: 10.21817/ijet/2017/v9i3/170903s080.

[27] P. J. Binduhewa, M. Barnes, and A. Renfrew, "Standard microsource interface for a microgrid," *IET Semin. Dig.*, vol. 2008, no. 12380, 2008, doi: 10.1049/ic:20080431.

[28] G. P. P. System, "Modeling and Simulation for an 8 kW Three-Phase," *Res. Artic.*, pp. 603–612, 2017.

[29] C. Yongning, L. Yan, L. Zhen, C. Ziyu, and L. Hongzhi, "Study on Grid-connected Renewable Energy Grid Code Compliance," *iSPEC 2019 - 2019 IEEE Sustain. Power Energy Conf. Grid Mod. Energy Revolution, Proc.*, pp. 72–75, 2019, doi: 10.1109/iSPEC48194.2019.8974936.

[30] M. B. E. N. Smida and A. Sakly, "Particle Swarm Optimization Control of a Grid Connected Solar / Wind Energy System," vol. 4, pp. 18–23, 2017.

[31] W. He, X. Zhang, W. Wei, and L. Shi, "Parameters Tuning of Photovoltaic Power Generation System with Static Synchronous Compensator Based on Chaos Orthogonal Particle Swarm Optimization," *IOP Conf. Ser. Earth Environ. Sci.*, vol. 384, no. 1, 2019, doi: 10.1088/1755-1315/384/1/012053.

[32] T. P. Sahu and T. V. Dixit, "Modelling and analysis of perturb and observe and incremental conductance MPPT algorithm for PV array using Ċuk converter," *2014 IEEE Students' Conf. Electr. Electron. Comput. Sci. SCEECS 2014*, vol. 4, no. 2, pp. 213–224, 2014, doi: 10.1109/SCEECS.2014.6804468.

[33] S. Sezen, A. Aktas, M. Ucar, and E. Ozdemir, "A three-phase three-level NPC inverter based grid-connected photovoltaic system with active power filtering," *16th Int. Power Electron. Motion Control Conf. Expo. PEMC 2014*, no. September 2014, pp. 1331–1335, 2014, doi: 10.1109/EPEPEMC.2014.6980697.

[34] M. Sarvi and A. Azadian, *A comprehensive review and classified comparison of MPPT algorithms in PV systems*, no. 0123456789. Springer Berlin Heidelberg, 2021.

[35] H. Islam *et al.*, "Performance evaluation of maximum power point tracking approaches and photovoltaic systems," *Energies*, vol. 11, no. 2, pp. 7–9, 2018, doi: 10.3390/en11020365.

[36] K. Deželak, P. Bracinik, K. Sredenšek, and S. Seme, "Proportional-integral controllers performance of a grid-connected solar pv system with particle swarm optimization and ziegler–nichols tuning method," *Energies*, vol. 14, no. 9, 2021, doi: 10.3390/en14092516.

[37] C. N. Rowe, T. J. Summers, R. E. Betz, and T. G. Moore, "A virtual Point of Common Coupling voltage for improved droop control in microgrids," *15th Int. Power Electron. Motion Control Conf. Expo. EPE-PEMC 2012 ECCE Eur.*, pp. 1–8, 2012, doi: 10.1109/EPEPEMC.2012.6397453.

[38] I. V. Banu and M. Istrate, "Study on three-phase photovoltaic systems under grid faults," *EPE 2014 - Proc. 2014 Int. Conf. Expo. Electr. Power Eng.*, no. Epe, pp. 1132–1137, 2014, doi: 10.1109/ICEPE.2014.6970086.

[39] R. Krishna, *Grid Connected Three-Level Converters - Studies for Wave Energy Conversion*, vol. 78. 2014.

[40] S. Görtz, "Battery energy storage for intermittent renewable electricity production. A review and demonstration of energy storageapplications permitting higher penetration of renewables," *Examensarbete för Civil. i Energitek.*, p. 82, 2015, [Online]. Available: https://www.diva-portal.org/smash/get/diva2:818683/FULLTEXT01.pdf.

[41] M. Abdel-Salam, A. Ahmed, and M. Mahrous, "Transient analysis of grid-connected wind-driven PMSG, DFIG and SCIG at fixed and variable speeds," *Innov. Syst. Des. ...*, vol. 2, no. 3, 2011, [Online]. Available: http://www.iiste.org/Journals/index.php/ISDE/article/view/222.

[42] S. Paul, “Islanding Detection in Grid-Connected 100 KW Photovoltaic System Using Wavelet Transform,” *Int. J. Innov. Res. Sci. Eng. Technol.*, vol. 5, no. 5, pp. 92–98, 2016.

[43] W. Bower, W. Bower, I. Llc, J. Reilly, and R. Associates, “AdvancedMicrogrid_Integration-Interoperability_March2014.pdf,” no. March, pp. 1–56, 2014.

[44] C. Science, “VOLTAGE REGULATION OF DC-MICROGRID WITH PV AND BATTERY Voltage Regulation of DC-Microgrid with PV and Battery Case Western Reserve University Case School of Graduate Studies,” 2017.

[45] S. Salman, X. Ai, and Z. Wu, “Design of a P-&-O algorithm based MPPT charge controller for a stand-alone 200W PV system,” *Prot. Control Mod. Power Syst.*, vol. 3, no. 1, 2018, doi: 10.1186/s41601-018-0099-8.

[46] S. Algburi, “Stand-Alone Photovoltaic System,” no. March 2016, 2017.

[47] A. Rhma and M. Khemliche, “Optimal Fuzzy Logic Controller Based on PSO for the MPPT in Photovoltaic System,” pp. 1–6, 2014.

[48] M. F. Roslan, A. Q. Al-Shetwi, M. A. Hannan, P. J. Ker, and A. W. M. Zuhdi, *Particle swarm optimization algorithm-based PI inverter controller for a grid-connected PV system*, vol. 15, no. 12 December. 2020.

[49] O. Lodin, I. Kaur, and H. Kaur, “Predictive-P&O MPPT algorithm for fast and reliable tracking of maximum power point in solar energy systems,” *Int. J. Recent Technol. Eng.*, vol. 7, no. 6, pp. 264–268, 2019.

[50] T. Bogaraj, J. Kanagaraj, and E. Shalini, “Fuzzy Logic Based MPPT for Solar PV Applications,” vol. 2, no. 6, pp. 1566–1571, 2014.

[51] C. N. M. Ho, V. S. P. Cheung, and H. S. H. Chung, “Constant-frequency hysteresis current control of grid-connected VSI without bandwidth control,” *2009 IEEE Energy Convers. Congr. Expo. ECCE 2009*, pp. 2949–2956, 2009, doi: 10.1109/ECCE.2009.5316436.

[52] J. Yu, M. Su, and Y. Sun, “A novel current control method for grid connected photovoltaic system,” *Asia-Pacific Power Energy Eng. Conf. APPEEC*, no. 1, 2011, doi: 10.1109/APPEEC.2011.5748441.

[53] A. Bidram, S. Member, and A. Davoudi, “Hierarchical Structure of Microgrids Control System,” pp. 1–14, 2012.

[54] A. A. Kadum, “PWM control techniques for three phase three level inverter drives,” *Telkomnika (Telecommunication Comput. Electron. Control.*, vol. 18, no. 1, pp. 519–529, 2020, doi: 10.12928/TELKOMNIKA.V18I1.12440.

[55] Q. Zheng, J. Li, X. Ai, J. Wen, and J. Fang, “Overivew of grid codes for photovoltaic integration,” *2017 IEEE Conf. Energy Internet Energy Syst. Integr. EI2 2017 - Proc.*, vol. 2018-Janua, pp. 1–6, 2017, doi: 10.1109/EI2.2017.8245501.

[56] Z. Draft, “Tariff Guidelines and Methodology for,” no. January, 2019.

[57] N. Grid *et al.*, “The grid code - UK,” no. 5, 2017, [Online]. Available: https://www.nationalgrid.com/sites/default/files/documents/8589935310-Complete Grid Code.pdf.

[58] A. B. Rey-Boué, R. García-Valverde, F. D. A. Ruz-Vila, and J. M. Torrelo-Ponce, “An integrative approach to the design methodology for 3-phase power conditioners in Photovoltaic Grid-Connected systems,” *Energy Convers. Manag.*, vol. 56, pp. 80–95, 2012, doi: 10.1016/j.enconman.2011.11.012.

[59] X. Hou, H. Han, C. Zhong, W. Yuan, M. Yi, and Y. Chen, “Improvement of transient stability in inverter-based AC microgrid via adaptive virtual inertia,” *ECCE 2016 - IEEE Energy Convers. Congr. Expo. Proc.*, pp. 0–5, 2016, doi: 10.1109/ECCE.2016.7855195.

[60] L. Kafle, “Frequency Control of Wind and Pv Based Isolated Microgrid.” 2016.

[61] B. V Rajanna, “Grid Connected Solar PV System with MPPT and Battery Energy Storage System,” *... Trans. Electr. Eng. Comput. ...*, no. December, pp. 8–25, 2020, [Online]. Available: http://www.iteecs.com/index.php/iteecs/article/view/5.

[62] C. Z. Ally and E. C. W. De Jong, “Robust PI control of a grid-connected voltage source inverter for virtual inertia response in weak grid conditions,” *SEST 2019 - 2nd Int. Conf. Smart Energy Syst. Technol.*, pp. 1–6, 2019, doi: 10.1109/SEST.2019.8848990.

[63] T. Yuvaraja, “Transient Power Flow in Micro grids with Signal Stability Energy,” *IOSR J. Electr. Electron. Eng.*, vol. 8, no. 4, pp. 70–74, 2013, doi: 10.9790/1676-

0847074.

[64] M. A. Khan, A. Haque, F. Blaabjerg, V. S. B. Kurukuru, and H. Wang, “Intelligent transition control between grid-connected and standalone modes of three-phase grid-integrated distributed generation systems,” *Energies*, vol. 14, no. 13, 2021, doi: 10.3390/en14133979.

[65] Y. Li, S. Member, D. M. Vilathgamuwa, and S. Member, “Design , Analysis , and Real-Time Testing of a Controller for Multibus Microgrid System,” vol. 19, no. 5, pp. 1195–1204, 2004.

[66] S. Fahad, A. J. Mahdi, W. H. Tang, K. Huang, and Y. Liu, “Particle Swarm Optimization Based DC-Link Voltage Control for Two Stage Grid Connected PV Inverter,” *2018 Int. Conf. Power Syst. Technol. POWERCON 2018 - Proc.*, no. 201807100000006, pp. 2233–2241, 2019, doi: 10.1109/POWERCON.2018.8602128.

[67] N. Rasmussen, “Understanding power-, crestand surge-factor,” *EngineerIT*, no. JANUARY, pp. 20–21, 2011.

[68] S. Derbie and S. D. Gont, “Design of a Standalone Photovoltaic System for a Typical Household around Dessie City-Ethiopia ASSESSMENT OF POWER RELIABILITY AND IMPROVEMENT POTENTIAL BY USING SMART RECLOSERS View project Design of a Standalone Photovoltaic System for a Typical Househo,” *Am. J. Electr. Electron. Eng.*, vol. 7, no. 1, pp. 1–7, 2019, doi: 10.12691/ajeee-7-1-1.

[69] IFC, “Utility-Scale Solar Photovoltaic Power Plants,” pp. 35–39, 2015.

[70] M. S. Jadin, I. Z. M. Nasiri, S. E. Sabri, and R. Ishak, “A sizing tool for PV standalone system,” *ARPN J. Eng. Appl. Sci.*, vol. 10, no. 22, pp. 10727–10732, 2015.

[71] W. Al-Saedi, S. W. Lachowicz, D. Habibi, and O. Bass, “Voltage and frequency regulation based DG unit in an autonomous microgrid operation using Particle Swarm Optimization,” *Int. J. Electr. Power Energy Syst.*, vol. 53, no. 1, pp. 742–751, 2013, doi: 10.1016/j.ijepes.2013.06.002.

[72] D. K. Dheer, N. Soni, and S. Doolla, “Improvement of Small Signal Stability Margin and Transient Response in Inverter-Dominated Microgrids,” *Sustain. Energy, Grids Networks*, 2015, doi: 10.1016/j.segan.2015.12.005.

[73] J. Hernandez-Alvidrez *et al.*, “PV-Inverter Dynamic Model Validation and

Comparison under Fault Scenarios Using a Power Hardware-in-the-Loop Testbed," *2018 IEEE 7th World Conf. Photovolt. Energy Conversion, WCPEC 2018 - A Jt. Conf. 45th IEEE PVSC, 28th PVSEC 34th EU PVSEC*, pp. 1412–1417, 2018, doi: 10.1109/PVSC.2018.8547488.

[74] B. F. Towler, "Solar Power Solar Power," *Reinhuette*, pp. 1–27, 2019.

[75] A. E. W. H. Kahlane, L. Hassaine, and M. Kherchi, "LCL filter design for photovoltaic grid connected systems," *Third Int. Semin. new Renew. energies*, vol. 8, no. 2, pp. 227–232, 2014.

[76] A. (NREL) Nagarajan, "Greening the Grid : Best Practices for Grid Codes for Renewable Energy Generators," 2018.

[77] T. Converters, U. Borup, F. Blaabjerg, S. Member, and P. N. Enjeti, "Sharing of Nonlinear Load in Parallel-Connected," vol. 37, no. 6, pp. 1817–1823, 2001.

[78] V. Rallabandi, O. M. Akeyo, N. Jewell, and D. M. Ionel, "Incorporating battery energy storage systems into multi-MW grid connected PV systems," *IEEE Trans. Ind. Appl.*, vol. 55, no. 1, pp. 638–647, 2019, doi: 10.1109/TIA.2018.2864696.

[79] Q. Zhong and S. Member, "Harmonic Droop Controller to Reduce the Voltage Harmonics of Inverters," vol. 60, no. 3, pp. 936–945, 2013.

[80] M. Saleh and W. Brandauer, "Design and implementation of CCNY DC microgrid testbed How does access to this work benefit you ? Let us know !," 2016.

[81] M. Kubeitari, A. Alhusayn, and M. Alnahar, "Space Vector PWM Simulation for Three Phase DC/AC Inverter," *Int. J. Electr. Comput. Eng.*, vol. 6, no. 12, pp. 1402–1407, 2012, doi: 10.5281/zenodo.1060621.

[82] N. Chitra, P. Sivakumar, S. Priyanaka, and A. Devisree, "Transient behaviour of a microgrid and its impact on stability during pre and post islanding -A novel survey," *Int. J. Eng. Technol.*, vol. 7, no. 2, pp. 326–330, 2018, doi: 10.14419/ijet.v7i2.24.12076.

[83] Zaheeruddin and K. Singh, "Intelligent frequency control in microgrid: Fractional order fuzzy PID controller," *J. Intell. Fuzzy Syst.*, vol. 39, no. 1, pp. 195–212, 2020, doi: 10.3233/JIFS-190963.

[84] P. Hou, J. Wang, Y. Xu, K. Huang, and J. Li, “Research on the dynamic characteristics of microgrid with pulsed nonlinear load,” *2016 IEEE 8th Int. Power Electron. Motion Control Conf. IPEMC-ECCE Asia 2016*, vol. 2015, no. 3, pp. 1732–1736, 2016, doi: 10.1109/IPEMC.2016.7512555.

[85] M. Liserre, F. Blaabjerg, and A. Dell’aquila, “Step-by-step design procedure for a grid-connected three-phase PWM voltage source converter,” *Int. J. Electron.*, vol. 91, no. 8, pp. 445–460, 2004, doi: 10.1080/00207210412331306186.

[86] Q. Tang, N. Liu, and J. Zhang, “Optimal operation method for microgrid with wind/PV/diesel generator/battery and desalination,” *J. Appl. Math.*, vol. 2014, 2014, doi: 10.1155/2014/857541.

[87] E. C. El Alaoui, H. Ayad, and S. Doubabi, “Fuzzy Anti-Windup Schemes for PID Controllers,” vol. 1, no. 3, pp. 295–306, 2006.

[88] K. Premkumar, T. Thamizhselvan, M. Vishnu Priya, S. B. Ron Carter, and L. P. Sivakumar, “Fuzzy anti-windup pid controlled induction motor,” *Int. J. Eng. Adv. Technol.*, vol. 9, no. 1, pp. 184–189, 2019, doi: 10.35940/ijeat.A1113.109119.

[89] D. Ronzani, “Advanced Anti-Windup Techniques for the Limitation of the Effects of,” 2017.

[90] M. Yang, L. Niu, and D. Xu, “Antiwindup design for the speed loop PI controller of a PMSM servo system,” *Turkish J. Electr. Eng. Comput. Sci.*, vol. 21, no. 5, pp. 1318–1327, 2013, doi: 10.3906/elk-1112-25.

[91] X. L. Li, J. G. Park, and H. B. Shin, “Comparison and evaluation of anti-windup PI controllers,” *J. Power Electron.*, vol. 11, no. 1, pp. 45–50, 2011, doi: 10.6113/JPE.2011.11.1.045.

[92] P. Giroux, O. Tremblay, G. Sybille, and P. Brunelle, “Microgrid Dynamic Operation,” pp. 1–10.

[93] J. Vasquez, J. Guerrero, J. Miret, M. Castilla, and L. Garcia De Vicuna, “Hierarchical control of intelligent microgrids,” *IEEE Ind. Electron. Mag.*, vol. 4, no. 4, pp. 23–29, 2010, doi: 10.1109/MIE.2010.938720.

[94] L. Pi, “Integral Anti-Windup for PI Controllers,” pp. 1–15, 2004.

APPENDICES

Appendix A: Appendices Related to data collection

Data from Internet: Weather Data accessed from NASA by using ASTU student Cafeteria latitude and longitude. (Accessed on February 10, 2021 from https://power.larc.nasa.gov/data-access-viewer/)

ASTU student Cafeteria

Location: Latitude 8.5632   Longitude 39.2909

Months of a year	Maximum temperature at 2m(°C)	Minimum temperature at 2m(°C)	Optimal solar irradiance(KW/m2/day)
January	26.03	11.02	7.13
February	27.46	12.21	6.75
March	27.99	14	6.54
April	27.05	14.87	6.23
May	27.62	15.14	6.43
June	27.39	15.36	5.92
July	24.66	14.53	5.27
August	24.03	14.25	5.32
September	24.51	14.23	5.77
October	24.97	12.07	6.57
November	25.08	10.64	7.2
December	25.01	10.37	7.42
Annually	25.98	13.23	6.38

Appendix B: (P&O) MPPT MATLAB algorithm

```
function D   = PandO(V, I, Dmax, Dmin, deltaD, Dinit, Scan_On, DeltaD_Scan)

% MPPT controller based on the Perturb & Observe algorithm.


% D output = Duty cycle of the boost converter (value between 0 and 1)

% V input = PV array terminal voltage (V)

% I input = PV array current (A)

% D = 1 - Vinput/Voutput (increasing D decrease Vin)


persistent Vold Pold Dold Scan_On_Old Pmax D_Pmax V_Pmax;

%

if isempty(Vold)

    Vold=0;

    Pold=0;

    Scan_On_Old=0;

    Dold=Dinit;

    Pmax=0;

    D_Pmax=0;

    V_Pmax=0;

end

P= V*I;

if Scan_On==1 || Scan_On_Old==1

    if Scan_On_Old==0

        Scan_On_Old=1;
```

```
        D=Dmin;
    else
        D=Dold+DeltaD_Scan;
    end
    Dold=D;
    if P>Pmax
        Pmax=P;
        D_Pmax=D;
    end
    if D >= Dmax
        Scan_On_Old=0;
        Pold=Pmax;
        Dold=D_Pmax;
        Vold=V_Pmax;
    end
else
    dV= V - Vold;
    dP= P - Pold;
    %
```

Appendix C: Microgrid parameters Matlab Script

```
% %%Microgrid Parameters
Ts=40e-7;  % Model sample time (s)
Fnom=50;   % System frequency (Hz)
***********************************************************************
```

```
%% Battery Energy Storage System
BESS.Frequency_Droop=1/2;      % Frequency droop (%)
BESS.Voltage_Droop=3;          % Voltage droop (%)
BESS.Droop_fn_Filter=10;       % Droop filter natural frequency (Hz)
% Power regulators:
BESS.PQref_RateOfChange=20;    % Pref & Qref rate of change (pu/s)
BESS.Kp_Preg=1.75;             % Proportional gain
BESS.Ki_Preg=80/5;             % Integral gain
BESS.Preg_RateChange=[10, -10]; % Output rate of change (pu/s)
BESS.Preg_Limits=[1.0, -1.0];  % Active power output limits (pu)
BESS.Qreg_Limits=[1.0, -1.0];  % Reactive power output limits (pu)
% Voltage regulator:
BESS.Kp_Vreg=5;                % Proportional gain
BESS.Ki_Vreg=25;               % Integral gain
BESS.Vreg_Limits=[1.5, -1.5];  % Output limits (pu)
% Current regulators:
BESS.Kp_Ireg=0.2;              % Proportional gain
BESS.Ki_Ireg=10;               % Integral gain
BESS.Ireg_Limits=[1.3, -1.3];  % Output limits (pu)
% PWM generator:
BESS.Fsw=2700;                 % PWM carrier frequency (Hz)
BESS.CarrierPhase=90;          % PWM carrier phase (deg.)
BESS.fn_Filter=500;            % Measurement filter natural frequency (Hz)
BESS.Synchro_Duration=3;       % Time allowed for synchronization to distribution system
```

```
BESS.Kp_SyncReg=0.025/2;       % Proportional gain

BESS.Ki_SyncReg=0.03/2;        % Integral gain

BESS.SyncReg_Limits=[20e-3, -20e-3];  % Regulators output limits

% Imbalance Compensation:

BESS.Kp_Vreg2=5;               % Proportional gain

BESS.Ki_Vreg2=25;              % Integral gain

BESS.Vreg2_Limits=[0.5, -0.5];  % Regulators output limits

BESS.Kp_Ireg2=0.08;            % Proportional gain

BESS.Ki_Ireg2=5;               % Integral gain

BESS.Ireg2_Limits=[0.5, -0.5];  % Regulators output limits

%% Solar Plant

%DC link:

PV.H=1.0;                      % Capacitance in number of cycles of Pnom

% PV arrays power regulator (Not in MPPT mode):

PV.Kp_Preg=0.05;               % Proportional gain

PV.Ki_Preg=2;                  % Integral gain

PV.Preg_Limits=[0.8 0.1];      % Output limits (pu)

% Voltage regulator:

PV.Kp_Vreg=6;                  % Proportional gain

PV.Ki_Vreg=30;                 % Integral gain

%PV.Vreg_Limits=[1.2, -1.2];    % Output limits (pu)

% Current regulators:

PV.Kp_Ireg=0.2;                % Proportional gain

PV.Ki_Ireg=15;                 % Integral gain
```

%PV.Ireg_Limits=[1.2, -1.2];   % Output limits (pu)

% PWM generator:

PV.Fsw=2340;   % PWM carrier frequency (Hz)

PV.CarrierPhase=0;   % PWM carrier phase (deg.)

PV.fn_Filter=1000;   % Measurement filter natural frequency (Hz)

Appendix D: Inverter control sub block diagram of solar plant and BESS

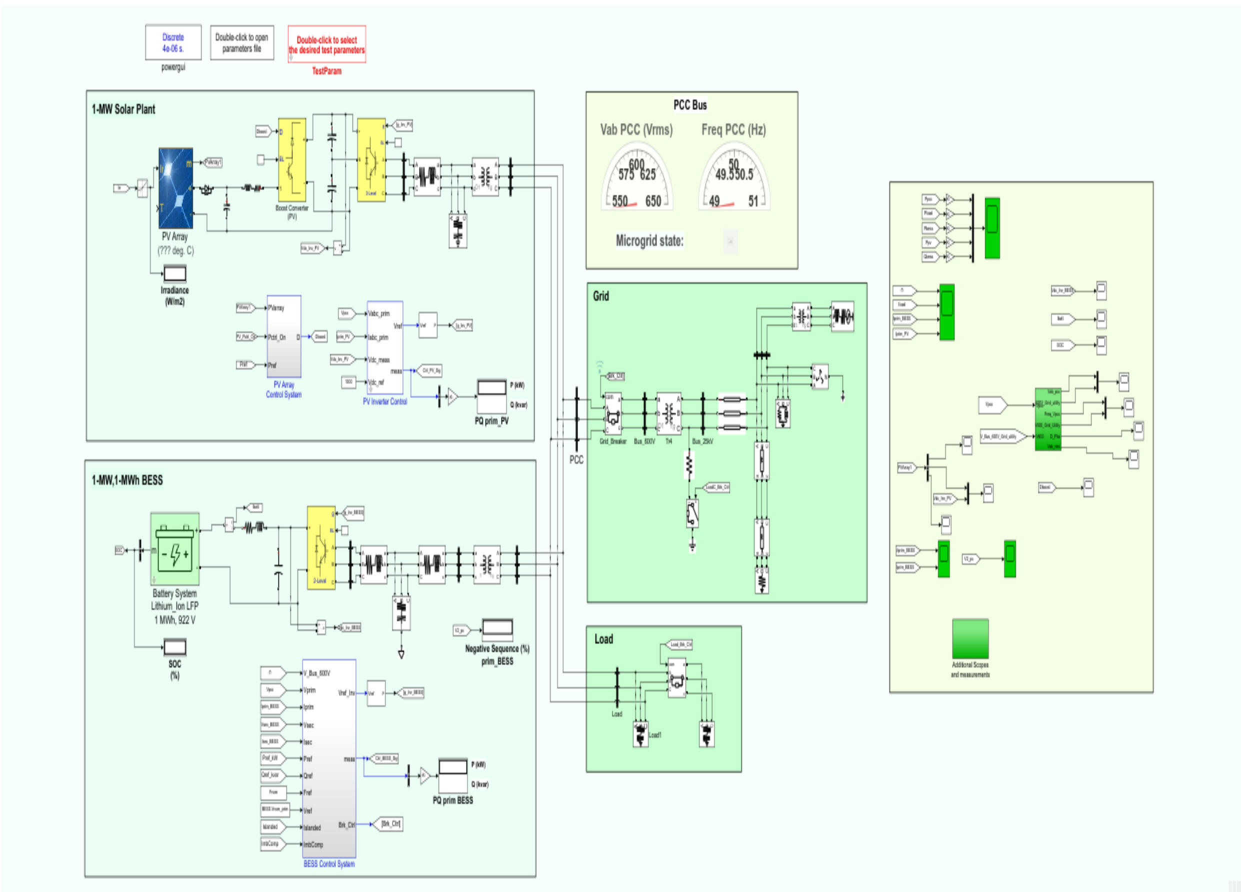

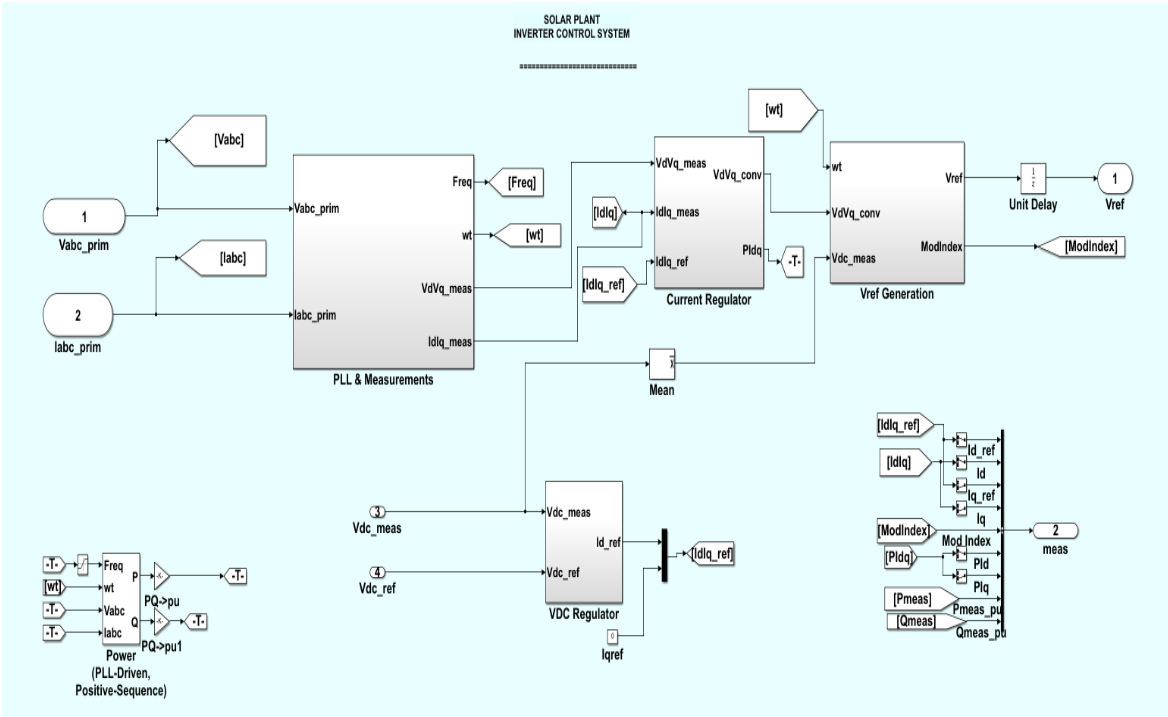
SOLAR PLANT
INVERTER CONTROL SYSTEM
[Vabc]
[Iabc]
Vabc_prim
Iabc_prim
PLL & Measurements
Freq
wt
VdVq_meas
IdIq_meas
[Freq]
[wt]
[IdIq]
[IdIq_ref]
VdVq_conv
Pldq
Current Regulator
Vdc_meas
Vref
ModIndex
Vref Generation
[ModIndex]
Unit Delay
Mean
Vdc_ref
Id_ref
VDC Regulator
Iqref
Power
(PLL-Driven,
Positive-Sequence)
PQ->pu
PQ->pu1
[PIdq]
[Pmeas]
[Qmeas]
Mod Index
Pmeas_pu
Qmeas_pu
meas

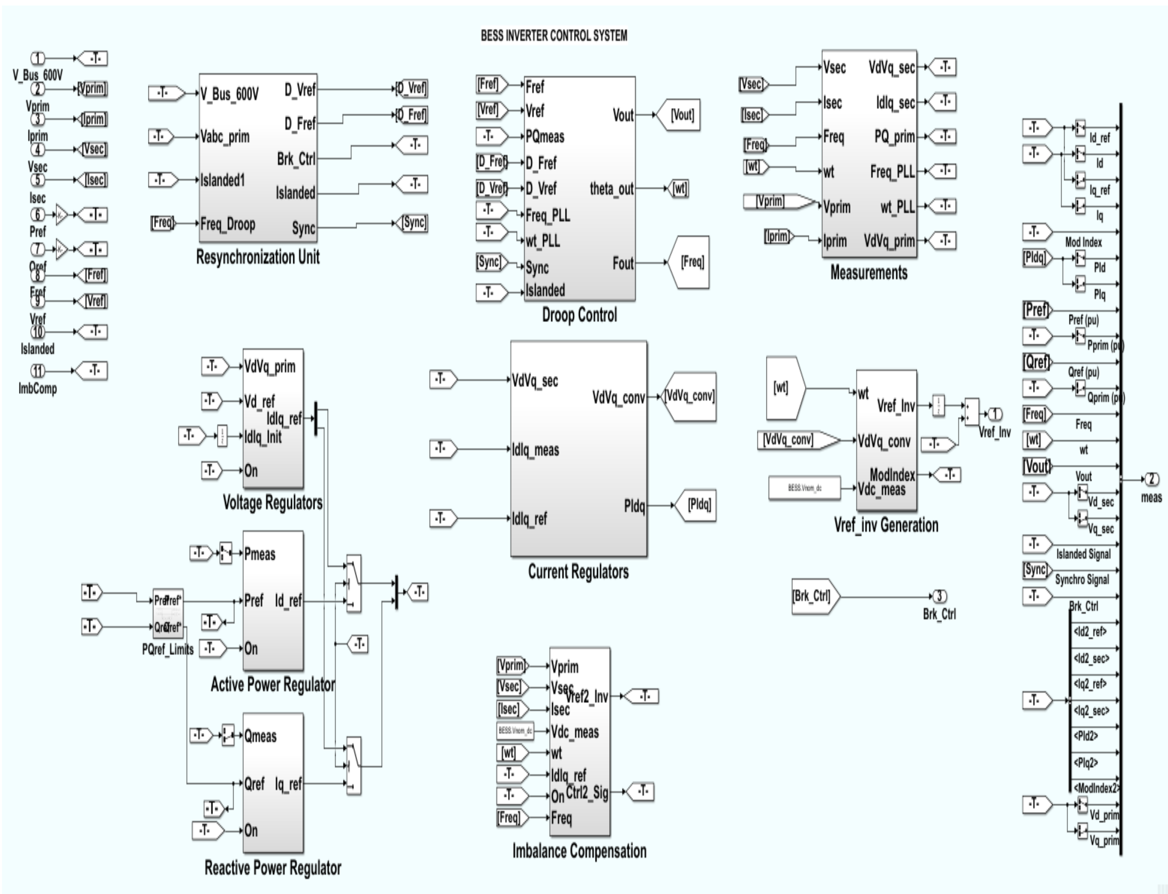
BESS INVERTER CONTROL SYSTEM
V_Bus_600V
Vprim
Iprim
Vsec
Isec
Pref
Qref
Fref
Vref
Islanded
ImbComp
Vabc_prim
Islanded1
Freq_Droop
D_Vref
D_Fref
Brk_Ctrl
Sync
Resynchronization Unit
PQmeas
Freq_PLL
wt_PLL
Vout
theta_out
Fout
Droop Control
VdVq_sec
IdIq_sec
PQ_prim
VdVq_prim
Measurements
Vd_ref
IdIq_Init
On
Voltage Regulators
Pmeas
Active Power Regulator
PQref_Limits
Qmeas
Reactive Power Regulator
IdIq_meas
IdIq_ref
VdVq_conv
Current Regulators
Vref_Inv
Vref_inv Generation
Brk_Ctrl
Vdc_meas
Vref2_Inv
Ctrl2_Sig
Imbalance Compensation
Islanded Signal
Synchro Signal
meas

Appendix E: Three Phase transformation

Clarke's transformation is a stationary frame transformation technique which converts time domain signals (e.g., voltage, current) from three-phase coordinates (abc) into two-phase orthogonal stationary coordinates (αβ). Consider a three-phase rotating vector Us which consists of A, B and C axis components. These three axis components can be represented in the two αβ coordinates by two components Uα and Uβ using the Clarke's transformation as shown in figure below. The three-phase rotating vector can be represented as:

$$\overrightarrow{U_S} = \left|\overrightarrow{U_S}\right| < \theta = \frac{2}{3}\left(u_a + u_b e^{j\frac{2\pi}{3}} + u_b e^{-j\frac{2\pi}{3}}\right) \quad (0.1)$$

where, $\overrightarrow{U_S} = \sqrt{U_\alpha^2 + U_\beta^2}$

and

$$\theta = \tan^{-1}\frac{U_\beta}{U_\alpha} \quad (0.2)$$

$$\begin{pmatrix} u_\alpha \\ u_\beta \\ u_0 \end{pmatrix} = \frac{2}{3}\begin{pmatrix} 1 & -\frac{1}{2} & -\frac{1}{2} \\ 0 & \frac{\sqrt{3}}{2} & -\frac{\sqrt{3}}{2} \\ \frac{1}{2} & \frac{1}{2} & \frac{1}{2} \end{pmatrix}\begin{pmatrix} u_a \\ u_b \\ u_c \end{pmatrix} \quad (0.3)$$

Park's transformation is the rotating frame transformation which converters three phase time varying quantities from three-phase coordinates (abc) into time invariant quantities in two phase orthogonal rotating coordinate.

$$u_{sd} = i_\alpha.\cos(\theta) + i_\beta.\sin(\theta) \quad (0.4)$$

$$u_{sq} = -i_\alpha.\sin(\theta) + i_\beta.\cos(\theta) \quad (0.5)$$

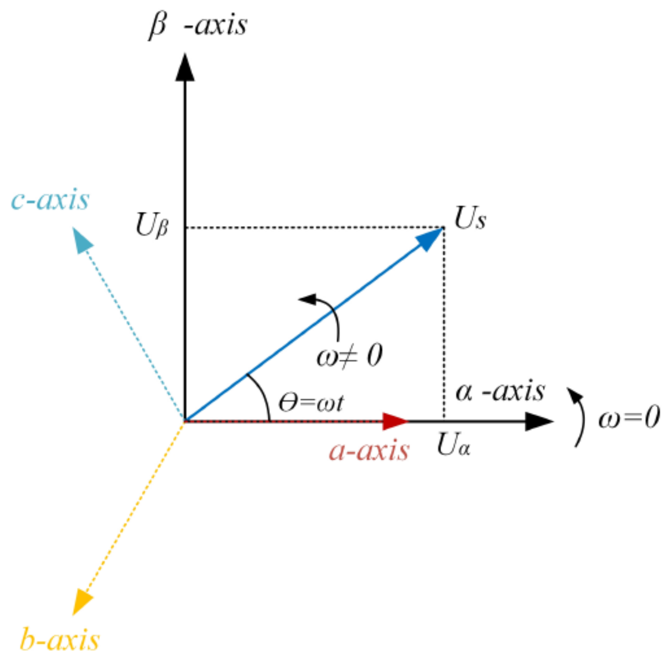

Figure 0.1Three phase transformation

Table 0-1 Summary of Transformation

a,b,c to α,β(Clarke Transform)	d, q,0-> α, β(Clarke To Park transform)
$u_\alpha = \frac{2}{3}(u_a) - \frac{1}{3}(u_b - u_c)$ $u_\beta = \frac{2}{\sqrt{3}}(u_b - u_c)$	$u_\alpha = i_{sd}.\cos(\theta) - i_{sq}.\sin(\theta)$ $u_\beta = i_{sd}.\sin(\theta) + i_{sq}.\cos(\theta)$
α, β to dq0	**a,b,c to α, β**
$u_{sd} = i_\alpha.\cos(\theta) + i_\beta.\sin(\theta)$ $u_{sq} = -i_\alpha.\sin(\theta) + i_\beta.\cos(\theta)$	$u_0 = \frac{2}{3}(u_a + u_b + u_c)$ $u_\alpha = \frac{2}{3}(u_a) - \frac{1}{3}(u_b - u_c)$ $u_\beta = \frac{2}{\sqrt{3}}(u_b - u_c)$